Development and Characterisation of $Glmp^{gt/gt}$ and $Glmp^{wt/wt}$ cell lines

Tora Daniela Moreiro Engh

Master thesis in Molecular Bioscience
Program option: Biochemistry

Department of Biosciences
The Faculty of Mathematics and Natural Sciences

UNIVERSITY OF OSLO
June 2017

Acknowledgments

Abstract

Glycosylated Lysosomal Membrane Protein (GLMP, formerly known as NCU-G1), is a *bona fide* lysosomal membrane protein with uncharacterised physiological function. A mouse model lacking detectable expression of *Glmp* has previously been made, using a gene-trap strategy. The predominant phenotype of the *Glmp*$^{gt/gt}$ mice is a slowly progressing liver fibrosis initiated shortly after birth, and they are indistinguishable from the *Glmp*$^{wt/wt}$ mice regarding growth, fertility and behaviour.

We hypothesise that the liver fibrosis is a symptom of a yet undescribed lysosomal disorder, caused by a deficiency in the endosomal-lysosomal system due to GLMP ablation. To characterise the effect of GLMP ablation at the cellular level, spontaneously transformed Mouse Embryonic Fibroblast (MEF) cell lines, derived from the *Glmp*$^{gt/gt}$ and *Glmp*$^{wt/wt}$ mice, were initially made (*Glmp*$^{gt/gt}$ MEF1 and *Glmp*$^{wt/wt}$ MEF1). The growth rate of the *Glmp*$^{gt/gt}$ and *Glmp*$^{wt/wt}$ MEF1 cell lines did not differ, but the *Glmp*$^{gt/gt}$ MEF1 cells were more sensitive to low cell densities in initial culture.

The cellular uptake capacity was compared between the *Glmp*$^{gt/gt}$ MEF1 cells and *Glmp*$^{wt/wt}$ MEF1 cells by monitoring uptake of fluorescently labelled endocytic ligands. Cellular uptake of both transferrin (Tf) and dextran was found to be equal between the genotypes of the MEF1 cells. The Epidermal Growth Factor (EGF) uptake of the *Glmp*$^{gt/gt}$ MEF1 cells had previously been found to be significantly impaired, when compared to *Glmp*$^{wt/wt}$ MEF1 cells. The impairment was initially thought to be caused by lowered synthesis or incorrect sorting of the EGF-receptor in the GLMP ablated MEF1 cells. To rescue the impaired uptake, the cellular uptake was studied in *Glmp*$^{gt/gt}$ MEF1 cells transiently expressing fluorophore labelled GLMP. Reintroduction of GLMP did not rescue the impaired uptake, and GLMP appeared toxic to the cells when introduced in high concentrations. A suspected protein partner of GLMP, Major Facilitator Superfamily Domain-containing protein 1 (MFSD1), was transiently expressed in *Glmp*$^{gt/gt}$ MEF1 cells, alone and alongside GLMP. Neither MFSD1 alone or MFSD1 and GLMP combined could rescue the impaired EGF uptake. To investigate whether the EGF impairment was caused by downregulated synthesis or improper sorting of EGF-receptor, the EGF uptake capacity of *Glmp*$^{gt/gt}$ MEF1 cells transiently expressing fluorophore labelled EGF-receptor was compared to control cells. Transient expression of additional EGF-receptor did improve the EGF uptake, thus impaired uptake was assumed to

be due to GLMP ablation somehow distorting the synthesis or causing upregulated degradation of EGFR.

To confirm the observations, additional MEF cell lines derived from the $Glmp^{gt/gt}$ and $Glmp^{wt/wt}$ mice were developed (MEF2-T and MEF3-T) by stable transfection with the Simian Virus40 (SV40) oncogene Large T antigen (TAg). A growth assay investigating the ability of the TAg transformed MEF2-T cells in low serum concentrations confirmed successful transformation.

The uptake capacity of Tf and EGF was then compared between the genotypes of the new confirmed cell lines ($Glmp^{gt/gt}$ and $Glmp^{wt/wt}$ MEF2-T). No difference was found when comparing the Tf uptake capacity between the MEF2-T genotypes, and the impaired EGF uptake found in the $Glmp^{gt/gt}$ MEF1 cells was not confirmed in the $Glmp^{gt/gt}$ MEF2-T cells. The EGF uptake capacity was also compared between $Mfsd1^{ko/ko}$ and $Mfsd1^{wtwt}$ MEF cells, and did not differ either. The observations were controlled by investigating the EGF uptake capacity in primary cells. The EGF uptake capacity did not differ between primary $Glmp^{gt/gt}$ and $Glmp^{wt/wt}$ MEF cells (MEF2-P) either, indicating that the impaired EGF uptake observed in the $Glmp^{gt/gt}$ MEF1 cells is an artefact of transformation, and not due to GLMP ablation. Tf uptake capacity was equal between the genotypes of the primary cells.

Preliminary karyotyping assays revealed that the $Glmp^{gt/gt}$ MEF1 cells are aneuploid, with four distinct $Egfr$ alleles. In addition, a chromosome cross-over site was observed on one of the four $Egfr$ gene containing chromosomes (Eskeland, R., unpublished). Preliminary western blot assays comparing EGF-receptor and Tf-receptor content in the GLMP ablated primary cells and cell lines (MEF1, MEF2-T and MEF2-P) revealed substantially lower EGF-receptor content in the $Glmp^{gt/gt}$ cells when compared to $Glmp^{wt/wt}$ MEF1 cells. The EGF content did not appear to differ between the genotypes of the MEF2-T cells or the MEF2-P cells. The Tf-receptor content was found to be equal between the genotype of the MEF1, MEF2-T and MEF2-P cells.

Based on these findings, the MEF1 cell lines have been rejected as suitable models for investigating the effect of GLMP ablation on the endocytic pathways. Furthermore, the uptake studies conducted on the MEF2-T and MEF2-P cell lines indicate that GLMP ablation does not affect EGF or Tf uptake capacity.

Table of content

x

1   Introduction

A mouse model lacking detectable expression of Glycosylated lysosomal membrane protein (GLMP) has previously been made, and the predominant phenotype in this model is a slowly progressing liver fibrosis [1, 2]. GLMP is a *bona fide* lysosomal membrane protein with uncharacterised physiological functions [3]. Deficient functions of proteins associated with the endosomal-lysosomal system is an underlying cause of a class of inheritable disorders collectively named Lysosomal Disorders, and over 50 such disorders are known [4]. Cell lines derived from transgenic mice are useful tools for characterising protein function *in vitro* [5], and in this thesis the aim was to develop and characterise Mouse Embryonic Fibroblasts (MEF) derived from the $Glmp^{gt/gt}$ and $Glmp^{wt/wt}$ mice. These MEF cells are intended as models for *in vitro* studies of the effect of GLMP ablation at the cellular level.

1.1 Liver fibrosis

1.1.1 Liver structure and function

The liver is a vital organ with numerous essential functions including nutrient processing, detoxification and blood glucose regulation. The liver is composed of parenchymal cells (hepatocytes) and various non-parenchymal cells. Non-parenchymal cells include Kupffer cells (KCs), Hepatic Stellate cells (HSCs), and Liver Sinusoidal Endothelial cells (LSECs). The hepatocytes are the main cell type in the liver [6]. Hepatocyte functions involve degradation, detoxification and modification of nutrients and other substances in the blood. Hepatocytes also synthetises bile acids and many of the blood plasma proteins (e.g. Albumin and Transferrin). Hepatocytes are organised in hexagonal lobules consisting of one cell thick plates with a central vessel called the sinusoid (figure 1B). The hexagonal lobules are organized around portal tracts containing a branch of hepatic artery, hepatic vein and a bile duct (figure 1A). Portal blood enriched with nutrients and other substances collected in the intestines flows from the portal vein through the sinusoids, where exchange between the circulatory system and the liver occurs. Oxygen rich blood is supplied by the hepatic artery converging with the blood from the hepatic vein. LSECs line the sinusoid walls, and the epithelial cell layer contains fenestrations that allow free passage of solutes. The blood is collected in a central vein at the end of the sinusoid [7]. HSCs reside in the sub-endothelial space between the hepatocytes and the LSECs, called "the space of Disse", functioning

mainly as storage cells for fat-soluble vitamins (i.e. Vitamin A). KCs, which are liver resident macrophages, reside in the sinusoids and defend against toxins and bacteria in the blood from the intestines (figure 1B) [6, 7].
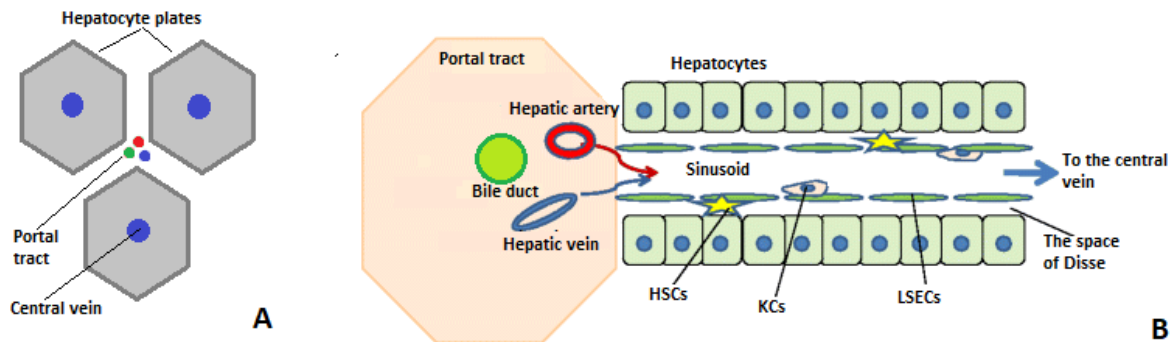
Figure 1: **Liver cell organisation**. (A) Cross section of hepatic lobules. Hepatocytes are organised in hexagonal lobules surrounding a central vessel called the sinusoid leading to a central vein. Each lobule is organised around a portal tract containing a hepatic artery (red), hepatic vein (blue) and a bile duct (green). (B) Organisation of liver cells in the hepatic lobule. The inner surface of the sinusoid is lined with Liver Sinusoidal Endothelial Cells (LSECs) containing fenestrations allowing for free passage of solutes. The space between the LSECs and the hepatocytes is called the space of Disse and is resided by vitamin A storing Hepatic Stellate Cells (HSCs). Liver-resident macrophages, Kupffer Cells (KCs) patrol the sinusoid. Blood flows through the sinusoids before being collected in a central vein. Figure adapted [7].

The liver possesses the unique ability to repair and renew itself following damage [8, 9]. The wound-healing process involves reorganisation of Extracellular Matrix (ECM) at the site of injury, and replacement of damaged hepatocytes through proliferation. In a healthy liver hepatocytes seldom proliferate, but following injury the proliferation rate increases dramatically. If the cause of injury ceases, the liver function and architecture can be completely restored [8, 9].

1.1.2 Liver fibrosis

Transient damage causes limited deposition and remodelling of ECM, which functions to encapsulate the site of injury while the tissue composition and volume is restored. After resolution, the excess ECM is degraded. Persistent injury might result in an ongoing wound-healing process where the ratio between proliferating and dying hepatocytes is skewed towards loss of functioning cells, causing accumulation of excess ECM eventually replacing the functional tissue. A condition referred to as liver fibrosis [10].

There are various causes of liver damage, including alcohol abuse, viral infections (e.g. Hepatitis), and inherited metabolic disorders. Liver fibrosis is a wound-healing process in

2

response to injury. It is characterised by accumulation of fibrous ECM which ultimately might compromise liver function by replacing the functional tissue. Ongoing fibrosis might result in development of nodules of proliferating hepatocytes surrounded by filamentous scar tissue, disrupted liver structure and altered blood flow. The end-state of fibrosis is termed cirrhosis, and if left untreated, cirrhosis might ultimately result in liver failure, cancer, and death [10-12].

In the healthy liver, the space of Disse consists of a low-density basement membrane-like matrix, composed of ECM molecules organised in a defined lattice meshwork. This meshwork provides cellular support and allows for free passage of solutes (figure 2) [13]. In the fibrotic liver, the quantitative and qualitative composition of the ECM is altered, and fibrous scar tissue accumulate and replace the functional tissue. Upregulated ECM synthesis, accompanied by downregulation of degradation, causes the deposition of excess ECM. Normal ECM contains mainly non-fibrous types of collagen, while the fibrotic scar tissue is comprised of fibrous collagen types that cross link and ultimately thicken to an extent where they are resistant to proteolytic degradation [11]. This scar tissue formation leads to loss of fenestrations in the sinusoidal wall, a process termed sinusoidal capilarisation (figure 2). The loss of fenestrations compromises liver function by hindering solute exchange between venous blood and hepatocytes [12].
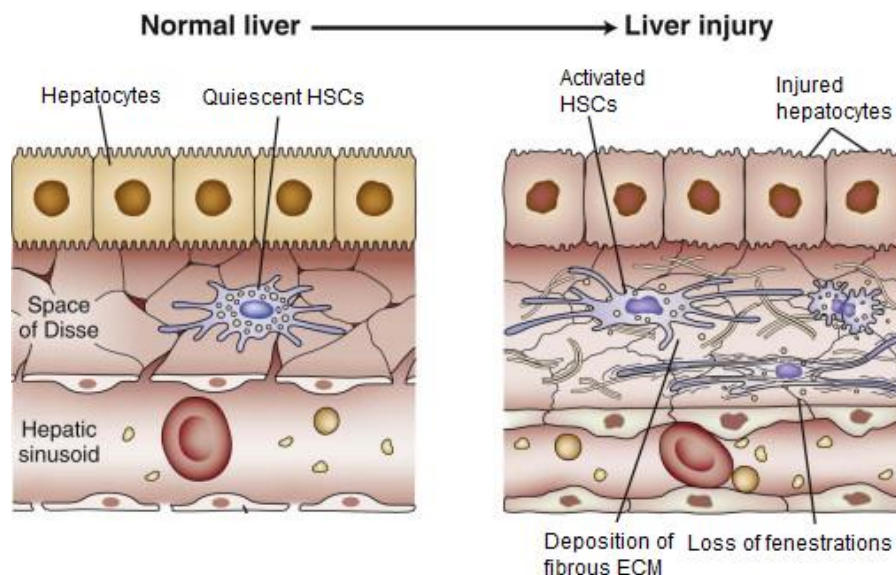
Figure 2: **Structural changes during fibrogenesis.** Following injury, Hepatic Stellate Cells (HSCs) are activated, and transdifferentiate into myofibroblast-like cells with altered phenotypic traits, involving loss of lipid droplets, higher proliferation rate, and increased deposition of fibrous Extracellular Matrix (ECM). The ECM composition of the sub-endothelial space, named the space of Disse, changes and accumulation of excess fibrous ECM leads to loss of fenestrations and blockage of solute exchange across the space of Disse, a phenomenon known as sinusoidal capilarisation. Figure adapted from [11].

The major ECM producing cells in the liver are HSCs, accompanied by recruited portal fibroblasts and myofibroblasts from the bone marrow [10]. Following injury HSCs are activated by various cytokines secreted by damaged hepatocytes and LSECs [14]. Activation of HSCs causes trans-differentiation of quiescent HSCs into fibrotic, mobile, proliferating and contractile myofibroblast-like cells (Figure 3). Activation also leads to loss of the lipid vitamin-A storage droplets [11]. Active HSCs migrate to the site of injury, and produce fibrous ECM to encapsulate the damaged area. The activated HSCs also secrete fibrotic mediators, maintaining self-activation, recruitment of immune cells, and downregulating degradation of ECM. This continues as long as damaged tissue is present. The contractile phenotype leads to increased portal resistance at the site of injury, and is linked with increased production of α Smooth Muscle Actin (α-SMA, a common marker for HSCs activation) [15].
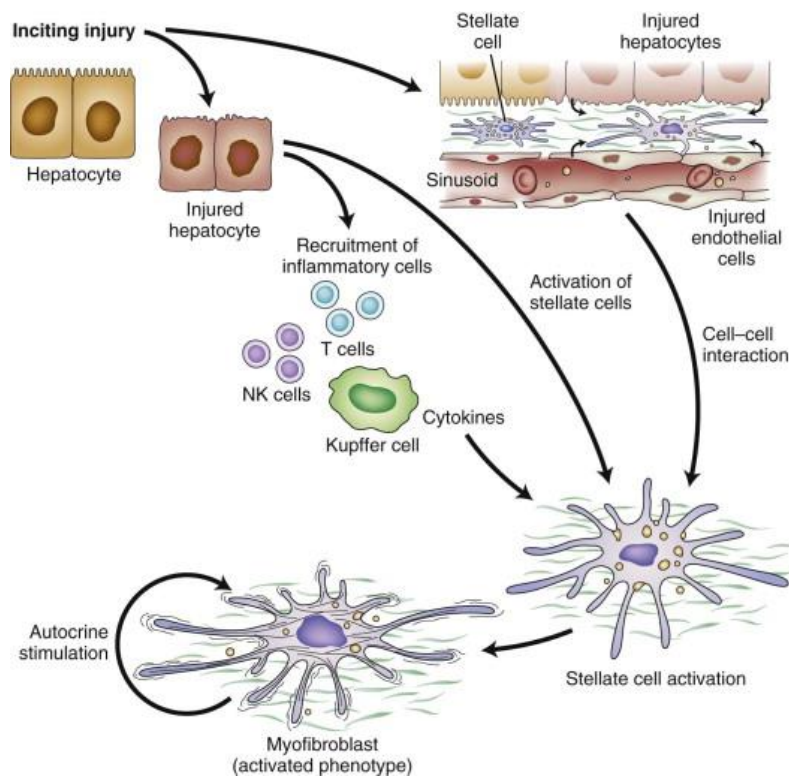
Figure 3: **Initiation and progression of fibrogenesis**. Injured Hepatocytes secrete inflammatory mediators recruiting leukocytes and promoting Hepatic Stellate Cell (HSC) activation. The inflammatory cells modulate the fibrosis progression, and secrete cytokines that further promote HSC activation. Activation causes HSCs to trans-differentiation into myofibroblast-like cells with new traits, including contractility, loss of lipid droplets, higher proliferation rate, and deposition of fibrotic Extracellular Matrix (ECM) at the site of injury. When the injury persists, the fibrosis is maintained in a self-enhancing cycle, where the participating cells stimulate each other and drive the fibrosis forward. Figure adapted from [11].

4

The inflammatory mediators secreted by the damaged cells and activated HSCs leads to recruitment of leukocytes and liver residential KCs, that migrate into the site of injury. The recruited cells remove dead and dying hepatocytes by phagocytosis, and secrete additional inflammatory mediators, which further promotes HSCs activation and recruitment of additional immune cells [16]. Ongoing insult causes paracrine and autocrine signalling cascades, maintaining the fibrotic state in a self-enhancing, possibly pathogenic manner. The wound-healing process which is present to encapsulate and resolve damage, develops into a pathogenic process where deposition of undegradable fibrous scar tissue replaces the functional tissue. This compromises the organ function with potentially lethal outcome [13].

1.2 GLMP and *Glmp*^{gt/gt} mice

1.2.1 Glycosylated Lysosomal Membrane Protein (GLMP)

Glycosylated Lysosomal Membrane Protein (GLMP), previously known as NCU-G1, was initially reported to be a nuclear protein with transcriptional regulatory function [17]. GLMP has later been identified as a *bona fide* lysosomal membrane protein [3, 18]. The lysosomal localisation of GLMP was determined by immunofluorescence assays where GLMP colocalised with the established lysosomal protein LAMP-1, confirmed by density centrifugation assays where GLMP was found primarily in the lysosomal fraction alongside LAMP-1 [3]. Another study showed that GLMP expression is controlled by Transcription Factor EB (TFEB), which coordinates expression of many lysosomal proteins, further confirming lysosomal residency [18]. GLMP is a small highly glycosylated type I integral membrane protein with a short C-terminal cytoplasmic tail, and a large luminal N-terminal domain containing nine predicted N-glycosylation sites, and a hydrophobic signal sorting sequence that is post-translationally removed [3] (Figure 4).
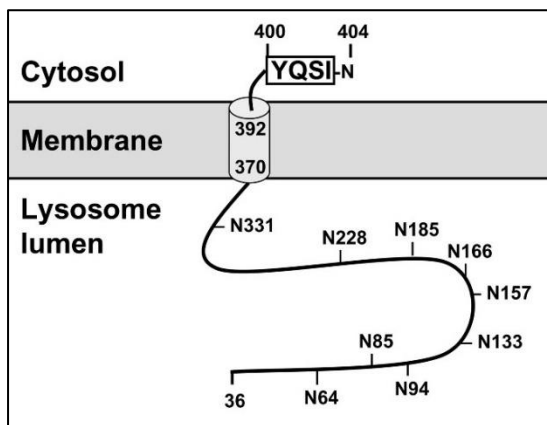
Figure 4: **Schematic representation if the predicted structure of GLMP.** GLMP is a type I integral lysosomal membrane protein with a short C-terminal cytoplasmic tail containing a predicted tyrosine-based lysosomal sorting signal (in box 400-403), a single transmembrane segment (encapsulated 370-392) and a large luminal N-terminal domain with nine predicted N-glycosylation sites (indicated with residue number), here shown after removal of the hydrophobic N-terminal signal peptide (1-35). Figure adapted from [3]

The molecular weight (MW) of the apoprotein is approximately 44 kDa, but the fully glycosylated form has a MW of 70-80 kDa [3]. The sequence does not resemble any known protein, except a small portion of the C-terminal tail, which resembles the C-terminal tail of the well-known lysosomal membrane proteins LAMP-1 and LAMP-2 [3]. GLMP is ubiquitously expressed and highly conserved, indicating important biological function, but this function has not yet been found [2, 17]. Recently, a mutation in the *Glmp* gene was shown to be the main cause of craniofacial fibrous dysplasia syndrome [19, 20].

To further investigate the physiological function of GLMP, a transgenic mouse model lacking detectable expression of GLMP was generated. This was achieved by inserting a gene-trap cassette into intron 1 of the *Glmp* gene. The gene-trap contains a neomycin-resistance cassette for positive selection and a polyadenylation site that inhibits transcription [2].

1.2.2 The *Glmp$^{gt/gt}$* mouse model

The *Glmp$^{gt/gt}$* mice are indistinguishable from the *Glmp$^{wt/wt}$* mice regarding growth, reproduction and behaviour [2]. The *Glmp$^{gt/gt}$* predominant phenotype is a slowly progressing liver fibrosis initiated shortly after birth [1]. The damage is not lethal and is less extensive after the mice reach adulthood, however the fibrosis is never reversed completely and the liver remains somehow distorted through the whole life-span of the animal [1]. At 1 week, infiltrating leukocytes are visible in histological sections. This increases with age, and is an indication of tissue inflammation and a common initial response to damage; this implicates postpartum initiation of liver injury and consequently fibrogenesis [1]. Several assays confirmed postpartum initiation of fibrosis. Macroscopical investigations of new-born *Glmp$^{gt/gt}$* mice show no visible liver damage (figure 5A). Sub-capsular bleeding is observed at 2-4 weeks, and sub-capsular contractions are observed at 3 months of age, causing distortion of the liver structure in the adolescent animals (figure 5A). Histological analysis of liver sections show no excess collagen in 1-week old individuals, confirming the absence of fibrogenesis at this age [1]. At 1 month, excess collagen is prominent in the *Glmp$^{gt/gt}$* liver (figure 5B). This is also confirmed by quantitative determination of hydroxyproline levels, a common method for measuring collagen. The hydroxyproline levels are equal in the new-born mice, but increase in the *Glmp$^{gt/gt}$* mice at 2-weeks of age, and remains elevated throughout the life-span of the animal [1].
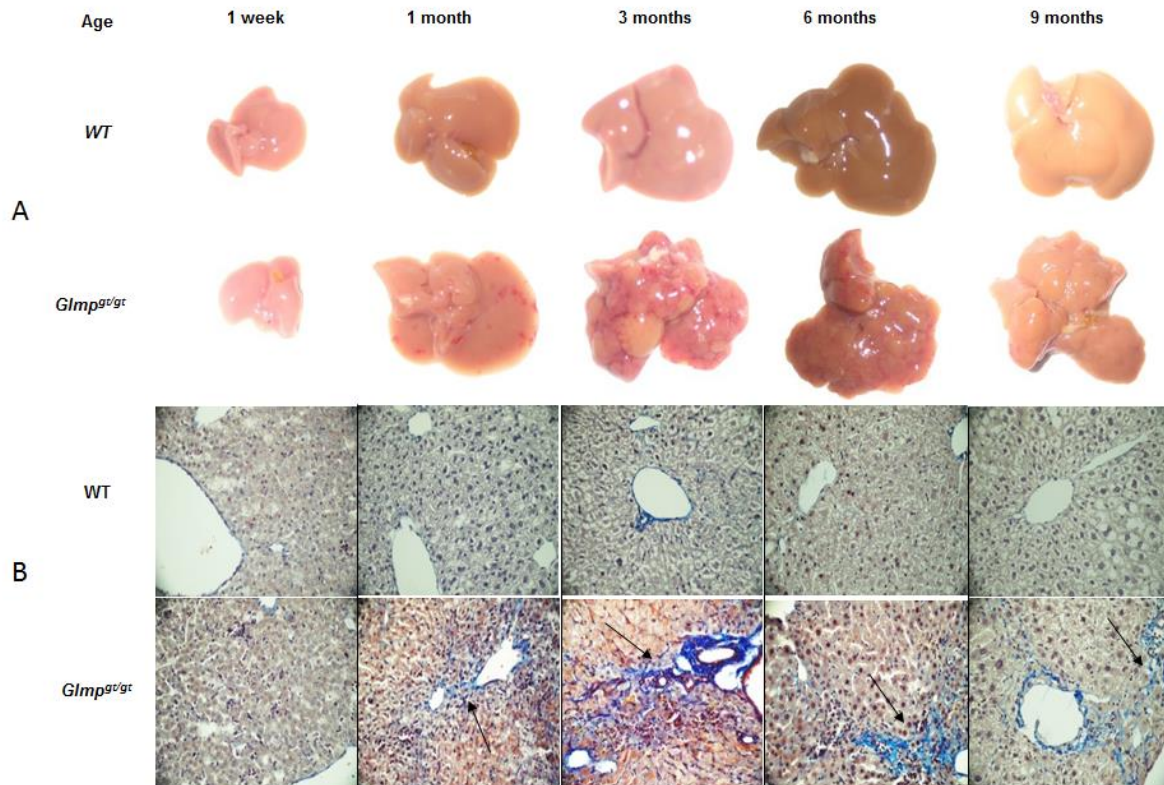
Figure 5. **Age-dependent development of liver fibrosis in *Glmp^gt/gt* mice**. (A) Images of livers from *Glmp^wt/wt* and *Glmp^gt/gt* mice ranging from the age of 1 week to 9 months. There is no visible difference at 1 week, indicating absence of damage at this age. Subscapsular contractions appear around 3 months of age in the *Glmp^gt/gt* livers, increasing up until 6 months giving the liver a nodular, distorted appearance. The surface smoothens out at 9 months. (B) Liver sections from various ages of *Glmp^wt/wt* and *Glmp^gt/gt* mice stained with collagen selective stain acid fuchsin orange G (Blue). Deposition of excess collagen is observed from 1 month of age in the *Glmp^gt/gt* mice (arrows). Figure adapted from [1] .

Hepatic Stellate Cells (HSCs) are the main ECM producing cells in the liver and key regulators of fibrogenesis. HSCs are usually quiescent vitamin A storage cells, but following an insult to the liver they are activated and transdifferentiate into myofibroblast-like cells. The gene expression pattern changes, which includes increased expression of alpha smooth muscle actin (α-SMA), a common and well-established marker for activated HSCs [11, 14, 21]. Activation of HSCs has long been regarded as the central mechanism in liver fibrosis[22]. Relative gene expression analysis revealed no significant difference in α-SMA mRNA content in the new-born mice, confirming the absence of activated HSCs, and hence the absence of fibrogenesis, at this age [1]. The α-SMA mRNA level increases in the *Glmp^gt/gt* mice after the first month and remains significantly elevated (figure 6). At 4.5 months of age, blood serum analysis reveal elevated serum transaminase levels, increased bile acid, lowered serum albumin levels and mild anaemia, consistent with liver damage [1]. Evidence of

proliferating hepatocytes is also present, as is expected in order to replace lost hepatocytes. Between the age of 3 and 6 months the hepatocyte proliferation is not able to compensate for the total hepatocyte loss, leading to activation of the oval cell compartment. Over all the damaging effects seem to be dampened after the animal reach adult size, but the fibrosis is never reversed, and parts of the liver structure remains distorted. [1]

GLMP ablation is most damaging when the animal grows and the liver adapts to degrading and processing nutrients, pathogens, and toxins associated with oral nutrient intake, which

Figure 6 **Relative gene expression analysis of Alpha smooth muscle actin(α-SMA) in *Glmp^gt/gt* mice.** mRNA expression was measured by qPCR, showing increased expression starting at one month, peaking at 3.5 months. α-SMA is a common marker for activated Hepatic Stellate Cells (HSCs), which are the main drivers of fibrogenesis. (n = 4, *p < 0.05, **p < 0.01, ***p < 0.005 vs. WT). Values are presented as mean ± s.e.m, figure adapted from [1]

unlike the nutrient intake via the umbilical cord is not sterile. GLMP ablation appears to be less damaging after the animal reaches adult size and the liver ceases to grow. The animals maintain sufficient liver function, as the damage is mild and the fibrosis dampened in the adult mice [1]. Despite the reducing disparities at 9 months, the fibrosis and injury is not reversed completely, as confirmed by the consistently elevated levels of hydroxyproline. Furthermore, oval cell compartment activation appeared vital to compensate the loss of hepatocytes, but also contributes to cancer development; 60% of the *Glmp^gt/gt* mice aged 12-18 months had increased numbers of liver tumours compared to *Glmp^wt/wt* mice [1, 23].

We hypothesise that the liver fibrosis is a manifestation of a yet undescribed lysosomal disorder, and that GLMP ablation alters the endocytic function. To investigate the effect a simpler model system is useful. There is no replacement for animal models for determination of *in vivo* function of any protein or pathway. However, the cost, complexity, and time consumption often makes it beneficial to develop alternative models. The use of cultivated cells has long been a part of biological research [5]. They serve as *in vitro* models for biological processes and responses at a cellular level, making them suitable for investigating cellular events. A great advantage of using cultivated cells is the ability to investigate cellular responses under highly controlled conditions. When studying cellular events *in vivo* it is

8

difficult to determine whether the observations are directly or indirectly connected to the applied stimuli, as the cells are part of bigger and more complex environment.

1.2.3 *In vitro* models for characterisation of protein function

One objective of this thesis is to develop an *in vitro* model, intended for initial characterisation of the effect of GLMP ablation at the cellular level. Cultivated fibroblasts derived from transgenic mice are commonly used for characterisation of protein function and responses *in vitro*. Characterisation of function at the cellular level is often approached by comparing mutant cells to wildtype cells [5, 24]. One example of this is a study that demonstrated that PPARγ coactivator-1 (PGC-1) depends on histone acetyltransferases steroid receptor coactivator–1(SCR-1) for transcriptional activity; this was determined by comparing *SRC-1^{wt/wt}* and *SRC-1^{ko/ko}* cells [25].

When developing a model system, it is important to be aware of the limitations and proper applications. Cultivated cells are suitable for investigating cellular function *in vitro*, but the observations do not necessarily represent the situation *in vivo*. The cellular environment in live animals is far more complex than the environment in the culture vessel. *In vivo* responses often include intercellular interactions between different cell types, the extracellular matrix, solutes and signal molecules. The observed responses and reactions are often due to larger interaction networks, an environment impossible to replicate *in vitro*. However, this complexity makes it difficult to determine whether the observed responses are solely due to the imposed altered gene function or whether they are part of a bigger network. Limiting the complexity of the model is useful for understanding the basic cellular mechanisms of single proteins or genes. Cells in culture are ideal models for such studies as their environment is in large part controlled by the conditions imposed on them by their handler [5, 24, 26].

Primary cells are the preferred *in vitro* model, as their behaviour generally resembles the *in vivo* behaviour more closely than immortalised cells. Any immortalisation event ultimately alters the characteristics and behaviour of the cells, sometimes to an extent that compromises the mechanisms of interest. Despite the possible conflicting changes in phenotypic traits after an immortalisation event, several advantages make the use of immortalised cell lines preferable to primary cells. Primary cells have shorter lifespan than immortal cells and can only be subcultured a limited amount of times, referred to as the Hayflick limit, where the cells enter a senescent state and cease to divide [27]. Immortalisation occurs when cells

obtain traits allowing them to divide beyond their Hayflick limit [5, 27]. Immortalised cell lines are also cheaper and easier to maintain than primary cells, and yield almost endless amount of material. They are easily stored and provide purer populations beneficial for consistency and reproducibility [28]. However, excessive subcultivation can lead to genotypic and phenotypic changes [29]. It is not uncommon that immortal cell lines are aneuploid, meaning that they contain an abnormal number of chromosomes. Heteroploidy can also occur, where different cells in the same population have varying chromosomal content. Rodent cells are more unstable than human cells, and are therefore more likely to transform spontaneously. They are also more prone to mutations which might alter the cellular functions of interest [28, 30]. To confirm findings from cell lines it is often useful to develop several independent cell lines derived from the same transgenic mouse lineages. Confirming findings in additional cell lines derived from the same source reduces the possibility of the observed effects being artefacts of the immortalisation or any undetected mutation present in the cell line. However, it is still important to confirm any significant findings in primary cells when possible, before ultimately confirming the findings in the animal model [5, 28].

Fibroblasts can be isolated from a variety of tissues including tail, lungs, and embryos. The use of embryonic tissue for cultivation of fibroblasts is common and yields robust cells that are easily cultured. However, fibroblast isolation from embryonic tissue is more time consuming than the use of external tissue. Successful mating and proper detection of impregnation is time consuming, and if the isolation is not successful several weeks might pass before new embryos can be harvested. When using tail or ear the tissue may be collected at any time. An advantage of using embryonic tissue, compared to external tissue, is the sterility. The foetus itself is sterile and good sterile technique prevents contamination in the primary culture [5, 24, 26, 31]. Contamination compromises the authenticity of the results, as it might alter the cellular responses, and proper sterile technique and equipment is essential [28, 30, 32].

Embryos may be harvested at almost any stage during pregnancy, but 12.5 to 13.5 days is preferred due to factors as size and cell type content. At this age, the embryo is large enough to be dissected with the naked eye, but still young enough to contain a substantial amount of fibroblasts. Older embryos are larger and easier to dissect, but also contain more

differentiated cells not desired in a fibroblast culture. Younger embryos are small and the removal of the red organs and brain is difficult [24, 31, 33].

It is important to ensure that the protein of interest is active in the chosen cell line, failing to do so would give a model useless for the intended purpose. In this project, the *Glmp^{gt/gt}* and *Glmp^{wt/wt}* cell lines are intended as models to study the impact of GLMP ablation on the endocytic pathways. Previous studies show that GLMP is ubiquitously expressed in all tissues of the *Glmp^{wt/wt}* mice and that the *Glmp^{gt/gt}* mice lack detectable expression of GLMP [2].

Spontaneously transformed Mouse Embryonic Fibroblast (MEF) cell lines (designated *Glmp^{gt/gt}* and *Glmp^{wt/wt}* MEF1 in this thesis), derived from the *Glmp^{gt/gt}* and *Glmp^{wt/wt}* mice has previously been successfully generated. Gene expression analysis confirmed the absence of detectable GLMP expression in the *Glmp^{gt/gt}* MEF1 cells (Kong, X. Y., unpublished).

1.3   The Endosomal-Lysosomal system

All events involving formation of intracellular vesicles by invagination of the plasma membrane can be collected under the general term endocytosis. The endocytic pathway mediates internalisation of components ranging from fluids, solutes, and membrane proteins, to entire cells. The endosomal-lysosomal system is responsible for processing, sorting, storing and degrading anything internalised by endocytosis, and therefore plays a key role in numerous cellular pathways [34, 35]. The system can also be accredited regulation of intracellular communication by controlling plasma membrane composition, thereby controlling the sensibility of the cell to extracellular signals [36].

1.3.1 Endosomes end endosomal maturation

The endosomal-lysosomal system consists of dynamic membrane-enclosed compartments, which according to function and traits can be divided into early endosomes, recycling endosomes, late endosomes, and lysosomes [35]. The system can be roughly divided in three parts; a recycling cycle, the degradation pathway and a feeder pathway mediating interaction between them. The recycling cycle is responsible for recycling plasma membrane components, and includes Early Endosomes, Recycling Endosomes and the primary endocytic vesicles in the peripheral area of the cell (figure 7) [36]. Most of the internalised

goods are recycled back via the early endosome, the rest is directed further down the endocytic pathway. The degradation pathway leading to the lysosome functions to degrade macromolecules, not only delivered from endosomes, but also intracellular components marked for degradation, in addition to cargo from phagosomes and autophagosomes. The feeder pathway, coordinated by the Late Endosomes, facilitates transport from the recycling pathway to the degradative pathway, in addition to transport of lysosomal proteins from the Trans Golgi Network (TGN) to the lysosomes (figure 7) [35, 36].
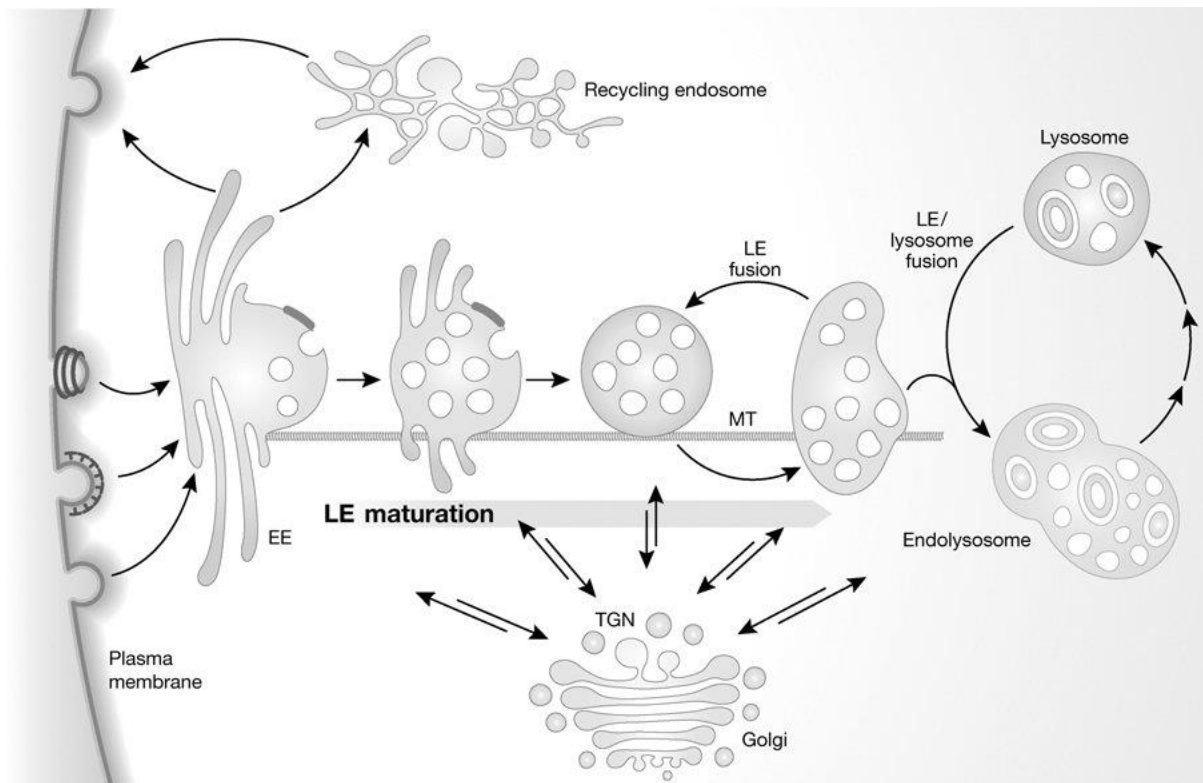
Figure 7. **The endosomal-lysosomal system.** Invaginations at the plasma membrane bud off and primary endocytic vesicles carrying fluids and internalised material are made. The primary endocytic vesicles fuse with each other and with Early Endosomes (EE), where most of the cargo and membrane is sorted back to the membrane directly or via a recycling endosome. The EE is transported along microtubules (MT) and several events occur during this migration, leading to maturation of EE into Late Endosomes (LE). The endosomal lumen acidifies, and an increasing number of Intraluminal vesicles form. Cargo destined for degradation is sorted into the intraluminal vesicles and endosomal components are exchanged by lysosomal components, facilitated by bidirectional vesicle transport with the Trans Golgi Network(TGN). LE fuse with each other and eventually with the lysosome, creating a hybrid organelle called endoslysosome where degradation takes place. Other degradation pathways lead to the lysosome, including phagocytosis and autophagocytosis (not shown). In the last maturation step, the endolysosome is converted to a dense lysosome. Figure adapted from [36].

Sorting and trafficking in the endosomal-lysosomal system is regulated by small GTPases belonging to the Rab family of monomeric G proteins. The Rab proteins function as molecular switches, with a GTP-bound active form and a GDP-bound inactive form. Distinct

12

types of endosomes are regulated by specific Rab proteins, and Rab proteins therefore serve as markers for differentiating between types of endosomes. For instance, Rab5 is specific to early endosomes and Rab7 in specific to late endosomes, and the exchange of Rab5 to Rab7 is a hallmark event in the conversion from early endosomes to late endosomes. Rab functions include vesicle fusion, directing cargo along to the appropriate compartments and regulating endosome maturation [36, 37]

Endosomes are dynamic, and mature as they move along the endocytic pathway. Endosomal maturation involves several changes, including acidification, exchange of associated Rab proteins, increasing content of intraluminal vesicles and movement along microtubules towards the microtubule organising centre [36]. The luminal pH acidifies as the endosomes mature creating an acidic gradient from ~ pH 6.5 in the early endosomes to ~ pH 4.5 in the lysosome. The acidification is mediated by ATP-dependent proton pumps located in the endosomal and lysosomal membranes. The acidic luminal environment is important for several processes, like dissociation of ligands from their receptors at appropriate places, and facilitating the proper environment for acidic hydrolases in the lysosome [35].

Newly internalised cargo is delivered to the early endosomes via primary endocytic vesicles. The cargo is sorted, and only a small fraction continues to the late endosome. The formation of early endosomes is not fully understood, but most of the membrane and intraluminal liquid comes from fusing with primary endocytic vesicles. [34]. The inwards budding of endosomal membrane, and formation of Intraluminal Vesicles (ILVs), is initiated in the early endosomes. The amount of ILVs increases along the maturation pathway and is important for maturation from early endosome to late endosome [34]. The Endosomal Sorting Complexes Required for Transport (ESCRT) ensure correct sorting of ubiquinated membrane proteins destined for degradation in the lysosome, into the ILVs [35]. As the endosomes move along the microtubules, exchange mediated by sorting vesicles between the endosome and the TGN occurs. Endosomal components are sorted out and lysosomal components are delivered to the endosomes. The feeder function of the late endosomes involves sorting of cargo from delivered from the early endosomes, where the components are either directed towards the lysosome for degradation, or via the TGN for reuse at the plasma membrane. Transport from, and to, the TGN is mediated by the Retromer complex which can be regarded as having the opposite function of the ESCRT system [34, 35, 38].

Mature late endosomes fuse to form larger late endosomes, sometimes referred to as multivesicular bodies. Interaction with the lysosome happens either with "kiss-and-run" interactions, where transient fusions allows for exchange between the compartments, or by total fusion and formation of endolysosomes. Endolysosomes may be regarded as hybrid organelles, and facilitate degradation of ILV cargo. Following fusion of the late endosome and lysosomes, the lysosome structure is recovered. This can be regarded as the last maturation step, and the process includes content condensation and membrane renewal [39]. Lysosomal composition and content is described later.

1.3.2 Endocytosis

Endocytosis is the internalisation of material and fluids in membrane enclosed compartments. Several different mechanisms exist, usually divided into Clathrin-Mediated Endocytosis (CME) and Clathrin-Independent Endocytosis (CMI) (figure 8) [36]. Common for all these pathways is the formation of primary endocytic vesicles, that fuse with the Early Endosomes and are either sorted back to the plasma membrane or carried along for lysosomal degradation. The exception is phagocytosis, were the formed vesicle fuses directly with the lysosome [50].
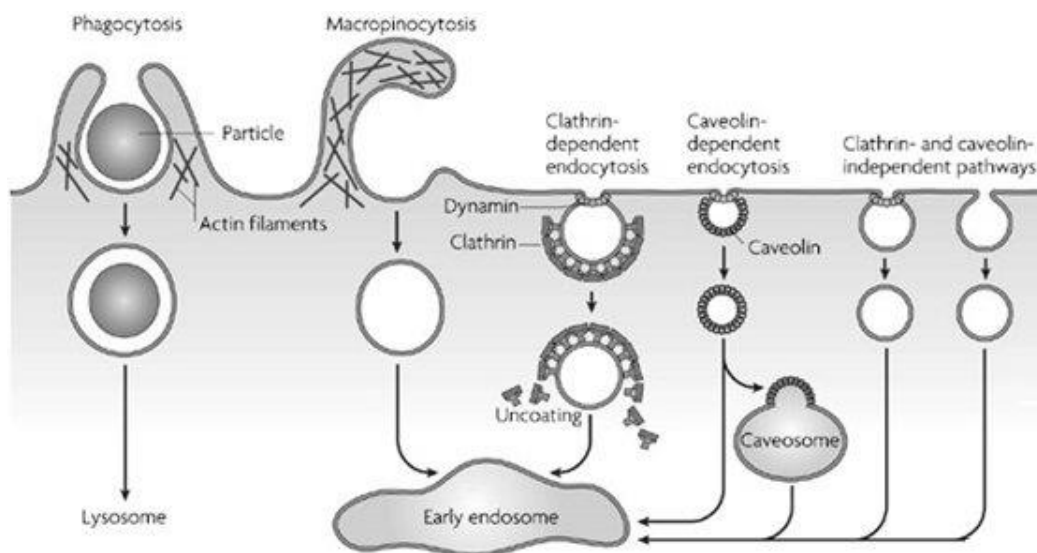
Figure 8. **Endocytic pathways**. There are several mechanisms for internalising extracellular material. Entire cells may be engulfed by specialised cells in a process called phagocytosis. The resulting vesicles, called phagosomes, fuse with lysosomes, killing the cell. The internalisation is mediated by actin remodelling of the plasma membrane. A similar actin-mediated process is associated with macropinocytosis, where fluids and non-specific solutes are internalised. The formation of primary endocytic vesicles is usually divided into clathrin-mediated and clathrin-independent endocytosis, including caveolin-dependent and clathrin- and caveolin-independent pathways. Figure adapted from [40]

14

1.3.2.1 Clathrin-mediated endocytosis

Clathrin-mediated endocytosis (CME) is the most common endocytosis mechanism. CME involves the packing of transmembrane proteins, and any associated ligands, into clathrin coated vesicles. The mechanism can be divided into five stages; initiation, cargo selection, coat assembly, partition from the membrane, and uncoating (figure 8) [41].

Initiation can be stimulated by the binding of cargo to a membrane receptor. One example of this is the internalisation of Epidermal Growth Factor Receptor (EGFR). EGFR is a receptor tyrosine kinase, with several different ligands including Epidermal Growth Factor (EGF) and Transforming growth factor-α (TGF-α). Upon ligand binding, two EGFR monomers dimerise and auto-phosphorylate, initiating an intracellular kinase signal cascade, followed by internalisation of the EGFR-ligand complex [42, 43]. Receptor destiny depends on the type of ligand; binding of EGF destines the EGFR for degradation in the lysosome, and binding of TGF-α allows for receptor recycling via the recycling pathway. TGF-α dissociates from EGFR in the early endosome, due to the decrease in pH. EGF remains bound to EGFR, and the EGF-EGFR complex is marked for degradation by a ubiquitin tag on the cytosolic tail of EGFR. The complex is then sorted into ILVs and transported through the endosomal-lysosomal pathway for degradation [35].

The internalisation event starts with activation of EGFR. Activated EGFR recruit adaptor proteins, and alongside other associate proteins, they coordinate formation of a clathrin lattice. As the invagination buds, EGF-EGFR complexes are clustered together in clathrin-coated pits (figure 8). The lattice stabilises the invagination, and as more clathrin proteins polymerise, a spherical vesicle is formed. This continues until only a small portion of the membrane is left in a shape resembling a neck. The dissociation from the plasma membrane is mediated by the GTPase Dynamin. Dynamin forms a loop around neck of the budding vesicle, and pinches it off in an energy-dependent manner. Once internalised, the clathrin-coated vesicle loses its coat and fuses with other primary endocytic vesicles and the early endosome for further processing of the cargo [36, 42, 43]. Internalisation of EGFR by clathrin-independent pathways has also been demonstrated, but requires high EGF concentrations. At physiological concentrations CME is the main internalising mechanism[44].

Another example of an endocytic receptor internalised through CME is the Transferrin-receptor (TfR). Unlike the EGFR-EGF complex, the TfR receptor is recycled back to the

plasma membrane alongside its ligand. Transferrin facilitates internalisation of iron, mediated by the iron carrying protein Transferrin (Tf). Tf is capable of binding two iron ions, and iron-loaded Tf binds the TfR, which leads to internalisation through CME. When the Tf-TfR-complex reaches the early endosome, the iron dissociates and is transported to the cytoplasm. Tf-TfR-complex is then recycled back to the plasma membrane, were the Tf (apo-form) dissociates from the TfR to collect more iron [45].

1.3.2.2 Clathrin-independent endocytosis

Clathrin-independent endocytosis is the formation of intracellular vesicles from the plasma membrane without the aid of clathrin. One such pathway is caveolin-dependent endocytosis. Caveolins are integral membrane proteins that accumulate at highly hydrophobic areas of the plasma membrane rich in cholesterol, sometimes referred to as lipid rafts [46, 47]. There are three main caveolin proteins: Caveolin-1, -2 and -3. Caveolin-1 is responsible for caveolae formation, which are flask shaped invaginations in the plasma membrane. The N-terminal of caveolin-1 has a hairpin shape that is inserted into the cytosolic leaflet of the plasma membrane. The C-terminal end is soluble and aligns along the membrane. Caveolin-2 is thought to have an accessory function, forming a heterodimeric complex with caveolin-1 [46, 48]. Caveolae are anchored to the plasma membrane via the cytoskeleton, only budding off into the cytosol upon binding of specific ligands (e.g. folic acid and Albumin). As in CME, the dissociation from the plasma membrane is aided by Dynamin (figure 8) [46, 47]. Once internalised, caveolar vesicles form multi-caveolar complexes named Caveosomes. Caveosomes does not fuse with lysosomes, but may interact with the endosomal-lysosomal pathway (figure 8) [46].

Clathrin- and caveolin-independent endocytosis involve formation of vesicles independent of protein coating that depends on cholesterol. This type of endocytosis is dependent on correct membrane composition, and may be Dynamin dependent or independent. Examples are Rho-A regulated (dynamin-dependent) and CDC42-regulated (Dynamin-independent) (figure 8) [36].

1.3.2.3 Macropinocytosis and phagocytosis

Macropinocytosis involves internalisation of large volumes of liquid, involving large self-fusing projections from the plasma membrane. The projectiles are a result of cytoskeleton

16

rearrangements, mainly involving actin. Fluid and solutes present in the surrounded area are unspecifically internalised within a membrane enclosed compartments called macropinosomes. The process usually occurs in response to growth factor stimulation (e.g. EGF) [36, 49].

Specialised cells possess the ability to internalise material as large as whole cells. Phagocytosis is initiated by recognition of an antibody on the target, followed by rearrangement of the plasma membrane, and formation of projections named pseudopodia. The target is then enclosed by the plasma membrane and internalised. The resulting compartment is called a phagosome, which fuses with the lysosome, resulting in degradation of the target[50].

1.3.2.4 Autophagy

Autophagy or "self-eating" is not an endocytic mechanism, but is associated to the endosomal-lysosomal system, and is therefore included in this section. The autophagic process is responsible for removing malfunctioning and unnecessary intracellular components, and serves as a means to overcome starvation. The process involves enclosing the target in double-membraned vesicle, creating an autophagosome, or by the direct uptake of cytosolic components by the lysosome (figure 9). The autophagosome then fuses with the lysosome and the content is degraded [51].

There are three different autophagic mechanisms: micro- and macro-autophagy, and chaperone-mediated autophagy. Micro-autophagy involves internalisation of cytosolic components by the lysosome, via invaginations of the lysosomal membrane or at the late endosome (figure 9B). Both non-selective and selective mechanisms are known. Non-selective micro-autophagy is present in all eukaryotic cells, but selective has only been observed in yeast [51-53].

The macro-autophagic process involves the expansion of an isolating membrane, thought to originate from the Endoplasmic Reticulum (ER) or the Trans Golgi Network [51]. The membrane encloses the target, and fuses to form a membrane-enclosed compartment known as an autophagosome. The autophagosome fuses with the lysosome, and the content is degraded by lysosomal acidic hydrolases (Figure 9A). The degradation products are then transported out to the cytoplasm by lysosomal permeases and transporters, to be reused by the

cell. Selection of cargo was originally thought to be unspecific, but there is evidence of specific targeting of protein aggregates and organelles via recognition by Microtubule-associated proteins (LC3) [51, 54].

Chaperone-mediated autophagy is degradation of specifically marked soluble proteins, which are translocated over the lysosomal membrane and degraded (figure 9C). Typical targets are misfolded proteins, and short-lived proteins. The mechanism is important for maintenance of cellular homeostasis, protein turn-over and for recycling amino acids. The presence of one or several pentapeptide signal sequences allows for recognition of the protein by cytosolic chaperones. The motif, often concealed within properly folded proteins, has specific characteristics necessary for recognition by chaperones. These include correct charge, and the presence of a basic and a hydrophobic residue. The motif is recognised by the chaperone heat shock cognate protein of 70 kD (hsc70). The chaperone-substrate complex binds to the cytosolic tail of Lysosome-associated Membrane Protein 2A (LAMP-2A). LAMP-2A is a heavily glycosylated lysosomal membrane protein, with one transmembrane domain, and a short C-terminal tail. The translocation event is poorly understood, but is thought to involve multimerization of LAMP-2A initiated by substrate binding. Once internalised, the protein is degraded, and the degradation products are transported to the cytoplasm for reuse [55, 56].
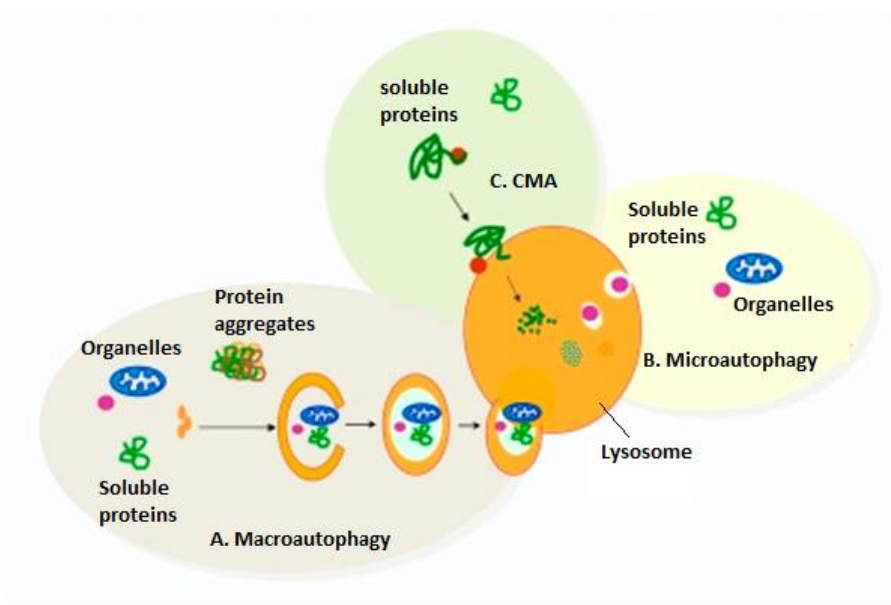
Figure 9, **Autophagic mechanisms**. A. Macroautophagy involves the wrapping of large cytosolic components by a double membrane, creating an autophagosome. The autophagosome fuses with the lysosome, where the cargo is degraded. B. Micro-autophagy involves the internalisation of cytosolic components by invaginations of the lysosomal membrane forming small vesicles in the lysosomal lumen, where the cargo is degraded. C. Chaperone-mediated autophagy (CMA) involves the translocation of marked protein over the lysosomal membrane mediated by the lysosomal receptor LAMP-2A. Figure adapted from [55].

1.3.3 The lysosome

Lysosomes are acidic organelles present in almost every type of animal cell, and serve as the main site for catalytic activity. The lysosome degrades endogenous and exogenous biomolecules delivered from the endocytic, phagocytic and autophagic pathways (section 1.3.1). Lysosomal function depends on two classes of proteins; soluble lysosomal acidic hydrolases and Lysosomal Membrane Proteins (LMPs) [57].

After translation, lysosomal proteins are transported from the Endoplasmic Reticulum (ER), via Golgi and the Trans Golgi Network, to the endocytosis pathway. This can occur directly to the endosomes, or indirectly via the plasma membrane [58].

1.3.3.1 Soluble lysosomal acidic hydrolases

There are 50 known lysosomal acidic hydrolases, all with specific target substrates, and collectively they constitute the total degradation capacity of the lysosome [57].

Hydrolases are enzymes that catalyses the brakeage of chemical bonds, by a hydrolysis mechanism. Lysosomal acidic hydrolases include glycosylases, lipases, proteases, phosphatases, and nucleases; hence the lysosome is equipped to degrade any biomolecules [58]. One common characteristic of the lysosomal acidic hydrolases is the narrow pH-optimum [59]. Correct folding and optimal function depends on an acidic environment. Most of the lysosomal acidic hydrolases lose their native conformation, and hence their function, at neutral pH [60]. In addition to the compartmentalisation of the acid hydrolases inside the lysosomal lumen, the pH-optimum serves as a protection against possibly damaging proteolytic activity outside the lysosome [60].

Lysosomal acidic hydrolases are initially translated with an additional N-terminal signal tag of 20-25 amino acid residues. The signal tag directs the translocation of the peptide into the ER lumen during translation. In the ER lumen, the signal tag is cleaved off. Simultaneously, the hydrolase is N-glycosylated with a pre-made oligosaccharide at specific Arginine residues. The hydrolases are then transported to the Golgi apparatus in vesicles where the oligosaccharide chains are further modified. One important modification is the addition of Mannose-6-Phospate (M6P) [58]. The M6P tag is recognised by M6P-receptors (M6PR) in the Trans Golgi Network (TGN). The receptors bind adaptor proteins, and Clathrin-coated vesicles are formed, followed by transport to the Endosomes, where the hydrolase is released

from the receptor. The receptor is recycled to the TGN, and the hydrolases are delivered to the lysosome (see section 1.3.1) [57]. M6PR-independent delivery pathways to lysosomes are also known [58]. One example is the route of the lysosomal β-Glucocerebrosidase, which is targeted to the lysosome in a M6PR-independent matter. Lysosomal Integral Protein 2 (LIMP-2) is the trafficking receptor facilitating correct sorting of β-Glucocerebrosidase to the lysosome [61].

1.3.3.2 Lysosomal Membrane Proteins (LMPs)

The lysosomal membrane is vital for maintaining lysosomal function and to separate the acidic environment of the lysosomal lumen from the cytoplasm. The lysosomal membrane contains a vacuolar-type H^+-ATPase (V-ATPase), which functions to maintain the low luminal pH-level [62].

The membrane contains many different highly specialised LMPs, with various roles such as transmembrane transport, maintenance of luminal acidity and facilitating membrane fusion [63]. Due to the acidic environment and the high content of hydrolases, most LMPs are highly glycosylated creating a continuous glycoprotein barrier alongside the luminal surface of the lysosomal membrane. The glycoprotein coat is estimated to be around 8 nm thick, and is thought to play an important function in regulating lysosomal integrity and stability [64].

Unlike the acidic hydrolases, with a few exceptions, LMPs are not modified with M6P in Golgi. The sorting of LMPs instead depend on their cytosolic tails, which carries a lysosome specific signal sequence. The sequence interacts with adaptor proteins that associate with clathrin, and clathrin-coated vesicles are made [58]. The vesicles are transported from the TGN to the endosomes, and then to the lysosomes as described earlier. Another route is indirectly via the plasma membrane, where the LMPs follow the normal endocytosis pathway, as opposed to the direct delivery described above [65].

The most abundant types of LMPs are the Lysosomal Associated Membrane Proteins 1 and 2 (LAMP-1 and LAMP-2), and the Lysosomal Integral Membrane Proteins 1 and 2 (LIMP-1 and LIMP-2) [66]. It is estimated that 50% of all LMPs are LAMP-1 and LAMP-2 proteins [67]. LAMP-1 and LAMP-2 are homologous, but distinct type I transmembrane proteins [66]. Both proteins have a single transmembrane segment, a short C-terminal tail, and a large N-

terminal domain. The un-glycosylated apoprotein form of both LAMP-1 and LAMP-2 has a MW of approximately 40 kDa. The fully glycosylated MW is approximately 120 kDa [68].

LAMP-1 and LAMP-2 deficiency is lethal at the embryonic level in combination, but mice deficient in either LAMP-1 or LAMP-2 are fertile and viable. This suggests a common function *in vivo*. LAMP-2 deficient mice display more severe phenotypes than LAMP-1 deficient mice, and it is therefore speculated that LAMP-2 has a more specific function. LAMP-2 deficiency causes accumulation of autophagosomes in heart and muscle tissue [67]. The LAMP-2 mRNA has three alternative splicing possibilities, and three isoforms of LAMP-2 exist (LAMP-2A, -2B and -2C) [69].

A study of LAMP-1 and LAMP-2 ablated Mouse Embryonic Fibroblasts (MEF) cells with reconstituted phagocytosis showed normal internalisation of particles through phagocytosis, but the phagosome was unable to recruit Rab7 and fuse with the lysosome, suggesting that the LAMPs have a function in phagosome maturation. The same study showed impaired movement of late endosomes along the microtubule in the LAMP1/LAMP2 ablated MEF cells [70].

Another type of abundant LMPs is LIMP-1 and LIMP-2. The N-terminal and C-terminal ends of both LIMP-1 and LIMP-2 are located on the cytoplasmic side of the lysosomal membrane, and both proteins have highly glycosylated luminal domains [66].

Over-expression of LIMP-2 has been shown to cause enlarged endosomes and impaired traffic from the enlarged endosomes. This indicates a role of LIMP-2 in the biogenesis of endosomes, possibly in controlling the balance between invagination and vesicle formation in endosomes [71].

The lysosomal membrane contains more than a hundred different LMPs. Proteomic analysis has proposed many candidate LMPs, but many of these have not been confirmed. In the majority of the confirmed lysosomal resident LMPs the function is still unclear [63]. As the lysosome is the main site for catabolism in the cell, many of the uncharacterised LMPs are expected to be transporters, facilitating translocation of degradation products from the lysosomal lumen to the cytoplasm [72].

1.3.3.3 Lysosomal disorders

Deficient function of lysosomal proteins or non-lysosomal proteins associated to the endocytic pathway, often caused by mutations, might result in distortion of lysosomal function, and over 50 Lysosomal Disorders (LDs) are known [4]. The majority of these are due to malfunctioning soluble hydrolases, but many LDs caused by non-enzymatic proteins are also known, both lysosomal and non-lysosomal [73]. A common feature of LDs is the accumulation of undegraded substrate (caused by hydrolase deficiency) or of monomeric compounds inside endosomes and lysosomes (due to malfunctioning membrane transporters) [4, 73, 74]. Deficiencies leading to improper maturation of endosomes and autophagosomes have also been demonstrated [75].

Accumulation of undegraded substrates or degradation products within the lysosome can cause secondary substrate accumulation. This may occur when accumulation of the first substrate inhibits the function of proteins initially not genetically affected [76]. The accumulation of both primary and secondary substrates, not only affects the endosomal-lysosomal system, but the overall cell function [73]. Despite the fact that almost all cells contain lysosomes, storage is often restricted to tissues and cell types with high substrate turnover, as well as cell types with low proliferation rate, such as neurons. Most LDs have neurodegenerative phenotypes [73-75].

Due to a wide variety of displayed symptoms, LDs are often difficult to diagnose and classify. This applies not only to distinct LDs, but also when the disorder is caused by deficiency in the same protein. The majority of LDs are progressive, and the severity and extent depends on the amount and identity of the accumulated substrate [77].

The most common LD is Gaucher Disease [78, 79], which is caused by the deficient function of the soluble hydrolase β-glucocerebrosidase, and subsequent accumulation of its substrate glucocerebroside and other glycolipids in the lysosome, particularly in macrophages. Macrophages with this sort of deficiency are often referred to as Gaucher Cells [79, 80].

There are three types of Gaucher Disease, in which type 2 and 3 affect the nervous system and type 1 which affect the liver, spleen, and bones [78, 79]. The disease phenotype is mostly restricted to macrophages, as these cells degrade glycolipids of phagocytosed leukocytes and red blood cells [80]. Gaucher cells infiltrate various tissues, including bone marrow and liver [74]. Enlarged livers (hepatomegaly) are often observed in patients with type 1 Gaucher

Disease, and the infiltrating Gaucher cells cause inflammation, that potentially progresses to liver fibrosis [74, 81].

Another well-known LD caused by a malfunctioning soluble hydrolase is Pompe's disease, also known as glycogen storage disease II (GSD II). Pompe's is caused by deficient function of a lysosomal soluble hydrolase, α-glucosidase, which catalyses the hydrolysis of α-glucosidic bonds in glycogen [82]. Deficient function of α-glucosidase causes accumulation of lysosomal glycogen[83]. Phenotypes include respiratory problems and muscle weakness. The disease onset varies depending on enzyme activity in the affected individual. In the most severe cases, Pompe's Disease is lethal within the first year[84].

1.4 MFSD1 – Possible protein partner?

Major Facilitator Superfamily Domain containing protein 1 (MFSD1) is a member of the Major Facilitator Superfamily Domain containing (MFSD#) protein family, which consists of secondary active transporters, commonly referred to as atypical solute carriers. MFSD1 was found to be a candidate novel lysosomal membrane protein, responsive to the known lysosomal transcription factor EB (TFEB) [85]. Proteomic analysis has identified its presence in lysosomes and phagosomes [86]. Immunofluorescent assays showed colocalisation of MFSD1 and the well-established lysosomal membrane protein LAMP-2 in HeLa cells [85], and in lysosomes in differentiated osteoclasts [87]. MFSD1 has therefore been thought as a viable novel candidate lysosomal membrane transporter. However, MFSD1 was shown not to colocalise with LAMP-2 in mouse neurons, revealed by a fluorescent double-staining assay described in a more recent study [88], but was found to localize in the plasma membrane. The same study conducted a relative gene expression assay on various organs derived from WT mice, and found that *Mfsd1* expression was highest in the kidney and liver.

Indications of possible cooperation between GLMP and MFSD1 have come from a collaboration partner (Markus Damme, University of Kiel, Germany). Preliminary data suggested inhibition of GLMP expression in *Mfsd1$^{ko/ko}$* SV40 TAg transformed MEF cells (designated MEF-M in this thesis). The cells where included in the cellular uptake assays, and MFSD1 was considered a protein of interest in the transient transfection assays.

2   Aims of the study

Glycosylated Lysosomal Membrane Protein (GLMP) is a *bona fide* lysosomal protein with unknown function. To investigate the physiological function of GLMP, a mouse model lacking detectable GLMP expression has been generated (*Glmp$^{gt/gt}$* mice). The predominant phenotype in these mice is a slowly progressing liver fibrosis initiated shortly after birth. Otherwise the mice are indistinguishable from their wild type siblings regarding growth, reproduction, and behaviour.

We hypothesise that the liver damage is due to a malfunction in the endocytic system caused by GLMP ablation, and that the phenotype is a trait of a yet undescribed lysosomal disorder. To investigate which part of the endocytic pathway is affected, an *in vitro* Mouse Embryonic Fibroblast (MEF) model has been generated.

The main objective of this study is fourfold, and aims to initiate investigation of the effect of GLMP ablation at the cellular level by:

1. Developing Mouse Embryonic Fibroblast (MEF) cell lines derived from the *Glmp$^{gt/gt}$* mouse model by stable transfection with Simian Virus 40 Large T antigen.

2. Initiating characterisation of the various *in vitro* models by comparing growth rate and cellular uptake capacity between the genotypes of GLMP ablated cells, as well as in MFSD1 knock out cells.

3. Studying the impact of transiently expressed GLMP, MFSD1 and EGFR on cellular uptake in GLMP ablated cells.

4. Comparing cellular protein levels of different endocytic receptors in *Glmp$^{gt/gt}$* and *Glmp$^{wt/wt}$* MEF cells using Western immunoblotting techniques.

3 Methods

3.1 Animal experiments

The *Glmp*^{gt/gt} and *Glmp*^{wt/wt} mice were used for isolation of primary embryonic fibroblasts. To create *Glmp*^{gt/gt} and *Glmp*^{wt/wt} MEF cell lines primary embryonic fibroblasts were cultivated and transformed by stable transfection with the oncogene Large T antigen from Simian Virus 40 (SV40 TAg, section 3.2.5). The primary *Glmp*^{gt/gt} and *Glmp*^{wt/wt} cells were also used for uptake assays, described in section 3.4.1.

3.1.1 Isolation of embryonic fibroblasts

Standard procedure:

- Subject must be pregnant female, optimally at 12.5 days post coitus.

- Euthanise by cervical dislocation and place on dissecting board with abdomen facing upwards.

- Soak the fur of the abdomen area thoroughly with 70% ethanol. (It is important that the area is completely soaked).

- Make a 3mm cut across the lower abdominal region, lift up the skin and cut towards the thorax using a pair of blunt scissors.

- Using a clean pair of blunt scissors cut through the abdominal wall and release the uterine horns at the connecting point at the bottom of the Y (Be careful not to damage any of the intestines, this might cause contamination).

- Place in petri dish with 1 X sterile PBS (Appendix C, table C3.1) to remove excess blood.

(Inside sterile hood)

- Separate the embryos by cutting the uterus between the embryos and move the separated embryos to a petri dish with fresh 1 X sterile PBS.

- Release embryos from their embryonic membranes and placentas, and move to a dish with fresh 1x sterile PBS. Approximately four embryos per dish.

- Remove the red organs by gently scraping with a pair of pointed tweezers, ideally there should be no visible red tissue left. Wash away as much blood as possible.

- Cut off the head and move the remaining tissue to a petri dish with fresh 1 X sterile PBS on ice. Repeat for the remaining embryos.

- With the petri dish still on ice, remove as much of the PBS as possible.

- Mince the tissue as thoroughly as possible by using two scalpels.

- Add 1.5 mL ice-cold Trypsin EDTA per embryo and transfer to a 50 mL centrifuge tube.

- Pipette vigorously 10 times with a graded pipette.

- Incubate in a 37˚C preheated water bath for 10 min, swirl the tubes continuously.

- Add ice cold growth medium (Appendix C, table C1.1) up to 45 mL and let the suspension sediment at 1x g at RT for approximately 5 minutes or until all visible pieces of tissue sediment.

- Carefully remove supernatant. Transfer to a new 50-mL centrifuge tube. Pipette from the liquid surface to avoid the sediment swirling into the supernatant. Make sure no visible pieces of tissue are moved along with the supernatant.

- Centrifuge at 500 x g for 5 min at RT.

- Discard supernatant and resuspend pellet in 13 mL preheated (37 ˚C) growth medium.

- Transfer to T75 flask and disperse cells evenly by moving the vessel sidewise and lengthwise approximately 8 times.

- Grow in humidified cell incubator (37˚C and 5% CO_2)

3.2 Cell biological methods

The methods described in this section were used for all Mouse Embryonic Fibroblast (MEF) cell lines used in this thesis (Table 1).

Table 1. **Overview of cell lines.**

Name	Cell type	Genotype
MEF-1	Spontaneously transformed MEF (Kong, X. Y. unpublished)	$Glmp^{gt/gt}$ and $Glmp^{wt/wt}$
MEF2-P	Primary MEF	$Glmp^{gt/gt}$ and $Glmp^{wt/wt}$
MEF2-T	SV40 TAg transformed MEF	$Glmp^{gt/gt}$ and $Glmp^{wt/wt}$
MEF-M	SV40 TAg transformed MEF (Damme, M., Unpublished)	$Mfsd1^{ko/ko}$ and $Mfsd1^{wt/wt}$

Different cell culture vessels of varying sizes were applied and table 2 is an overview of volumes applied adjusted to vessel size.

Table 2 **Customised volumes for different vessel sizes.**

Vessel size: Solution	T75	T25	6-well / 35mm	12-well
PBS (1X)	10 mL	4.5 mL	1 mL	0.5 mL
Trypsin EDTA	1.5 mL	0.5 mL	0.2 mL	0.1 mL
Growth medium (after trypsination)	10 mL	4.5 mL	2 mL	1 mL
Growth medium (total in vessel)	13 mL	4.5 mL	2 mL	1 mL

Cells were stored in liquid nitrogen and thawed when required. All methods described in this section were performed in a sterile cell culture hood. All cell medium and solutions were preheated to 37 ºC using a water bath unless stated otherwise. The cells were grown in a humidified cell incubator (37˚C and 5% CO_2).

3.2.1 Thawing frozen cells

Standard procedure:

- Collect appropriate cryo vial with cells from the liquid nitrogen tank.

- Thaw cells by swirling them in a 37˚C preheated water bath. Leave a small piece of ice in the vial.

- Transfer cells to a 50-mL centrifuge tube containing 10 mL growth medium (appendix C, table C1.1).

- Centrifuge at 500 x g for 5 min at RT, discard supernatant. This step removes DMSO.

- Resuspend pellet in appropriate amount of preheated growth medium (table 2), depending on desired application and cell density (if necessary count cells, see section 3.2.3).

- Transfer to a new culture flask/ dish. Disperse cells evenly by moving the vessel sidewise and lengthwise approximately 8 times.

- Grow cells in cell incubator (37˚C and 5% CO_2).

3.2.2 Harvesting, sub-cultivation and trypsination

Standard procedure:

- Control cells under microscope to ensure proper density and morphology (growth to maximum 60- 80% confluency recommended to maintain normal growth rate).

- Remove growth media.

- Wash three times with 1X sterile PBS (appendix C, table C3.1).

- Add Trypsin-EDTA (table 2), distribute evenly over cell vessel surface.

- Incubate for 2 min in cell incubator (37˚C, 5% CO_2).

- Tap vessel gently to loosen cells.

- Add preheated growth medium (appendix C, table C1.1), and make a cell suspension by pipetting up and down approximately 8 times or until cells are evenly distributed.

- Transfer to a centrifuge tube.

- Centrifuge at 500 x g for 5 min at RT.

- Remove supernatant and resuspend pellets in appropriate volume of growth medium (table 2). (For smaller vessels, an automated pipette might be more useful. To reduce the stress inflicted on the cells, it is recommended to cut off a portion of the pipette tip when resuspending the cells).

- Transfer desired amount of cell suspension to a cell culture vessel containing fresh growth medium.

- Disperse cells evenly by moving the vessel sidewise and lengthwise approximately 8 times.

- Grow cells in cell incubator (37˚C and 5% CO_2).

3.2.3 Cell quantification

To ensure appropriate cell density for the uptake studies (section 3.4) and SV40 TAg transformation (section 3.2.5), quantification is a necessary part of the standard procedure. As a part of the characterisation of *Glmp*$^{gt/gt}$ and *Glmp*$^{wt/wt}$ MEF1, growth rate was analysed. To investigate growth rate, cells of each genotype were seeded out in equal amounts in T75 cell culture flasks, and quantified after 24 h, 48 h, 56 h and 64 h.

All cells where counted using Countess™ Automated Cell Counter (Invitrogen). For the growth analysis, quantification of cells using a Bürker counting chamber was conducted in addition.

3.2.3.1 Cell quantification using Countless™ Automated Cell Counter

In principle, this machine counts cells by analysing an image of trypan blue stained cell suspension. This is achieved by mixing a small amount of cell suspension with an equal amount of trypan blue stain 0.4% (Invitrogen). The mixture is then added to a Countless™ Cell Counting Chamber Slide (Invitrogen), with a small chamber with a fixed volume. Live cells exclude trypan blue and dead cells internalise the trypan blue. The countless then distinguishes between the two by staining patterns, and counts total cell amount, and estimates cell density in the suspension. The machine also estimates cell size and roundness if desired. Capacity 1×10^4 cells/ mL – 1×10^7 cells/ mL with highest accuracy between 1×10^5 cells/ mL – 4×10^6 cells/ mL. [89]

Standard procedure:

- Harvest cells as in section 3.2.2.

- Make sure the cell suspension is homogenous by swirling the tube.

-   Mix 20 µl cell suspension with 20 µl trypan blue.

-   Add mix to one of the sides of the disposable cell counting slide until pocket is filled up.

-   Insert the slide at the front of the machine, the screen will now display an image of the cells.

-   Zoom in and adjust the focus with the knob on the side.

-   Press start and the amount of total cells per mL, live cells per mL and viability will be displayed on the screen. The data can also be transferred to an USB stick if desired.

3.2.3.2 Cell quantification using Bürker counting chamber

The Bürker counting chamber is a sort of microscope slide, with two engraved areas with nine 1 mm^2 squares subdivided by double lines (0.5 mm apart), further divided into 16 group squares with 0.2 mm frames (figure 10). [90]

Standard procedure:

-   Harvest cells as described in section 3.2.2.

-   Fasten a cover slip on top of chamber. It might be useful to moisten the coverslip by breathing gently on it.

-   Make sure the cell suspension is homogenous by swirling the tube.

-   Add the cell suspension with a pipette under the coverslip. The coverslip should not float on the liquid and the liquid should cover the entire area.

-   Place slip on light microscope and count cells inside the three large diagonal squares A, B and C in both areas. All cells inside the small squares (A1, A2, A3, A4 and
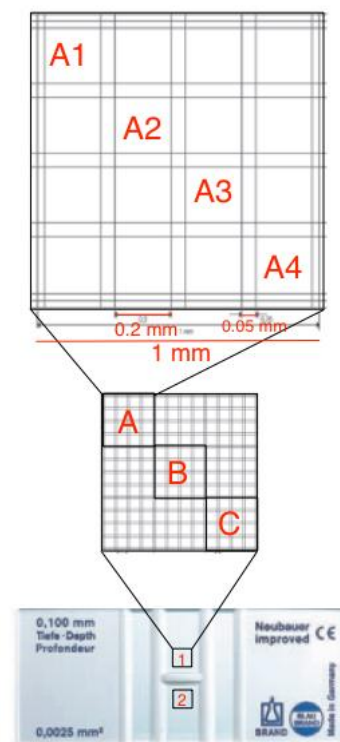
Figure 10 **Bürker counting chamber.** For quantification of cells in suspension. A cover slip is placed over the engraved area, and a small volume of cell suspension is added beneath the coverslip. Cells are counted in the diagonal squares of each engraved area (A1-A4, B1-B4, and C1-C4). Figure adapted from [90].

so on) must be counted, including cells overlapping two predetermined connecting sides (Figure 10).

- Calculate the diagonal mean and use formula 1.1 to estimate cell density in the cell suspension.

$$\text{Formula 1.1} \qquad \frac{Diagonal\ mean\ \cdot 2,1}{100} = X \cdot 10^6 \frac{cells}{mL}$$

3.2.4 Transient transfection

Transfection is the process of introducing foreign nucleic acids into eukaryotic cells. This can be done physically by electroporation and other pore-introducing methods, or chemically by complex formation with lipids or polymeric compounds that enable crossing of the cell membrane. The polyPLUS jetPRIME® transfection reagent is positively charged and forms complexes with the negatively charged nucleic acid, with a ratio resulting in an overall positively charged complex. The complex interacts with the negatively charged cell membrane and triggers cellular uptake via endocytosis, resulting in internalisation of the complex in an endocytic vesicle. Once inside the cytoplasm the nucleic acid is released from the vesicle [91].

During transient transfection, the foreign genetic material is not incorporated in the genome. The plasmid is only present a limited period, before being degraded or diluted by cell division. Hence, any gene product carried by the introduced gene will only be expressed a limited time period.

EGF uptake was shown to be impaired in $Glmp^{gt/gt}$ MEF1 cells, when compared $Glmp^{wt/wt}$ MEF1 cells (Heyward, C.A., unpublished). In order to investigate if reintroduction of ablated/down regulated proteins would rescue the uptake capacity, reintroduction of these proteins through transient transfection using various plasmid vectors was conducted. GLMP was reintroduced in $Glmp^{gt/gt}$ MEF1 cells by transient transfection, using a plasmid expressing GLMP with an N-terminal EGFP tag (Appendix D, Plasmid D2). A plasmid expressing EGFP-tagged MFSD1 was also introduced in these cells in two separate experiments, one of which the GLMP carrying plasmid was co-transfected alongside the MFSD1-plasmid , and one with the MFSD1-plasmide alone. A plasmid expressing EGFP tagged EGF-receptor (Appendix D, Plasmid D5) was also introduced to $Glmp^{gt/gt}$ MEF1 cells by transient transfection.

Due to the suspected toxic nature of GLMP when introduced in large amounts, pRFP (Appendix D, Plasmid D4) was used as a transfection control. After optimisation, the levels of GLMP in the transiently transfected cells was too low to visualise using the applied microscope. The use of pRFP caused successfully transfected cells to express RFP in the cytoplasm, hence making them easier to distinguish from non-transfected cells. To ensure proper DNA to reagent ratio, an empty plasmid vector, pSG5, was added when needed (Appendix D, Plasmid D1). The cellular uptake capacity in the transient expression assays was compared to control cells transfected with empty plasmid vector pSG5.Plasmid quantity used in the different set ups are listed in table 3.

Table 3 **Plasmid quantities used for introduction of transiently expresses proteins in uptake assays.**

Protein: Introduced:	RFP	SG5	EGFR-EGFP	GLMP-EGFP	MFSD1-EGFP
EGF-Receptor	0.5 µg	0.75 µg	0.75 µg	-	-
GLMP	0.5 µg	0.75 µg	-	0.75 µg	-
GLMP and MFSD1	0.5 µg	-	-	0.75 µg	0.75 µg
Control-transfected	0.5 µg	1.5 µg	-	-	-

All cells were transfected using jetPRIME® DNA & siRNA transfection reagent kit. All reagents and solutions are at RT.

Standard procedure:

- Seed cells to desired density in 35mm cover glass-bottomed dish (MatTek). This depends on the growth rate and optimisation might be required. (15 000 cells / dish was used for MEF1).

- Dilute 2 µg DNA into 200µl jetPRIME® buffer (table 3). Mix by vortexing.

- Add 4 µl jetPRIME® reagent and mix 10 seconds by vortexing. Spin down briefly.

- Incubate 30 min at RT (kit suggests 10 min; extended incubation time allows for formation of more complexes).

- Add 200 µl of transfection mix drop wise evenly on to cells.

- Gently rock the dish from side to side.

- Incubate at in humidified cell incubator (37˚C, 5% CO_2).

- Analyse after 24 h or later.

3.2.5 Immortalisation with SV40 large T antigen

To transform primary MEFs to a stable immortal cell line, cells harvested in section 3.1.1 where transfected with a plasmid expressing Simian Virus 40(SV40) Large T antigen (TAg) (appendix D, Plasmid D3). TAg function involves inactivating tumour suppression mechanisms, and is a well-established method for immortalisation of several mammalian cell types [92]. TAg was stably transfected into primary cells (MEF2-P) of both genotypes with a plasmid containing the TAg cDNA (Appendix D, Plasmid D3) using jetPRIME® DNA & siRNA transfection reagent kit.

Standard procedure:

- Seed primary cells (MEF2-P) into 6-well plates, 150 000 cells per well, let grow in humidified cell incubator (37˚C, 5% CO_2) O/N.

- Add 2 µg TAg-plasmid to 200µl jetPRIME® buffer. Mix by vortexing.

- Add 4 µl jetPRIME® reagent and mix 10 seconds by vortexing. Spin down briefly.

- Incubate 30 min at RT (kit suggests 10 min; extended incubation time allows for formation of more complexes).

- Add 200 µl of transfection mix drop wise evenly on to cells.

- Gently rock the dish from side to side.

- Incubate for 4 hours in cell incubator (37˚C, 5% CO_2).

- Remove medium and wash gently 2 times with preheated 1 x sterile PBS (appendix C, table C3.1).

- Add fresh, preheated growth medium (appendix C, table C1.1).

- Grow cells in humidified cell incubator (37˚C, 5% CO_2) until confluent.

- Harvest cells as in section 3.2.2, and move one vessel size up. Monitor cells, and change medium every other day until confluent. When confluent, harvest cells and move up a vessel size until the cells are able to inhabit a T75 cell culture flask.

Verification of successful transformation

Serum-supplemented medium is required for survival and growth of primary embryonic fibroblasts. SV40 TAg transformed MEF cells may survive and expand in growth medium containing little to no serum [92]. To verify successful transformation equal amounts of MEF2-P and MEF2-T cells of both genotypes were seeded out in cell culture plates using growth medium containing 10% FBS, 1% FBS and 0% FBS (figure 11) and monitored daily for a week.
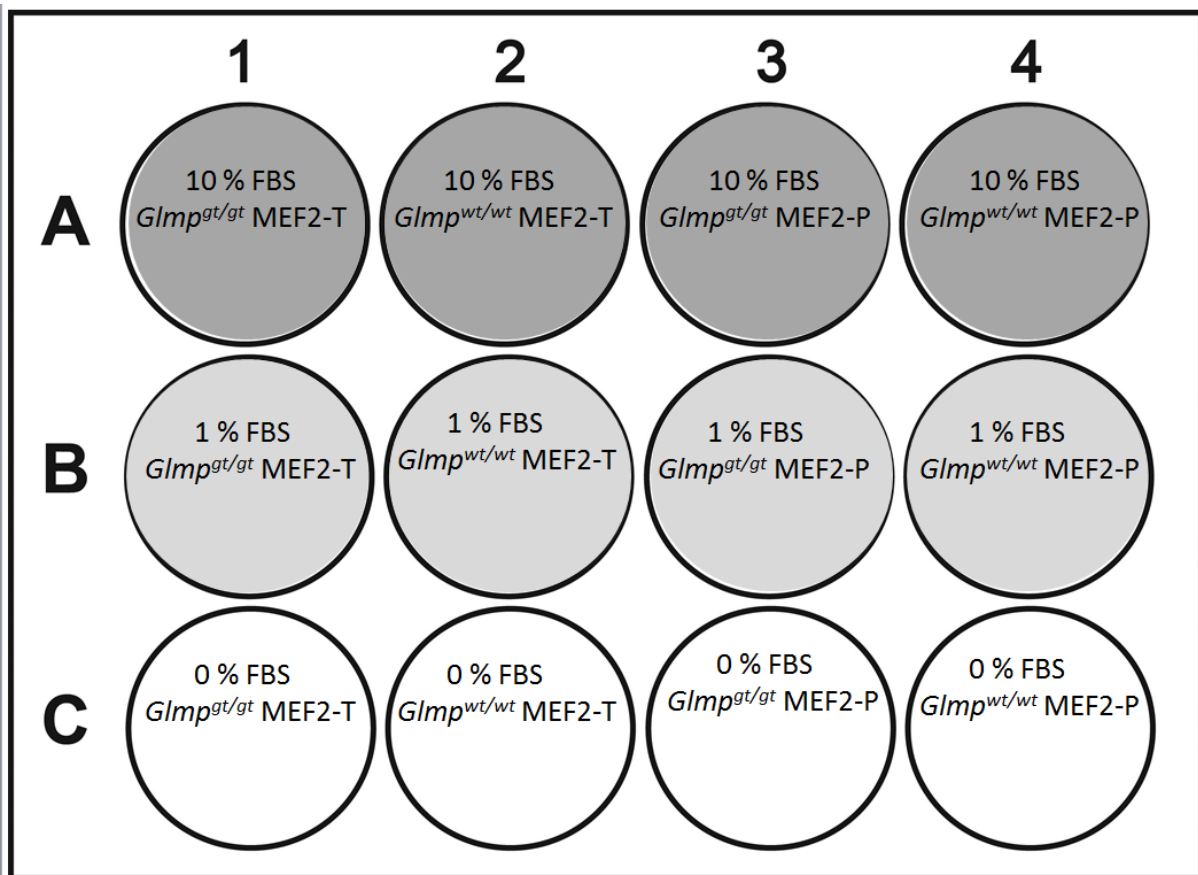
Figure 11 **Set up for transformation verification assay.** Transfected *Glmp$^{gt/gt}$* and *Glmp$^{wt/wt}$* MEF cells (MEF-T) and untransfected primary *Glmp$^{gt/gt}$* and *Glmp$^{wt/wt}$* MEF cells (MEF-P) were seeded out in equal amounts with various Fetal Bovine Serum (FBS) content in growth medium.

- Seed cells as demonstrated in figure 11 using growth medium with 10% FBS (appendix C table C2.1). Cell amount depends of well size (We used 30 000 cell per well in 6-well plates).

- Grow cells in humidified cell incubator (37˚C, 5% CO_2) O/N (this allows for the cells to adhere to the culture plate bottom and grow at optimal conditions prior to limiting their resources).

- Wash thoroughly 3 times with 1 mL 1 x PBS (Appendix C, table C3.1).

- Add growth medium with appropriate amount of FBS (figure 11) to the wells.

- Monitor cells daily for one week, medium change might be necessary to remove dead cells.

- The cells growing in fully supplemented medium (10% FBS) are expected to grow at optimal rate for both transformed and un-transformed cells. Successful transformation may be verified if transformed cells survive in limited medium when the primary cells do not.

3.2.6 Cryopreservation

- For optimal preservation, cells at 60% confluence are recommended.

- Freeze stable medium is required (appendix C, C1.2).

- Harvest cells according to 3.2.2. In the last step resuspend cells in freeze medium. Amount depends on what cell density is desired per cryo vial.

- Distribute a volume of 1.5 mL per cryo vial.

- Place cryo vial O/N in a -80 ˚ C freezer, inside a box containing paper (to ensure a slower freezing process) before transferring the vial to liquid nitrogen tank for storage.

3.3 Biochemical methods

To compare the Epidermal Growth Factor-receptor (EGFR) and Transferrin-receptor (TfR) content in the two genotypes, proteins were harvested from spontaneously transformed *Glmp*$^{gt/gt}$ and *Glmp*$^{wt/wt}$ *MEF* cells (MEF1), SV40 TAg transformed *Glmp*$^{gt/gt}$ and *Glmp*$^{wt/wt}$ MEF cells (MEF2-T), and primary *Glmp*$^{gt/gt}$ and *Glmp*$^{wt/wt}$ MEF cells (MEF2-P). The protein extract was then separated by SDS-PAGE gel electrophoresis, transferred to a membrane through western blot, and visualised. Signal strengths were then compared between the genotypes to provide insight into potential differences between the genotypes in the different cell lines. A household protein, β-Actin, was used as loading control. After visualisation of EGFR and TfR bands, the membranes were stripped and β-Actin bands were visualised.

3.3.1 Harvesting protein

Standard procedure:

- Wash cells thoroughly four times with 1x sterile PBS at RT.

- Add 1 mL RIPA lysing buffer (Appendix C, table C3.3) with protease inhibitor. The inhibitor should be added upon appliance and not to stock solution.

- Incubate for 30 min at 4°C.

- Harvest cells using a cell scraper.

- Transfer to centrifuge tube.

- Pass cell suspension forcefully five times through a 22G syringe.

- Centrifuge at 10 000 x g for 10 min at 4ºC.

- Transfer supernatant to sterile Eppendorf tubes.

- Store at -80 ºC.

3.3.2 Protein quantification

Protein concentrations were determined by Bradford protein assay. The protein solution is mixed with coomassie Brilliant Blue G250 dye (Biorad) and quantification is based on absorption variations between the blue and red form of the dye, where the blue form is stabilised when in complex with protein and the red form is predominant in free form. A standard curve with known protein concentrations must be obtained and concentrations are determined by linear regression.

Tecan Sunrise™ plate reader was used to measure absorbance.

Standard procedure:

- Make a dilution series for the standard curve from a bovine serum albumin solution with known concentration (for instance: 0.0, 0.05, 0.1, 0.2, 0.3, 0.4 and 0.5 µg/µL).

- Dilute coomassie Brilliant Blue G250 dye (Biorad) 1:5 with milliQ-H_2O and filtrate.

- Transfer 10µL of standard solutions and extract to a 96-well plate in triplicates.

- Add 200µL diluted and filtered dye to each well.

- Incubate at RT for 5 min.

- Measure Abs_{595nm}.

- Make a standard curve from the standard solutions and calculate concentrations by linear regression.

3.3.3 SDS-PAGE

Sodium Dodecyl-Sulphate Polyacrylamide Gel Electrophoresis (SDS-PAGE) is a method commonly used to separate proteins in solution according to size. In gel electrophoresis proteins would migrate in the electrical field according to their net charge, shape, and size. In SDS-PAGE the charge and shape factor is excluded by introducing SDS and the proteins are separated solely by size.

SDS is a negatively charged anionic detergent that forms complexes by hydrophobic interactions between the SDS hydrophobic tail and the hydrophobic areas that are exposed on

denatured proteins. The SDS / amino acid residue ratio is approximately 1 SDS molecule per 2 amino acid residues and since each SDS molecule carries a negative charge the complex formation also causes the proteins to linearize due to repelling forces between SDS head groups. This will result in an overall negative charge. All proteins will migrate towards the anode and the only factor influencing migration speed is protein size and the pore size in the gel.

The SDS-PAGE procedure is equal for all detection methods, but note the reduced volume of MW-weight standard used for fluorescence detection.

Standard procedure:

Mix in Eppendorf tube on ice:

- 5µl NuPAGE ® LDS Sample buffer (Novex)

- 2 µl NuPAGE ® Reducing agent (Novex)

- x µl protein extract (20 µg protein)

- milliQ H2O to 20 µl total volume

- Spin down briefly.

- Pierce a hole in the lid using a syringe.

- Denature proteins on heat block at 80º C for 10 min.

- Spin down briefly.

- Set up electrophoresis equipment, remember to remove the white sticker at the bottom of the gel sandwich, and remove the comb carefully prior to mounting it.

- Fill the chamber with NuPAGE® 1x MOPS SDS running buffer (Novex) and carefully wash each well with MOPS running buffer.

- Apply samples and 5 µl molecular weight standard (1µL for fluorescence detection).

- Run at 175 V for approximately 1 h 15 min.

3.3.4 Western immunoblotting

Western blot is a commonly used technique to detect proteins of interest in complex protein samples separated by gel electrophoresis. Proteins are transferred from a gel to a membrane and detected directly or indirectly with a signal/reporter labelled antibody. Two different visualisation methods were used depending on antibodies availability. The methods vary substantially and are described separately in the membrane handling section. Note that specialised PVDF membrane is required when using fluorescently labelled antibodies.

Standard procedure:

- Moisten Whatman paper and sponges in cold blotting buffer (appendix C, table C3.4).

- Release the SDS-PAGE gel and place in cold blotting buffer for 10 min.

- Moisten the membrane in methanol for 1 min before transferring it to cold transfer buffer on a rocking plate.

- Place a stir magnet into the electrophoresis chamber, and fill with transfer buffer.

- Place the cassette with the white part (anode-side) down in a tub filled with cold transfer buffer.

- Pack the cassette according to figure 12.
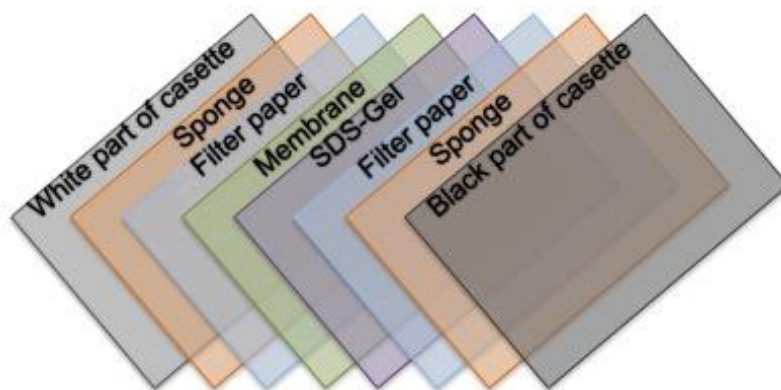
Figure 12 **Cassette packing order for Western blotting.**

- Roll over the package to remove any air bubbles; presence of air bubbles will affect transfer.

- Place cassette into electrophoresis chamber. Make sure the white side faces the anode.

- Insert cooling element.

- Run O/N at 4ºC and 20 V with stirring.

3.3.5 Membrane treatment and immunodetection

After transferring the proteins to the membrane, it is necessary to saturate the membrane with non-relevant proteins to inhibit unspecific antibody binding. This is called blocking and is achieved by incubating the membrane in blocking buffer. The blocking buffer contains fat-free milk rich in proteins that will bind available binding sites on the membrane, hence inhibiting unspecific binding of antibodies. For fluorescent visualisation, the membrane is dried and rehydrated instead of blocked in buffer. After blocking the membrane is incubated with a primary antibody that binds the protein of interest and finally the membrane is incubated with a secondary antibody with a signal tag for visualisation.

Horseradish peroxidase (HRP) conjugated secondary antibodies were used for detection of EGFR and loading control β-Actin. HRP is an enzyme reporter that catalyses oxidation of luminol, emitting light through the process of chemiluminescence. Lifescience™ Amersham™ ECL™ Prime Western Blotting Detection Reagent was used as HRP substrate for Enhanced Chemiluminescence (ECL) detection. [93]

A fluorophore conjugated secondary antibody was used for detection of TfR. The fluorophore is capable of absorbing photons at specific wavelengths by transferring an electron to a higher energetic state. When the electron returns to its ground state, a lower energy photon is emitted. The emitted light is of a different wavelength than the absorbed light, making it possible to detect emitted light without detecting light at the excitation wavelength. [94]

After visualisation of EGFR and TfR bands, the membrane was stripped using Restore™ PLUS Western Blot Stripping Buffer (Thermo Scientific). ECL visualised β-actin was used as loading control

Image Station 4000R Pro (Kodak) was used for imaging of ECL visualisation and Odyssey CLx (LI-COR) was used for fluorescent detection and imaging. Antibodies and concentrations are listed in table 4.

Table 4 **Antibodies used for detection of EGFR and TfR.**

Antibody:	Concentration	Detection method
Anti-EGFR polyclonal Ab (sheep. ES04, Fitzgerald)	1:1000	-
Anti-TfR Monoclonal Ab (Mouse H68.4, Thermo Fischer)	1:1000	-
Anti β-actin(C4) Monoclonal Ab (Mouse, SC-47778 Santa Cruise Biotechnology, inc.)	1:2000	-
Peroxidase Anti-Mouse Polyclonal Ab (Donkey, code: 715035150, Jackson ImmunoResearch Laboratories, inc.	1:10 000	ECL
Peroxidase Anti-Goat Polyclonal (donkey, SC-2020, Santa Cruise Biotechnology, inc.	1:10 000	ECL
IRDye® 800CW Polyclonal anti-Mouse (Goat, Prod# 925-32210, LI-COR)	1:10 000	Fluorescence

Standard procedure ECL visualisation:

- Open cassette and carefully cut the membrane in one corner (this is to remember orientation).

- Transfer membrane to a 50-mL tube containing blocking buffer (Appendix C, table C3.4) with protein side facing inwards.

- Incubate on roller platform for 1h at RT.

- Exchange blocking buffer with blocking buffer containing primary antibody (table 4).

- Incubate on roller platform at 4 ºC O/N. (for β-Actin detection 1h at RT is sufficient).

- Remove primary antibody.

- Rinse with 10 mL TBS + 0.1% tween (Appendix C, table C3.1).

- Wash three times with TBS + 0.1% tween on roller incubator 10 min RT.

- Add blocking buffer with secondary antibody (table 4).

- Incubate on roller incubator at RT for 1 h.

- Wash three times with 10 mL 1x TBS + tween 10 min on roller incubator.

- Use Lifescience™ Amersham™ ECL™ Prime Western Blotting Detection Reagent for visualisation. Mix equal amounts of solution A and B in an Eppendorf tube packed in foil to protect from light.

- Let the reaction mix reach RT.

- Add mix dropwise on to the protein side of the membrane and incubate for 1 min at RT before imaging.

Standard procedure fluorescent visualisation:

- Open cassette and carefully cut the membrane in one corner (this is to remember orientation).

- Place membrane with protein side facing upwards on a clean glass plate until completely dry (approximately 30 min).

- Rehydrate membrane in TBS + 0.1% tween (Appendix C, table C3.1) for 30 min on rocking plate at RT.

- Place membrane with protein side facing inwards in a 50-mL tube and add 3 mL blocking buffer (Appendix C, table C3.4) containing primary antibody (table 4).

- Incubate on roller platform at 4 ºC O/N.

- Remove primary antibody.

- Rinse with 10 mL TBS + 0.1% tween (Appendix C, table C3.1).

- Wash three times with PBS + 0.1% tween on roller platform 10 min RT.

- Add blocking buffer with secondary antibody (table 4).

- Incubate on roller incubator at RT for 1 h.

- Wash three times with 10 mL 1x TBS + tween 10 min on roller platform.

- Wash two times with 1x TBS 10 min on roller platform.

- Visualise according to excitation wavelength of secondary antibody. The PageRuler™ prestained protein ladder (BioRad) is visible in the 700nm channel.

Standard procedure for stripping membranes:

- Place membrane with protein side facing inwards in a 50-mL centrifuge tube.

- Add 10 mL Restore™ PLUS Western Blot Stripping Buffer (Thermo scientific).

- Incubate on rolling plate 15 min at RT.

- Remove stripping buffer.

- Wash 3 times with 1 x TBS + Tween.

- The membrane is now ready for blocking.

3.3.6 Analysing Western Blot results

ImageJ 1.51j was used to compare signal density of complementary bands for ECL detection. The software has a built-in function for western analysis that plots the signal density on a curve with width on the x-axis and signal density on the y-axis. The area beneath the curve is then determined and when analysing several peaks, results are displayed as percentage of total area for each peak. The results are therefore relative to the other bands analysed at the same time [95]. In this assay, the complementary genotypes were analysed together, to reveal any potential difference in expression.

Image Studio™ (LI-COR) was used to determine signal intensity in the fluorescence detection.

The signal density of the loading control, β-Actin, was used to adjust the differences in loading.

3.4 Confocal laser scanning microscopy

Fluorescent imaging allows for localization and quantification of fluorescently labelled molecules within living cells, and this section describes the methods applied to reveal potential differences in uptake capacity of selected fluorophore tagged ligands comparing Glycosylated Lysosomal Membrane Protein (GLMP) ablated and Major Facilitator Superfamily Domain-containing protein 1 (MFSD1) ablated cells to their WT counterparts. The methods were also applied to investigate if introduction of additional transiently expressed Epidermal Growth Factor-receptors (EGFR) and reintroduction of transiently expressed GLMP/MFSD1 could alter the uptake. The methods are only semi-quantitative, but serve the intended purpose of revealing significant differences, and narrowing the area of interest for further investigation in future studies.

When a photon of proper wavelength hits a fluorophore, it is absorbed, and an electron is transferred to a higher energy orbit. This exited state is unstable, and upon returning to ground state, a photon is released. Some of the energy obtained from the initial excitation is lost to the surroundings, and consequently, the emitted photon is of lower energy and longer wavelength than the absorbed one [96]. This makes it possible to detect emitted light from sites where a fluorophore is present, while excluding irrelevant wavelengths. The amount of emitted light is also directly correlated to the number of fluorophores, and hence, correlates to the amount of substrate internalised by the cell.

In confocal microscopy, fluorophores are excited by a laser of proper wavelength, often scanning the sample. A pinhole placed in position with the focal plane of the microscope allows for exclusion of any light not emitted from this position. This yields sharper images with less background haze than images obtained using conventional wide field microscopes, where the entire sample is illuminated and most emitted light is detected (fig 13). The depth of field in confocal microscopes is narrow, allowing for capturing of thin optical sections that might be stacked together to form sharper three-dimensional reconstructions[97, 98]. In the method applied here, only the widest section of the cells were analysed and used as a representative for the ligand content in the whole cell.
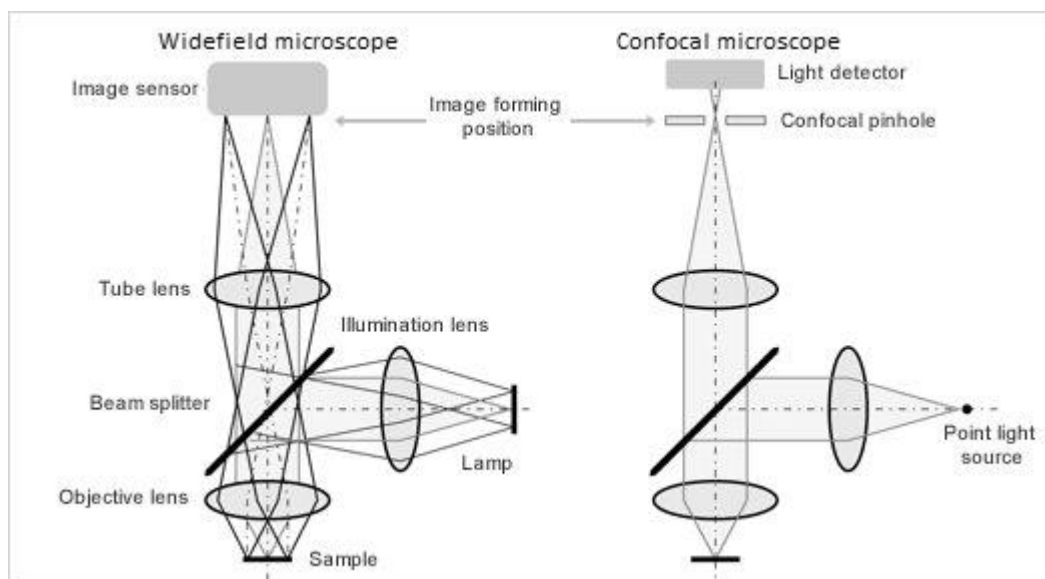
Figure 13. **Light path in wide field and confocal microscopes.** In the confocal microscope, the sample is illuminated by a point light source which is focused on a single point. Scattered light not emitted from the focal plane (not shown) is excluded by a pinhole that conjugates the focal position of the objective lens. In wide field microscopes, the whole sample is illuminated. Figure adapted from [98].

All imaging was conducted on Olympus IX81 inverted confocal microscope with a cell incubator (37 ºC) and a PLAPO 60x/1.10 NA oil immersion objective.

3.4.1 Ligand uptake assay

Live cells were used for uptake studies to compare endocytic activity between the genotypes and after introduction of various proteins through transient transfection (Overview in table 6). The cells were cultivated in 35 mm cover glass-bottomed dishes (MatTek). In the transient expression assays cells were transfected as described in section 3.2.4 prior to imaging. Fluorescently labelled ligands (table 5) where added to the live cells, and images of the cells where captured after an incubation period. The images were analysed, and the intra-cellular signal strength was determined.

Table 5: **Overview of the applied Fluorophore complexes applied in the uptake assays**

Complexes applied in uptake assays
Epidermal Growth Factor, Biotinylated, complexed to Alexa Fluor™ 647(EGF-Alexa647), Thermo Fischer Scientific, Catalog # E35351
Transferrin from Human Serum, Alexa Fluor™ 488 Conjugate (Tf-Alexa647), Thermo Fisher Scientific, Catalog # T13342
Dextran, Alexa Fluor™ 546; 10,000 MW, (Dextran-Alexa546), Thermo Fischer Scientific, Catalog # D22911

Table 6: **Overview of performed cellular uptake assays.**

Celltype:	Preformed uptake assays:
MEF1 GLMP$^{gt/gt}$ vs MEF1 GLMP$^{wt/wt}$	EGF-Alexa647*, Tf-Alexa647, Dextran-Alexa546
MEF1 GLMP$^{gt/gt}$ + GLMP-EGFP vs control	EGF-Alexa647
MEF1 GLMP$^{gt/gt}$ + MFSD1-GFP vs control	EGF-Alexa647
MEF1 GLMP$^{gt/gt}$ + GLMP-EGFP and MFSD1-GFP vs control	EGF-Alexa647
MEF1 GLMP$^{gt/gt}$ + MFSD1-GFP vs control	EGF-Alexa647
MEF1 GLMP$^{gt/gt}$ + EGFR-EGFP	EGF-Alexa647
MEF-M MFSD1^{ko} vs MFSD1^{wt}	EGF-Alexa647
MEF-P GLMP$^{gt/gt}$ vs GLMP$^{wt/wt}$	EGF-Alexa647, Tf-Alexa647

*Performed by Catherine Heyward.

3.4.1.1 Standard procedure for EGF-Alexa647 and Tf-Alexa647 uptake assays:

- Seed cells on 35 mm cover glass-bottomed dish (MatTek) according to growth rate in 2 mL preheated growth medium (appendix C, table C1.1). There should be a sufficient number of cells for analysis, but the cells should not be confluent. ($1.5 \cdot 10^4$ cells for MEF1/MEF2-T, $2.0 \cdot 10^4$ cells for MEF-M, and $3.0 \cdot 10^4$ cells for MEF2-P).

- Grow O/N in humidified cell incubator (37˚C, 5% CO_2).

- Wash cells three times with 1 mL preheated 1x sterile PBS.

- Add 2 mL microscope medium (appendix C, table C1.3).

- Add a drop of immersion oil to objective.

- Place the cover glass bottom part of the dish on the plate above the objective and carefully raise the objective using the knob on the side until the oil comes in contact with the cover glass.

- Focus in z-plane until cells are in focus.

- Add ligand solution (Final concentration in dish 25 µg/mL, preferably added in a total volume of 100 µL for optimal distribution).

- Capture image every 15 seconds for 30 min (important that all microscope parameters are equal between the two compared samples.)

-   Capture additional images of other out of frame cells within 10 min of the time-laps imaging.

3.4.1.2 Standard procedure for Dextran-Alexa546 and Tf-Alexa647 in primary cells

Note: due to high background a different approach was necessary when monitoring dextran uptake in MEF1 and Tf uptake in primary cells. This method allows for uptake analysis with reduced background since non-internalised ligands are removed prior to imaging.

-   Seed cells according to growth rate (see section 3.4.1.1).

-   Grow O/N in humidified cell incubator (37˚C, 5% CO_2).

-   Wash cells three times with 1 mL preheated 1x sterile PBS.

-   Add 150µL ligand solution to the cover glass portion of the dish. Incubate 1h for dextran and 30 min for Tf.

-   Remove ligand solution.

-   Wash cells three times with 1 mL preheated 1x sterile PBS.

-   Add 2 mL preheated (37 ºC) microscope medium.

-   Incubate 1 h for dextran experiments or 30 min for Tf experiments.

-   Add a drop of immersion oil to objective.

-   Place the cover glass bottom part of the dish on the plate above the objective and carefully raise the objective using the knob on the side until the oil comes in contact with the cover glass.

-   Focus in z-plane until cells are in focus.

-   Capture images. It is important that the same parameters are used for complementing samples.

3.4.2 Image analysis

The captured images were analysed using ImageJ software version 1.51j. The intracellular mean grey values were determined and compared between the compliment samples in order to detect any significant differences. The mean grey value reflects the amount of light emitted at a particular wavelength within the region of interest (ROI), and hence reflects the amount of fluorescently labelled ligand within that area. This does not allow for any specific quantification of internalised ligand, but is useful to determine if there is any significant difference between the two samples.

Standard procedure:

- Open image with separated channels.

- Using the polygon area selection tool to select a single cell as a ROI as close to the cell as possible.

- In the channel representing ligand emission, measure the mean grey value within the ROI using the Ctrl +M command. It can be useful to include the min and max grey values to detect saturation of signal or other errors in the image. The results will be displayed in a separate results window.

- Select an area in the image that does not contain any cells, cell debris or other particles, and measure the mean grey value (background).

- Ligand signal = (intracellular mean grey value) – (background mean grey value).

3.5 Molecular biological methods

Competent *E. coli* cells were prepared in order to produce plasmids for transfection experiments. Commercial DH5α ™ Competent cells (Invitrogen) were also used.

3.5.1 Competent cell preparation

Standard procedure:

Aseptic environment required

- Select a few colonies of DH5α cells from a LB-plate and suspend in 100 mL LB-medium (appendix C, table C2.1).

- Incubate 3 h at 37º C in shaking incubator (this is the pre-culture).

- Measure OD_{600} and calculate amount from the pre-culture required to obtain $OD_{600}=0.05$ in 250 mL LB medium.

- Transfer to a 2 L flask and incubate at 18ºC O/N (16-18 h).

- Measure cell density (should be $OD_{600}=0.3-0.6$).

- Cool cells on ice and transfer to sterile centrifuge tubes.

- Centrifuge at 2500 x g for 10 min at 4ºC.

- Carefully discard supernatant.

- Resuspend pellet in 80 mL TB total (e.g. 40 mL / tube if 2 tubes are used).

- Incubate 10 min on ice.

- Centrifuge at 2500 x g for 10 min at 4 °C.

- Carefully discard supernatant and resuspend in 20 mL TB total.

- Add 350 µl sterile DMSO per tube mix gently and leave on ice for 5 min.

- Add additional 350 µl sterile DMSO per tube leave on ice 10 min.

- Transfer cells in 200 µl portions to ice cold PCR tubes (0.5mL) and shock freeze in liquid nitrogen.

- Store at -80 ℃.

Control:

Negative control:

Grow cells on LB agar plate with added antibiotics (appendix C table C2.1). The cells should not grow. Growth indicates contamination.

Positive control and transformation efficiency test

- Transform cells with 1 ng, 10 pg and 0.1 pg plasmid containing antibiotic resistance gene (section 3.5.2).

- Spread out cells out on LB agar plates (appendix C, Table C2.1) containing set antibiotic.

- Let grow O/N at 37 ℃.

- Count colonies and calculate number of cells transformed with 1 µg plasmid, should be 10^6-10^9 cells/µg.

3.5.2 Transformation of competent E. coli

Competent E. coli cells (DH5α) were used for plasmid production.

Standard procedure:

- Add 20 ng plasmid DNA in a total volume of 5µL to a sterile Eppendorf tube (1.5mL) on ice.

- Add 50 µL newly thawed competent DH5α per tube.

- Knock the tube gently and place back on ice.

- Incubate 30 min on ice.

- Heat shock for 30 sec at 42°C in a water bath.

- Place back on ice, incubate 2 min.

- Add 450 µL preheated S.O.C. medium (Appendix C, Table C2.2)

- Incubate in water bath at 37°C for 1 h, swirl the tubes occasionally.

- Add to 5 mL LB medium with appropriate antibiotic. Make sure the lid is not completely closed to allow air to enter the tube.

- Incubate O/N at 37°C on shaking incubator.

3.5.3 Isolation of plasmids

Plasmids were isolated using NucleoSpin® plasmid kit (Macherey-Nagel).

Standard procedure:

- Centrifuge the liquid cell culture for 30 sec at 11 000 x g at RT (in an 1.5 mL Eppendorf tube).

- Remove as much liquid as possible.

- Add 250 µL buffer A1, resuspend pellet by pipetting up and down (vortex if desired).

- Add 250 µL Buffer A2, mix gently by inverting the tube (do not vortex).

- Incubate at RT for 5 min.

- Add 300 µL buffer A3, mix gently by inverting tube until all blue colour disappears (do not vortex).

- Centrifuge for 5 min at 11 000 x g at RT (repeat if supernatant is not clear).

- Place NucleoSpin® Plasmid column in a collection tube.

- Transfer supernatant (max 750 µL) to column.

- Centrifuge for 1 min at 11 000 x g at RT.

- Discard flow through.

- Add 600 µL buffer A4 centrifuge for 1 min at 11 000 x g at RT.

- Discard flow through.

- Centrifuge for 2 min at 11 000 x g at RT.

- Move the NucleoSpin® Plasmid Column to a sterile Eppendorf tube.

- Add 40 µL buffer AE to the column, incubate 1 min at RT.

- Centrifuge for 1 min at 11 000 x g at RT.

- Discard column.

3.5.4 Quantification of plasmids

Plasmids isolated in 3.5.3 were quantified using Nanodrop 2000 spectrophotometer (Thermo scientific).

<u>Standard procedure:</u>

- Place a 2µl milliQ-H_2O or AE buffer on instrument.

- Close lid and measure blank.

- Wipe gently with filter paper.

- Place a 2µl sample solution on instrument.

- Close lid and analyse.

3.6 Statistical analysis

Statistical analysis was conducted using GraphPad Prism 7.02.

Data are presented as mean and s.e.m. and tested using unpaired two-tailed t-test. D'Agostino-Pearson omnibus normality test was used to test for normality, and data was log-transformed using equation:

$y = \log(y+1)$

$p^* < 0.05$ was considered statistically significant. The graphs represent three independent replicates.

4 Results

4.1 A new immortalised cell line

Primary embryonic fibroblasts from $Glmp^{gt/gt}$ and $Glmp^{wt/wt}$ mice were harvested and cultivated as described in section 3.1. The cells were successfully cultivated and two MEF cell line pairs (MEF2-T and MEF3-T) were generated by stable transfection with Simian Virus 40 (SV40) oncogene Large T antigen (TAg). Successful transformation of the $Glmp^{gt/gt}$ MEF2-T and $Glmp^{wt/wt}$ MEF2-T cell lines was confirmed by a growth assay where the MEF2-T cells were grown in growth medium with varying Fetal Bovine Serum (FBS) content in parallel with un-transformed primary cells (MEF2-P) derived from the same mouse model as negative control. In contrast to non-transformed MEF cells, TAg transformed cells are able to grow in medium with limited FBS content. TAg enables the cells to bypass growth restrictions and senescence by binding and inhibiting the tumour suppressors [92].

The behaviour of the genotypes of each cell type did not vary noticeably, and are therefore described in unison for this assay. MEF2-T collectively meaning both $Glmp^{gt/gt}$ and $Glmp^{wt/wt}$ transformed MEF cells, and MEF2-P both genotypes of primary cells.

After 48 h, both the MEF2-T cells and the MEF2-P in the 10% FBS containing medium were fully confluent. The MEF2-T and MEF2-P cells in the 1% and 0% FBS containing medium did not appear to have expanded since day one. All cells were harvested (section 3.2.2) and transferred to T25 cell culture flasks. The MEF2-T cells in the 10% FBS medium were diluted 1:2 upon transfer due to high growth rate.

After 72 h, there was visibly fewer cells in the 0% FBS for all set ups, when compared to the 1% and 10% FBS wells of the same cells. The MEF2-T cells were overall more confluent than the MEF-P.

After 96 h, MEF2-P cells were extinct in the 0% FBS flask and only a few cells were observed in the 1% FBS flasks. The MEF2-P cells were notably more confluent in the 10% FBS compared to the previous day, but not as confluent as the MEF2-T cells. The 1% FBS flasks of MEF2-T were less confluent than the 10% FBS flask, but the cells were healthy looking and noticeably more confluent than the day before. Only a few cells remained in 0%

FBS in the MEF2-T flasks, but these cells looked healthier compared to the MEF2-P cells in the 1% flasks, which appeared more flattened.

After 144 h, all MEF2-P cells were extinct, except a few cells in the 10% FBS, these cells appeared flat and unhealthy. The MEF2-T cells in 10% FBS were 100% confluent, and approximately 60% confluent in the 1% FBS. No cells were found in the 0% FBS MEF2-T flasks.

The MEF2-T cells did not grow optimally in 1% FBS medium, but survived and grew slowly. In contrast, the primary cells did not survive at all. In addition, MEF2-T cells were successfully subcultivated up until generation 17, and could possibly be subcultivated further, which was not investigated. The primary cells ceased to divide and died after 6-8 passages. These findings confirm successful transformation.

4.2 Comparison of genotype specific cellular uptake capacity

As a part of the characterisation of the different cell lines and the primary cells (MEF2-P), the cellular uptake capacity was compared between $Glmp^{wt/wt}$ and $Glmp^{gt/gt}$ MEF cells (MEF1 and MEF2-T), WT and MFSD1 Knock Out (KO) cells (MEF-M), and $Glmp^{gt/gt}$ MEF1 cells with transiently expressed proteins of interest and control cells transfected with an empty plasmid vector (pSG5, Appendix D, D1). The different cell types used in the uptake assays are listed in table 7.

Table 7 : **Overview of the various cell types used in the cellular uptake assays.**

Name	Cell type	Genotype
MEF-1	Spontaneously transformed MEF	$Glmp^{gt/gt}$ and $Glmp^{wt/wt}$
MEF2-P	Primary MEF	$Glmp^{gt/gt}$ and $Glmp^{wt/wt}$
MEF2-T	SV40 TAg transformed MEF	$Glmp^{gt/gt}$ and $Glmp^{wt/wt}$
MEF-M	SV40 TAg transformed MEF	$Mfsd1^{ko/ko}$ and $Mfsd1^{wt/wt}$

To reveal potential differences in cellular uptake capacity, ligand uptake assays were conducted as described in section 3.4.1. The assays do not determine total ligand concentration within the cells, but compare relative uptake between the two genotypes or compared to the control cells in the case of transient expression of proteins of interest. Any

significant difference would indicate impaired uptake capacity, and possible candidates for further investigations.

Alexa flour-647 Epidermal Growth Factor conjugate (EGF-Alexa647) and Alexa flour-647 transferrin conjugate (Tf-Alexa647) were used to compare cellular uptake through recycling and degradative receptor mediated endocytosis. Alexa Fluor-546 dextran conjugate (Dextran-Alexa546) was used to compare cellular uptake through nonspecific fluid-phase endocytosis. As noted in section 3.4.1, two different experimental set ups were used, depending on background signal and cell activity. The assays described in this section were all carried out in triplicates.

4.2.1 Cellular uptake in spontaneously transformed MEF cells from *Glmp*$^{wt/wt}$ and *Glmp*$^{gt/gt}$ mice (MEF1)

Immortalised MEF cells (MEF1) were created by spontaneous transformation using primary MEF from the *Glmp*$^{gt/gt}$ and *Glmp*$^{wt/wt}$ mice by former colleague Xiang Y. Kong (Unpublished). Both receptor mediated endocytosis and nonspecific fluid-phase endocytosis uptake capacity were compared in these cells.

The MEF1 cells did not have any significant difference in uptake capacity of Tf-Alexa647, investigated using the method described in section 3.4.1.1 (figure 14).
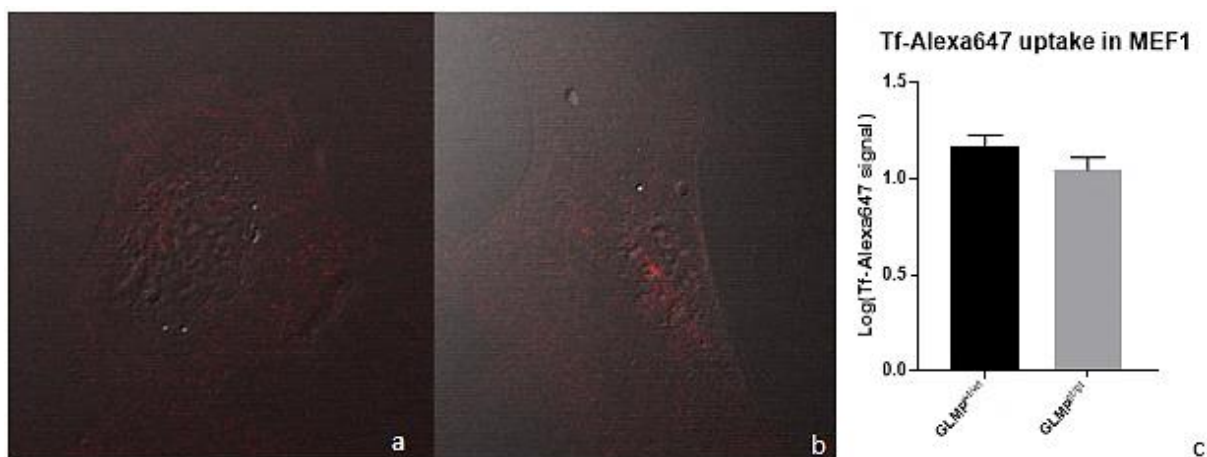
Figure 14: **Tf-Alexa647 uptake in MEF1.** Confocal image of the Tf-Alexa647 channel (Red) merged with transmission image of (a) *Glmp*$^{wt/wt}$ MEF1 cell and (b) *Glmp*$^{gt/gt}$ MEF1 cell. (c) Semi-quantitative measurements of internalised Tf-Alexa647. The signal is expressed as the mean of logarithm of the replicate means ± s.e.m. The cellular uptake capacity was found not to differ between the genotypes of the MEF1 cells (n=118 total cells analysed. p value 0.25 vs WT)

The Dextran-Alexa546 uptake assay did not reveal any significant difference either (Figure 15). This was investigated using the method described in section 3.4.1.2, due to high background.
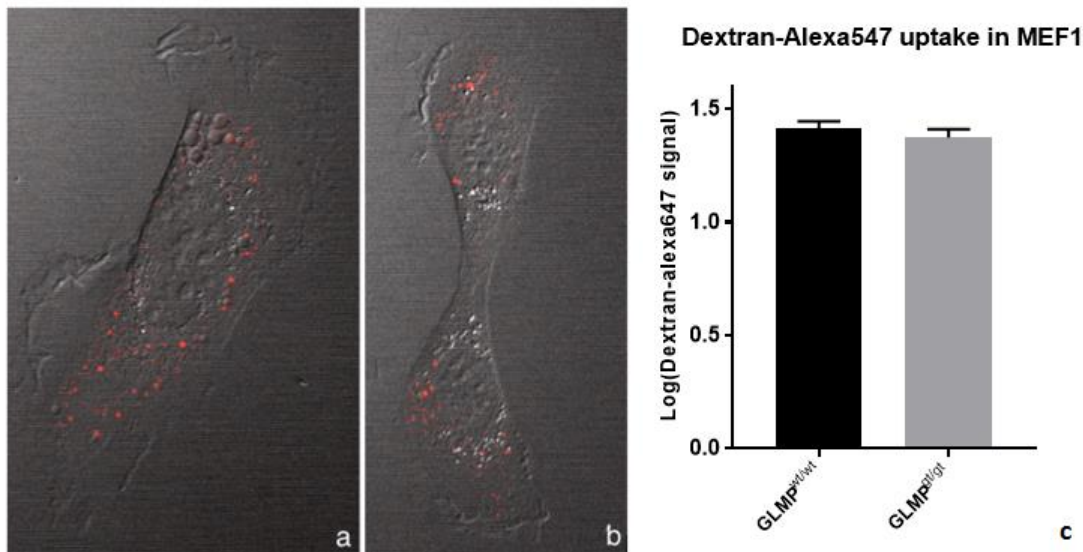
Figure 15: **Dextran-Alexa546 uptake in MEF1.** Confocal images of the Dextran-Alexa546 (Red) channel merged with transmission images of (a) $Glmp^{wt/wt}$ MEF1 cell and (b) $Glmp^{gt/gt}$ MEF1 cell. (C) Semi-quantitative determination of Dextran-Alexa546. The signal is expressed as the mean of logarithm of the replicate means ± s.e.m (n=164 total cells analysed. p value 0.46 vs WT).

Catherine A. Hayward, from the NorMIC Imaging Platform at the Department of Biosciences, compared the uptake capacity of EGF-Alexa647 between the MEF1 genotypes by monitoring and imaging the MEF1 cells over a longer time period, a method not described in this thesis. The $Glmp^{gt/gt}$ cells' uptake capacity of EGF-Alexa647 was significantly lower at all analysed time points (figure 16).
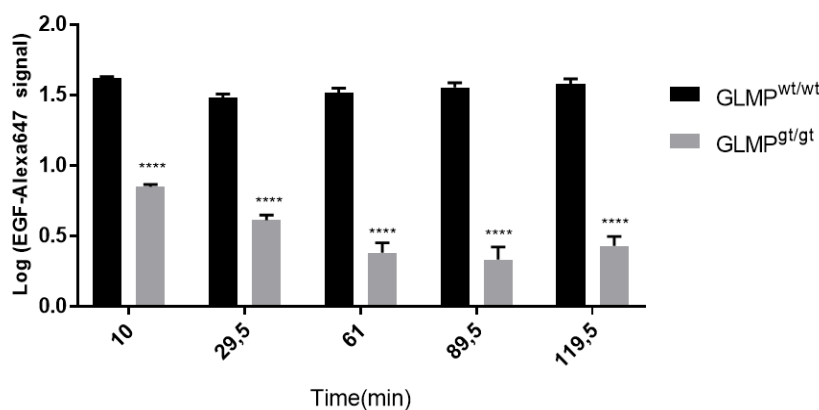
Figure 16: **Time dependent comparison of EGF uptake in MEF1 cells.** EGF-Alexa647 signal inside cells at different time points after ligand addition displayed as the logarithm of mean signal ± s.e.m. The cellular uptake capacity of EGF-Alexa647 in $Glmp^{gt/gt}$ MEF1 cells is highly impaired compared to WT MEF1 cells at all investigated time points. (n=8 cells per genotype, ****$p < 0.0001$ vs WT cells).

4.2.1.1 Cellular uptake in MEF1 transiently expressing proteins of interest

To investigate whether reintroduction of Glycosylated Lysosomal Membrane Protein (GLMP) to the $Glmp^{gt/gt}$ MEF1 cells could rescue the impaired EGF uptake capacity, a plasmid containing Enhanced Green Fluorescent Protein (EGFP) tagged GLMP cDNA (pGLMP-EGFP, Appendix D, plasmid D2) was transiently introduced through transfection as described in section 3.2.4. This allows for the cells to express GLMP-EGFP protein for a limited period, but due to GLMPs toxicity reintroduction was only possible at concentrations not visible in the applied microscope. A plasmid encoding Red Fluorescent Protein (pRFP, Appendix D, Plasmid D4) was used as transfection control. The successfully transfected cells expressed RFP in the cytoplasm, making it possible to distinguish them from untransfected cells. Control cells were equally treated and transfected with transfection control and an empty plasmid, pSG5 (Appendix D, Plasmid D1), in place of pGLMP-EGFP.

Reintroduction of GLMP did not rescue the uptake (Figure 17). The uptake capacity was even lower in the cells with transiently expressed GLMP than in the control cells. Visual observations revealed unhealthy cells, and the cell density was lower than in similar experiments using the same cells seeded out in equal numbers, even after several optimisation attempts.
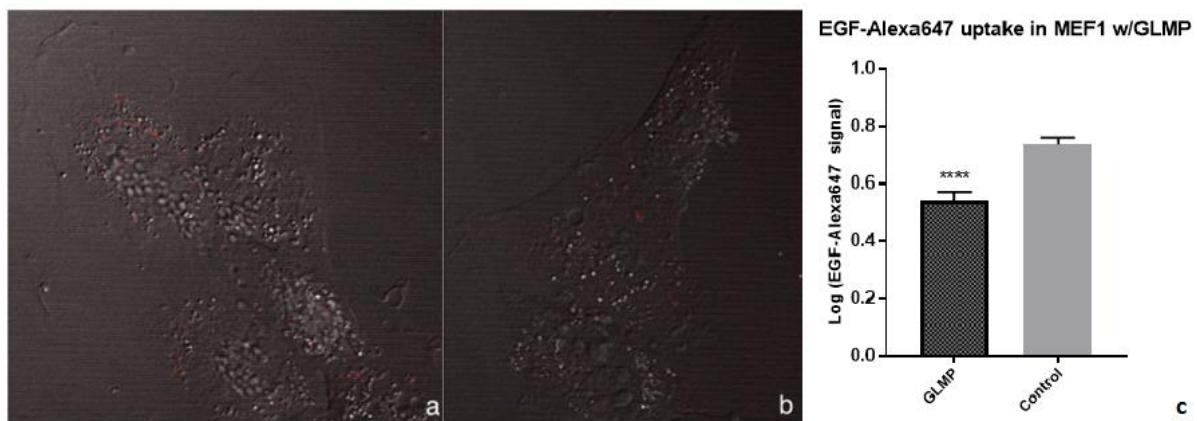
Figure 17: **EGF-Alexa647 uptake in MEF1 expressing GLMP and control cells.** Representative confocal images of EGF-Alexa647 (Red) uptake in $Glmp^{gt/gt}$ MEF1 cells (a) transiently expressing GLMP and (b) control cells transfected with an empty vector, both merged with a transmission image of the compliment cell. Transfection-control RFP channel is not included in the images. (C) Semi-quantitative determination of EGF-Alexa647 uptake in MEF1 $Glmp^{gt/gt}$ cells transiently expressing GLMP (dark grey) and control MEF1 $Glmp^{gt/gt}$ cells transfected with an empty plasmid vector (light grey). The signal is expressed as the mean of logarithm of the replicate means ± s.e.m. (n=267 total cells analysed. ****$p < 0.0001$ vs. control cells).

Two additional uptake assays with transiently introduced proteins were also performed in MEF1 cells. One assay introducing Green Fluorescent Protein tagged MFSD1 (MFSD1-EGFP), and one assay where both GLMP-EGFP and MFSD1-GFP were introduced simultaneously. Neither assay revealed any difference in cellular uptake of EGF-alexa647 compared to control cells (figure 18 and Figure 19). Visual inspection did not reveal as prominent health impacts and loss of cells after transfection as to the cells that were only transiently expressing GLMP.
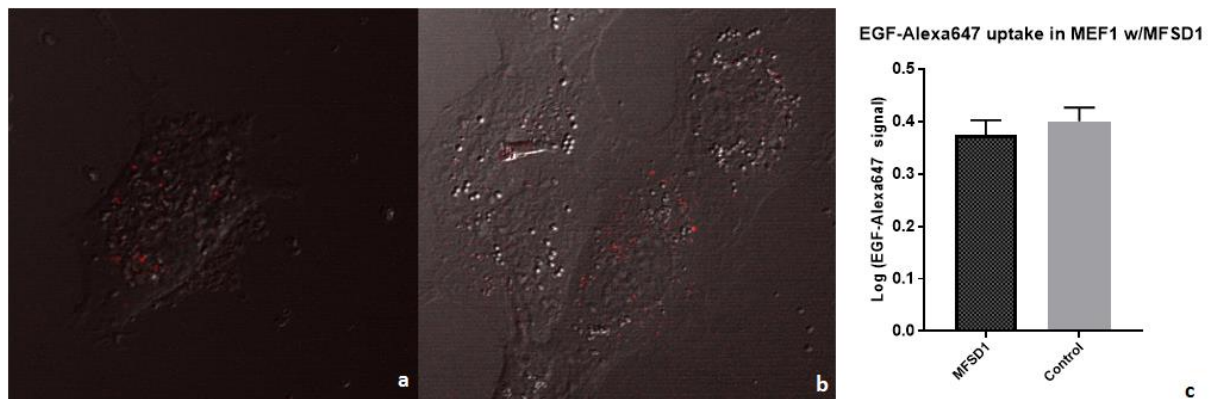
Figure 18: **EGF-Alexa647 uptake in MEF1 with transiently expressed MFSD-GFP**. Representative images of the EGF-Alexa647 (Red) uptake merged with transmission images, of *Glmp*^{gt/gt} MEF1 cells (a) transiently expressing MFSD1 and (b) control cells transfected with an empty plasmid vector. Transfection control RFP channel not included. (c) Semi-quantitative determination of EGF-Alexa647 signal inside cells transiently expressing MFSD1 (Dark grey) and control cells (light grey). The signal is expressed as the mean of logarithm of the replicate means ± s.e.m. Transient expression of MFSD1 did not alter the EGF uptake capacity in MEF1 cells. (n=139 total cells analysed. p-value 0.50).
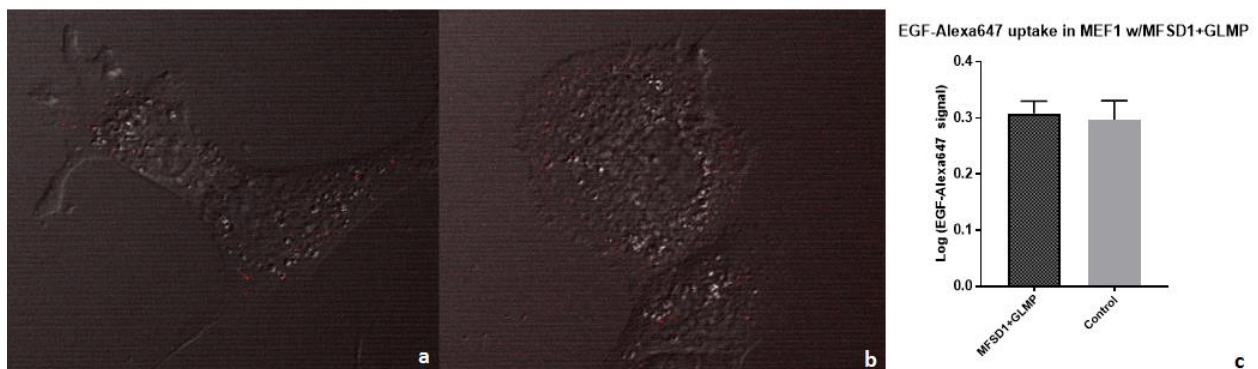
Figure 19: **EGF-Alexa647 uptake in MEF1 with transiently expressed GLMP-EGFP and MFSD-GFP.** . Representative images of the EGF-Alexa647 (Red) uptake merged with transmission images, of *Glmp*^{gt/gt} MEF1 cells (a) transiently expressing MFSD1 and GLMP and (b) control cells transfected with an empty plasmid vector. Transfection control RFP channel not included. (c) Semi-quantitative determination of EGF-Alexa647 signal inside cells transiently expressing MFSD1 and GLMP (Dark grey) and control cells (light grey). The signal is expressed as the mean of logarithm of the replicate means ± s.e.m. Transiently expression of MFSD1 did not alter the EGF uptake capacity in MEF1 cells. (n=174 total cells analysed. p-value 0.77).

To investigate whether the impaired EGF uptake was due to an error in the Epidermal Growth Factor Receptor (EGFR) synthesis or sorting, MEF1 $Glmp^{gt/gt}$ cells were transfected with EGFP tagged EGF-receptor (Appendix D, plasmid D5) as described in section 3.2.4 Transient expression of EGFR did increase the cellular uptake of EGF-Alexa647 significantly (figure 20). As in the GLMP and MFSD1 assays, EGFR concentrations were too low to be visible in the applied microscope. The improved uptake capacity following transient expression of EGFR indicates some sort of impairment of the EGFR synthesis, assuming the transiently expressed and native EGFR follow the same post-translational sorting route from the nucleus to the cell membrane.
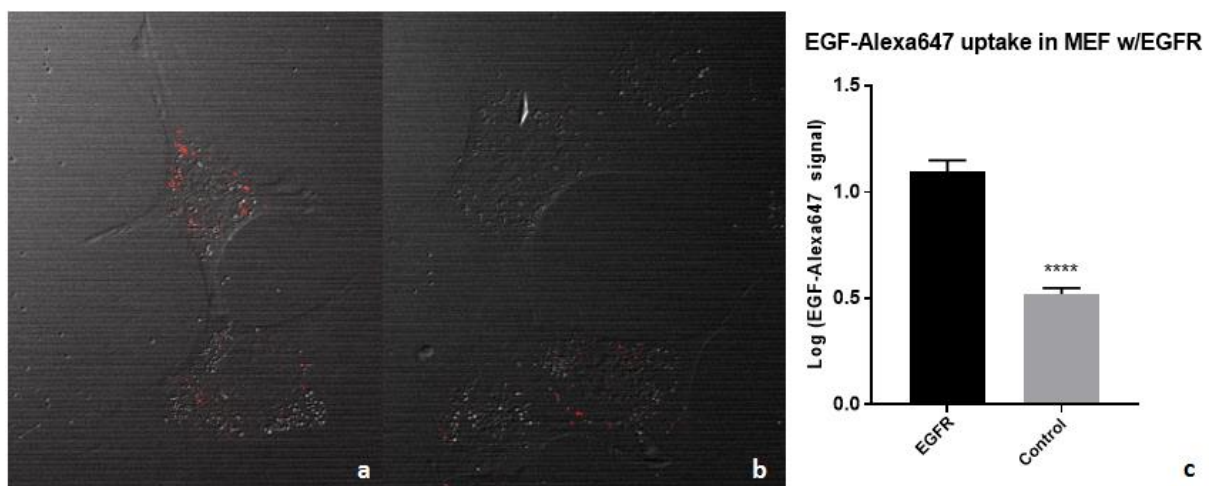
Figure 20: **EGF-Alexa647 uptake in GLMP ablated MEF1 with transiently expressed EGFP-EGFR.** Confocal images of the EGF-Alexa647 channel (Red) merged with transmission images of $Glmp^{gt/gt}$ MEF1 cells (a) transiently expressing EGFP-EGFR and (b) control cells. Transfection control RFP channel not included. (c) Semi-quantitative determination of EGF-Alexa647 signal inside cells transiently expressing EGFR (black) and control cells (grey). The signal is expressed as the mean of logarithm of the replicate means ± s.e.m. The uptake capacity was significantly improved in the cells transiently expressing EGFR. (n=132 total cells analysed. ****p< 0.0001 vs. EGFR).

To confirm that the impaired uptake capacity in MEF1 GLMP ablated cells was due to GLMP ablation, uptake assays were performed in the second cell line originating from the same mouse model (MEF2-T), and in primary cells (MEF2-P). EGF-uptake was also estimated in MEF-M cells.

4.2.2 EGF uptake capacity of *Mfsd1^{ko/ko}* and *Mfsd1^{wt/wt}* MEF cells (MEF-M)

The EGF-Alexa647 cellular uptake capacity of SV40 TAg transformed MEF cells derived from MFSD1 Knock Out (KO) and WT mice (MEF-M), created by our colleagues at the University of Kiel, was also analysed using the method described in section 3.4.1.1. No significant difference was found between the genotypes (figure 21).
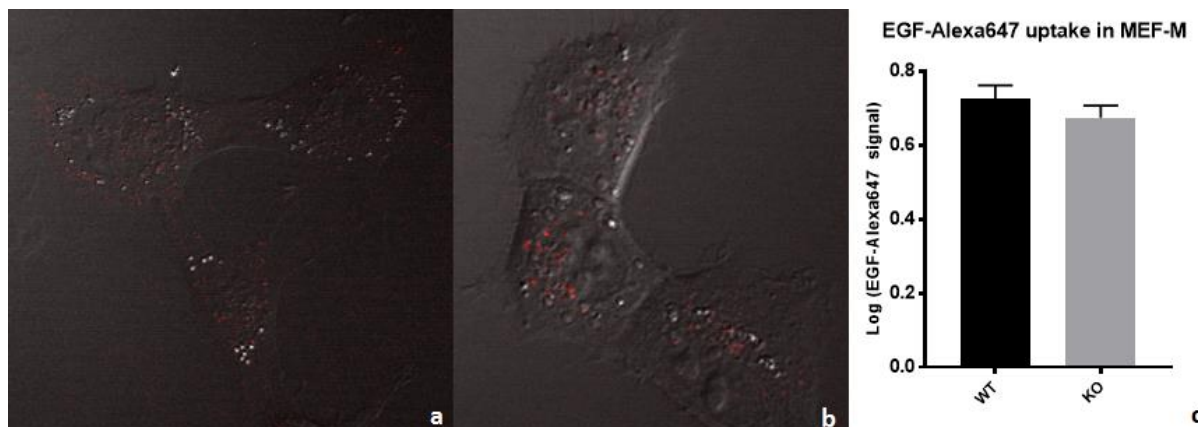
Figure 21: **Tf-Alexa647 uptake in MEF-M.** Confocal image of the Tf-Alexa647 channel (Red) merged with transmission image a representative (a) WT MEF-M cell and (b) *MFSD1^{ko/ko}* MEF-M cell. (c) Semi-quantitative measurements of internalised EGF-Alexa647. The signal is expressed as the mean of logarithm of the replicate means ± s.e.m. The cellular uptake capacity was found not to differ between the genotypes of the MEF-M cells (n=170 total cells analysed. p-value=0.31).

No further assays were performed on these cells.

4.2.3 Cellular uptake in SV40 TAg transformed MEF cells from *Glmp^{gt/gt}* and *Glmp^{wt/wt}* mice (MEF2-T)

Primary MEF cells were harvested, cultivated and immortalised by introducing SV40 Large T antigen (TAg) as described in section 3.2.5. After confirming successful transformation (section 4.1), cellular uptake capacity through receptor-mediated endocytosis was compared between *Glmp^{wt/wt}* and *Glmp^{gt/gt}* MEF2-T cells.

No difference between the genotypes was revealed in the cellular uptake capacity of Tf-Alexa647 or of EGF-Alexa647; both investigated using the method described in section 3.4.1.1 (figure 22 and 23). Dextran-Alexa546 uptake was not compared between the genotypes.
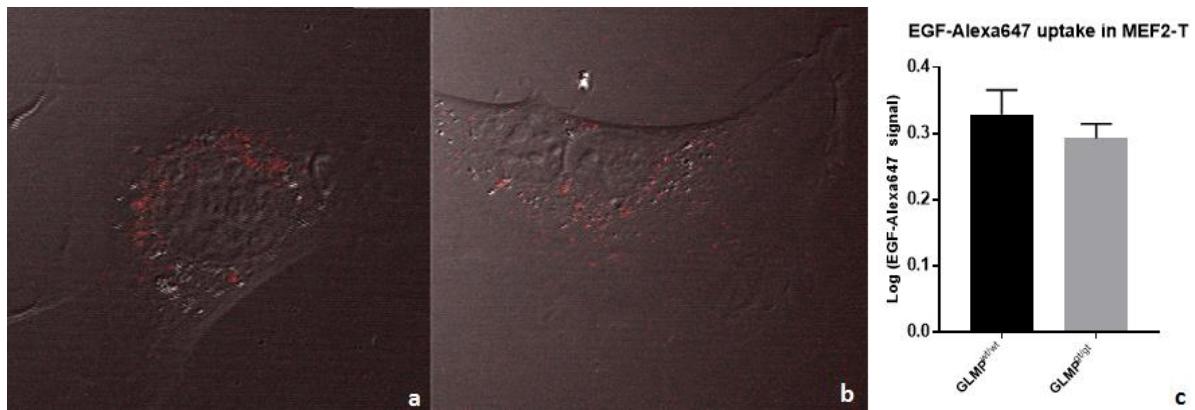
Figure 22: **EGF-Alexa647 uptake in MEF2-**T. Confocal image of the EGF-Alexa647 channel (Red) merged with transmission image a representative (a) *Glmp*$^{wt/wt}$ MEF2-T cell and (B) *Glmp*$^{gt/gt}$ MEF2-T cell. (C) Semi-quantitative measurements of internalised EGF-Alexa647. The signal is expressed as the mean of logarithm of the replicate means ± s.e.m. The cellular uptake capacity was found not to differ between the genotypes of the MEF2-T cells (n=148 total cells analysed. p-value=0.43).
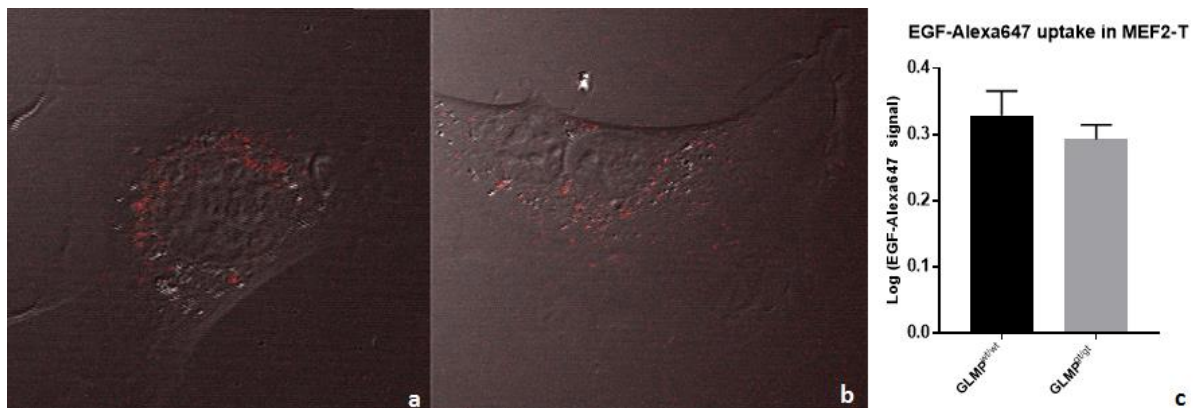
Figure 23: **Tf-Alexa647 uptake in MEF2-T.** Confocal image of the Tf-Alexa647 channel (Red) merged with transmission image a representative (A) *Glmp*$^{wt/wt}$ MEF2-T cell and (B) *Glmp*$^{gt/gt}$ MEF2-T cell. (C) Semi-quantitative measurements of internalised Tf-Alexa647 expressed as the mean of the logarithm of replicate means ± s.e.m. The cellular uptake capacity was found not to differ between the genotypes of the MEF2-T cells (n=193 total cells analysed. p-value=0.19).

The uptake capacity through non-specific fluid phase endocytosis was not compared between the MEF2-T genotypes.

Unlike MEF1 (section 5.2.1), the EGF-uptake capacity of MEF2-T did not differ between the genotypes. To investigate which of the cell lines more closely resemble the *in vivo* situation, the uptake capacity was compared in primary embryonic fibroblasts (MEF2-P).

4.2.4 Cellular uptake in Primary MEF cells from WT and *Glmp^{gt/gt}* mice (MEF2-P)

Primary embryonic fibroblasts (MEF2-P) were harvested and cultivated as described in section 3.1 and cellular uptake capacity was compared between *Glmp^{wt/wt}* and *Glmp^{gt/gt}* MEF2-P cells.

The uptake capacity of EGF-Alexa647 was compared between the genotypes using the method described in section 3.4.1.1. Inspections of the cells did not indicate any difference of uptake capacity (example cells are shown in figure 4 A and B). This was confirmed by comparing the mean grey value of the internalised ligand; no significant difference in cellular uptake was revealed (Figure 4 C).
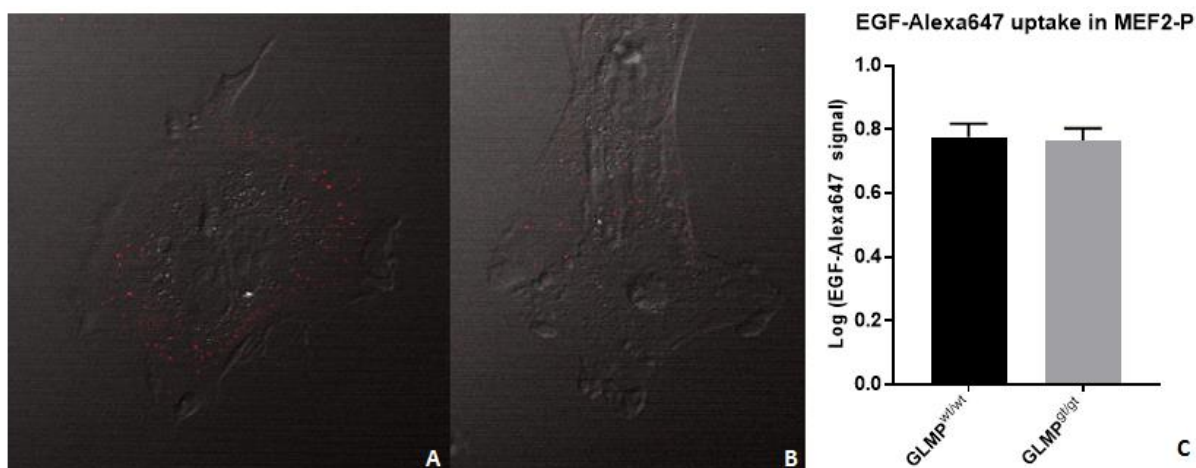
Figure 24: **EGF-Alexa647 uptake in MEF2-P.** Confocal images of the EGF-Alexa647 channel (red) merged with a transmission image of a representative primary (A) *Glmp^{wt/wt}* cell and (B) *Glmp^{gt/gt}* cell (MEF2-P). (C) Semi-quantitative measurements of internalised EGF-alexa647. The signal is expressed as the mean of logarithm of the replicate means ± s.e.m. No significant difference in cellular uptake of EGF-Alexa647 was found. (n=113 total cells analysed. p value 0.86 vs WT).

Similarly, the uptake capacity of Tf-Alexa647 in MEF2-P cells was also compared, but using the method described in section 3.4.1.2, due to high background signal. No significant difference in cellular uptake was revealed between the genotypes (Figure 5).
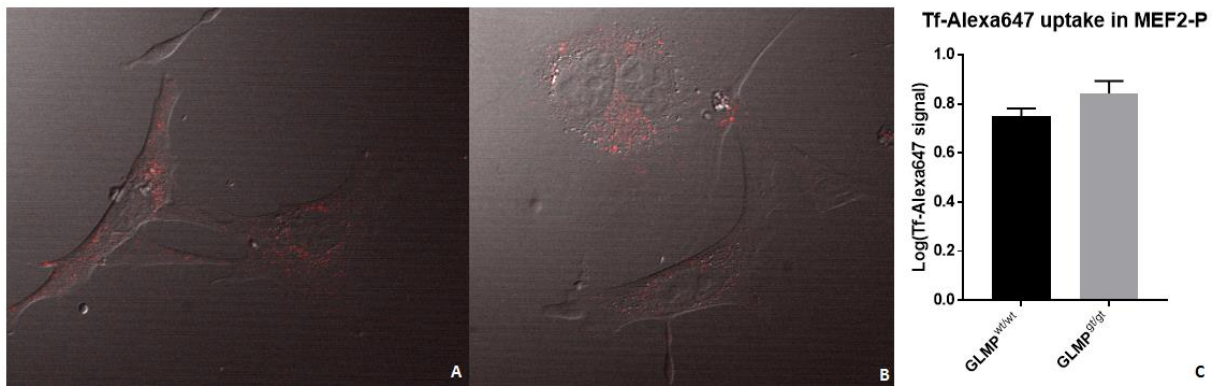
Figure 25: **Tf-Alexa647 uptake in MEF2-P.** Confocal images of the Tf-Alexa647 channel (red) merged with a transmission image of a representative primary (A) *Glmp*^{wt/wt} cell and (B) *Glmp*^{gt/gt} cell (MEF2-P). (C) Semi-quantitative measurements of internalised Tf-alexa647. The signal is expressed as the mean of logarithm of the replicate means ± s.e.m. No significant difference in cellular uptake of EGF-Alexa647 was found. (n=118 total cells analysed. p value 0.12 vs WT).

These findings correspond to the findings in the MEF2-T cells (section 5.2.2).

Dextran-Alexa546 uptake assay was not performed on the MEF2-P cells.

4.3 Growth analysis of spontaneously transformed MEF cells (MEF1)

Growth analysis of the spontaneously transformed MEF cells (MEF1), revealed no major difference in growth rate between the genotypes (figure 26). The cells were seeded out in equal numbers and counted after 24 h, 48 h, 56 h and 64 h, as described in section 3.2.3. The cells enter Log-phase after the first 24 h and were 100% confluent at 64 h.

The starting cell density had some limitations; the *Glmp*^{gt/gt} MEF1 cells did not grow at optimal rate if the initial cell number was lower than $2 \cdot 10^5$ cells per 75 cm^2 growth surface. The WT cells did not display such limitations in the investigated initial cell densities.
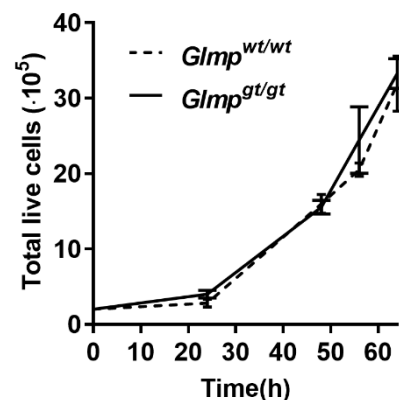
Figure 26 **Growth curve spontaneously transformed *Glmp*^{wt/wt} and *Glmp*^{gt/gt} MEF cells (MEF1).** Starting density $2 \cdot 10^5$ per 75 cm^2 growth surface. Cells were quantified after 24h, 48h, 56h, and 64h. *Glmp*^{wt/wt} MEF1 shown in dotted line and *Glmp*^{gt/gt} MEF1 in solid line. Results displayed as the mean of three replicates ± s.e.m.

4.4 Preliminary study: Western analysis of EGFR and TfR content in GLMP ablated cells

A preliminary western immunoblotting experiment was conducted to compare Epidermal Growth Factor Receptor (EGFR) and Transferrin Receptor (TfR) content between the genotypes of the various GLMP ablated cell lines. The *Mfsd1$^{ko/ko}$* and WT cells (MEF-M) were not included in this assay.

Proteins from confluent cell cultures of both genotypes were harvested from all cell lines (Section 3.3.1), and protein extract concentrations were determined (section 3.2.2.). The extracts were fractioned by SDS-Polyacrylamide Gel electrophoresis (SDS-PAGE) (section 3.2.3) and analysed by western immunoblotting (section 3.3.4). EGFR bands were visualised by electrochemiluminescence (ECL). The signal density was determined and compared between the genotypes (section 3.3.6). TfR bands were visualised and quantified using an antibody with a fluorescent tag (section 3.3.6). After visualisation of EGFR and TfR, the membranes were stripped (section 3.3.5) and β-actin, a house hold protein, was visualised as loading control using ECL detection.

The EGFR expression was then compared between the genotypes of the different cell lines, by comparing signal density between the bands (section 3.3.6). The signal density was also compared between the genotypes in the loading control, and only the MEF1 cells had a significant difference in EGFR content between the genotypes after correction for loading differences (figure 27). *Glmp$^{gt/gt}$* MEF1 EGFR content was estimated 60% lower than the EGFR content in the *Glmp$^{wt/wt}$* MEF1. The EGFR content in MEF2-T and MEF2-P did not deviate substantially between the genotypes after correction for loading differences (figure 27).
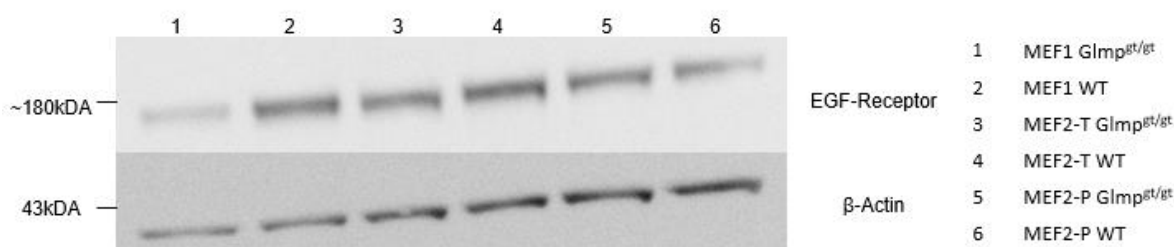
Figure 27: **EGFR content *Glmp$^{wt/wt}$* and *Glmp$^{gt/gt}$* cells**. Protein from *Glmp$^{wt/wt}$* and *Glmp$^{gt/gt}$* MEF1, MEF2-T and MEF2-P cells was harvested and fractioned by SDS-Polyacrylamide Gel Electrophoresis (SDS-PAGE). Protein Bands were transferred from the SDS-PAGE gel to a PVDF membrane by Western Blotting. The membrane was incubated O/N with primary anti-EGFR antigen, before incubation with horseradish peroxidase (HRP) tagged secondary antibody. Upper panel shows expression of Epidermal Growth Factor Receptor

(EGFR) in the genotypes of different cell types. Lower panel is loading control, house hold protein, β-Actin, detected after membrane stripping, both visualised with Electro Chemiluminescence (ECL) reagent.

The TfR content was compared between the genotypes of the different cell lines as well, using signal intensity (section 3.3.6). The signal density of the β-Actin bands was used to compare loading and correct for loading differences (section 3.3.6). The TfR expression in the MEF1, MEF2-T and MEF2-P cells did not appear to differ at all (Figure 28).
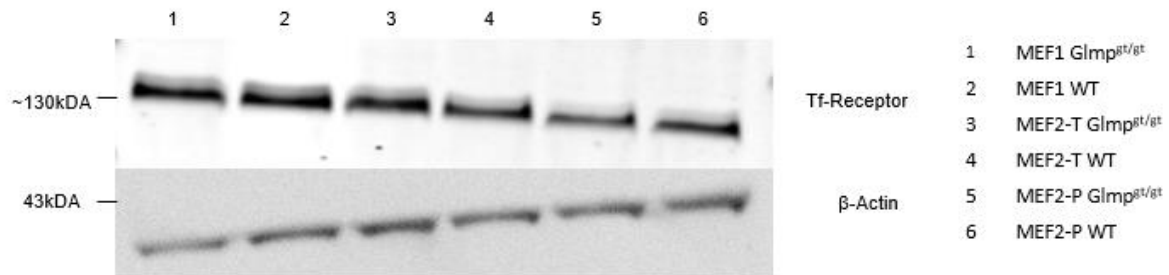
Figure 28: **TfR content in *Glmp^{wt/wt}* and *Glmp^{gt/gt}* cells.** Protein from *Glmp^{wt/wt}* and *Glmp^{gt/gt}* MEF1, MEF2-T and MEF2-P cells was harvested and fractioned by SDS-Polyacrylamide Gel Electrophoresis (SDS-PAGE). Protein Bands were transferred from the SDS-PAGE gel to a PVDF-FL membrane by Western Blotting. The membrane was incubated O/N with primary anti-TfR antigen, before incubation with a fluorophore-tagged secondary antibody. Upper panel shows expression of TfR in the genotypes of different cell types. Lower panel is loading control, house hold protein, β-Actin visualised with Electro Chemiluminescence (ECL) reagent.

5   Discussion

Mouse Embryonic Fibroblast (MEF) cell lines ($Glmp^{gt/gt}$ MEF2-T and $Glmp^{wt/wt}$ MEF2-T, $Glmp^{gt/gt}$ MEF3-T and $Glmp^{wt/wt}$ MEF3-T), made from primary embryonic fibroblasts ($Glmp^{gt/gt}$ MEF2-P and $Glmp^{wt/wt}$ MEF2-P), were successfully generated by introducing the Simian Virus40 (SV40) oncogene Large T antigen (TAg) through stable transfection. A growth assay comparing the growth ability of the MEF2-T cells and primary MEF2-P cells in growth medium with varying Fetal Bovine Serum (FBS) content was conducted to confirm transformation. The transformed cells could grow at lower serum concentrations than the primary cells, and were generally more viable. In addition to the ability to grow in low serum concentrations, the MEF2-T cells were also subcultured up to 17 times, and could probably continue for longer. The primary cells had shorter life-span, and entered a senescent state after 6-8 passages. These observations confirm successful transformation and generation of a new cell line. The $Glmp^{gt/gt}$ MEF2-T and $Glmp^{wt/wt}$ MEF2-T cells were intended as complementary cell lines to the $Glmp^{gt/gt}$ MEF1 and $Glmp^{wt/wt}$ MEF1 cell lines made by former colleague (Kong, X.Y., unpublished).

The cellular uptake capacity was compared between the genotypes of the spontaneously transformed $Glmp^{gt/gt}$ and $Glmp^{wt/wt}$ MEF cells (MEF1), primary $Glmp^{gt/gt}$ and $Glmp^{wt/wt}$ MEF cells (MEF2-P), the SV40 TAg transformed $Glmp^{gt/gt}$ and $Glmp^{wt/wt}$ MEF cells (MEF2-T), and SV40 TAg transformed MEF cells derived from a Major Facilitator Superfamily Domain-containing protein 1 (MFSD1) KO mouse lineage ($Mfsd1^{ko/ko}$ MEF-M and $Mfsd1^{wt/wt}$ MEF-M) (Damme, M., unpublished). Significant impairment of the cellular uptake capacity of Epidermal Growth Factor (EGF) was found in the $Glmp^{gt/gt}$ MEF1 cells, when compared to $Glmp^{wt/wt}$ MEF1 (Heyward, C. A., unpublished). No significant difference in EGF uptake capacity was found between the genotypes of MEF2-T, MEF2-P or MEF-M cells. Transferrin uptake capacity was investigated in all cell lines, except MEF-M, and did not reveal any difference between the genotypes. In addition, cellular uptake of Dextran was compared between the genotypes in MEF1 cells, and no difference was found here either. Growth analysis of the MEF1 cells showed equal growth rate between the genotypes.

To attempt to rescue the impaired EGF uptake capacity of $Glmp^{gt/gt}$ MEF1 cells, EGF uptake was monitored in $Glmp^{gt/gt}$ MEF1cells transiently expressing GLMP, MFSD1, GLMP and MFSD1 simultaneously, and EGF-receptors. The uptake capacity was significantly improved

by transient expression of additional EGF-receptors. Reintroduction of transiently expressed GLMP and MFSD1 did not improve the uptake capacity. Cells transiently expressing GLMP had even lower uptake capacity than the control cells.

Finally, a preliminary investigation of Transferrin Receptor (TfR) and EGF-receptor (EGFR) content in all $Glmp^{gt/gt}$ and $Glmp^{wt/wt}$ cell lines (MEF1, MEF2-P and MEF2-T) revealed substantially lower content of EGFR in $Glmp^{gt/gt}$ MEF1 cells compared to $Glmp^{wt/wt}$ MEF1 cells. No difference in EGFR content was found between the genotypes of the other cell lines. TfR content appeared to be equal between the genotypes of all the investigated cell lines.

5.1   A new cell model for characterisation of the effect of GLMP ablation at the cellular level

The use of MEF cells derived from transgenic mice for characterisation of protein function is common, and it enables the study of cellular events *in vitro* under controllable conditions [5, 24]. Although the use of primary cells is often preferred as they more closely resemble the *in vivo* behaviour, there are many advantages of using cell lines [5, 28, 99]. Primary cells have limited life-span, and can only be subcultivated until they reach their Hayflick Limit, where they enter a senescent state and eventually die [27, 100]. Transformed cells can divide beyond their Hayflick limit. They are easier and cheaper to maintain, more consistent, less time consuming, and can yield almost endless amount of material [5, 28]. It is important to note that *in vitro* models lack the tissue environment present in the whole animal, and that the observed responses and behaviour are not necessarily representative of the *in vivo* situation [5, 30]. However, if one is aware of the limitations and proper applications, there are numerous advantages and useful applications of cultured cells.

There are many approaches for developing transformed MEF cell lines from primary MEF cultures, the most common being stable transfection of SV40 TAg, and serial passage with possible spontaneous transformation. SV40 TAg transformation holds some advantages over spontaneous transformation. Serial passage to achieve transformation is time consuming, often requiring 20-25 subcultivations, and immortalisation might be hard to achieve. Spontaneously transformed MEF cell lines have been shown to have variable doubling rates, and lower and less consistent viable cell number compared to SV40 TAg transformed MEF cell lines[101]. Obtaining transformed cells using SV40 TAg is less time consuming, as

transformation is more reliable. In addition, TAg can be stably transfected into younger cells, and transformation can be achieved at a lower passage number. SV40 TAg transformed cell lines have been shown to have a more rapid and stable doubling rate than spontaneously transformed MEF cell lines [101].

TAg enables transformation by binding and inhibiting key regulators of the cell cycle, including tumour suppressor p53, heat shock chaperone hsc70, and tumour suppressors in the retinoblastoma family (Rb-family)[92]. One disadvantage is that TAg interacts with cell cycle dynamics, and should not be applied as an immortalisation method when studying cell cycle events [101]. The *Glmp*$^{gt/gt}$ and *Glmp*$^{wt/wt}$ cell lines (MEF2-T and MEF3-T) are intended as models to study the effect of GLMP ablation on the endocytic pathway, and TAg is not expected to influence the pathways of interest.

The transformation of MEF2-T was confirmed by a growth assay, investigating the ability of MEF2-T cells to grow at lower serum concentrations than primary MEF2-P cells. The ability of TAg transformed MEF cells to grow in low FBS concentrations is attributed to the ability of TAg to bind the tumour suppressors of the retinoblastoma (pRb) family and the pRb-related proteins p107 and p130[92]. TAg can bind pRb, p107 or p130, thereby inhibiting complex formation with transcription factor E2F [102, 103]. E2F transcription factors regulate cell proliferation, and E2F acts as growth supressing transcription factors when bound to pRb, p107, or p130 [104]. Binding to these proteins depends on a LXCXE motif, and point mutations within this domain has been shown to disrupt the ability to bind to pRb and pRb related proteins [105]. By inhibiting the actions of E2F, TAg enables the cells to bypass growth arrest, and proliferate in nutrient deprived medium [92].

Autophagic events have not yet been investigated in the new cell lines. As the autophagic mechanisms involve lysosomes, these pathways are of interest for future studies of the effect of GLMP ablation. Therefore, it should be emphasised that TAg has been shown to bind heat shock chaperone hsc70 [106]. TAg binding causes the release of bound unfolded proteins [107]. TAg also binds the tumour suppressor p53 [108], which is an inducer of autophagy [109]. These mechanisms might influence the autophagic events in SV40 TAg transformed cells. However, the levels of the autophagy induction marker LC3 was found not to differ between spontaneously transformed MEF cell lines and TAg transformed MEF cells lines. This indicates that TAg transformed MEFs can be useful models studying autophagy [101].

Genetic instability and phenotypic drift is a frequent problem with cultured cells [29, 30]. Aneuploidy and heteroploidy is common in cell lines, meaning the cells may have an abnormal number of chromosomes, and that the number of chromosomes might be heterogeneous within the same population [29, 30]. Rodent cell lines, and mouse lines in particular, are more genetically unstable than human cell lines, hence they immortalise and mutate much more easily [30]. The phenotypic characteristics have been shown to shift with increased passage numbers, and the behaviour can differ between high and low passage numbers [29]. One example of this was shown in Caco-2 cells, an established model of intestinal epithelium, which is used to predict drug absorption *in vivo.* Traits such as proliferation rate, cell density, and carrier-mediated transport were shown to depend on passage number, with significant difference between cells of different ages [29]. This has not been investigated in the cell lines applied in this thesis, but there was no great variance of passage numbers used for the uptake assays. Cells were replaced from the nitrogen tank stock regularly. However, one might speculate whether the extensive subcultivation needed to obtain spontaneous transformation causes them to deviate more from primary cells than TAg transformed cell lines, and that TAg transformed cell lines should be used at the lowest possible passage number. TAg was introduced to the MEF2-T and MEF3-T cell lines between passage number 2-4, and the MEF2-T cells uptake capacity was studied between passage 9-15, in contrast to MEF cells, which were studied between passage 23-45. Preliminary karyotyping assays preformed on the MEF1 cell lines revealed aneuploidy in the $Glmp^{gt/gt}$ MEF1 cell line, with a chromosome cross-over site on one of four chromosomes containing the *Egfr* gene (Eskeland, R., unpublished).

Growth analysis of the MEF1 cells revealed no substantial difference in growth rate between the $Glmp^{gt/gt}$ MEF1 and $Glmp^{wt/wt}$ MEF1 cell lines, but the $Glmp^{gt/gt}$ MEF1 cells were more sensitive to low densities in the starting population, while initial growth analysis not described here showed that the minimum cell density for optimal growth of $Glmp^{gt/gt}$ MEF1 cells was around $0.03 \cdot 10^5$ cells per cm^2 growth surface at day zero. The $Glmp^{wt/wt}$ MEF1 cells did not display such sensitivity in these assays. Whether this is due to genetic or phenotypic differences between the genotypes or due to GLMP ablation is speculative, and it must be emphasised that the $Glmp^{gt/gt}$ MEF1 cell line and $Glmp^{wt/wt}$ cell lines are distinct, with individual transformation events leading to immortalisation. Therefore, such differences cannot be accredited exclusively to the manipulation of the target gene.

70

To accredit any observed deviation between two genotypes to the manipulation of a target gene, the difference should be present in several independent cell lines derived from the same mouse lineage. However, confirming any significant findings in primary cells is always recommended when possible [5].

The *Glmp^{gt/gt}* and *Glmp^{wt/wt}* MEF1 cell lines were dismissed as suitable models for studying the effects of GLMP ablation on the endocytic pathway (see section 5.2). Characterising and comparing various traits and abilities is important to ensure that the observed difference between the genotypes is solely due to the GLMP ablation, and not due to other factors. Further characterisation (e.g. growth rate, viable cell count, karyotyping) of the MEF2-T and MEF3-T cell lines might be useful, and transformation must be confirmed in the MEF3-T cell lines.

5.2 No impairment of the cellular uptake capacity in GLMP ablated cell lines

The use of fluorophore tagged ligands to investigate endocytic events is widely used, with the most commonly used ligands being Tf and EGF conjugates. The study of Tf/TfR traffic is common for investigating cellular uptake capacity through recycling receptor-mediated endocytosis, and following EGF/EGFR internalisation is common for studying uptake capacity through degradative receptor-mediated endocytosis. Dextran conjugates are widely used to investigate fluid phase uptake (non-specific liquid phase endocytosis) [34, 110, 111].

The uptake capacity assays described in this thesis are intended as initial studies to narrow down the area of interest. Several factors have not been considered, including specific and non-specific binding. To correct for these factors, competition assays with unlabelled ligands should be performed. The unlabelled ligand will out-compete the labelled ligand at the specific binding sites, and the internalised labelled ligand can therefore be assumed to enter the cell unspecifically, as the unlabelled ligand does not out-compete unspecific binding [112-114]. Performing competition assays will give a more accurate quantitation of internalised ligand, by correcting for unspecifically internalised ligand. In addition, only one optical section of the cell was analysed. Analysing the whole cell, for instance by merging z-stack images and comparing the total amount of internalised ligand between the cells, would give a more correct idea of the uptake capacity.

Furthermore, the cell medium containing the labelled ligands was not replaced after ligand addition as described in section 3.4.1.1, and the cells were not washed prior to imaging. Therefore, any ligands adhering to the membrane were included in the detection. However, the assays were strictly used to compare the cellular uptake between the genotypes, or between cells transiently expressing proteins of interest and control cells, and not quantitatively. The uptake assays may therefore be viewed as preliminary, intended to reveal big differences to narrow down the area of interest.

The impaired uptake of EGF observed in the *Glmp*$^{gt/gt}$ MEF1 cells was initially thought to be connected to GLMP ablation. Tf and Dextran uptake capacity was also compared between the MEF1 genotypes, but no difference was found. This indicated that GLMP might have a function in EGFR trafficking or synthesis. To investigate if reintroduction of GLMP could rescue the uptake, *Glmp*$^{gt/gt}$ MEF1 cells transiently expressing GFP tagged GLMP was compared to cells transfected with an empty control plasmid. Unexpectedly, the cells transiently expressing GLMP had even lower uptake capacity than the control cells. This is probably due to GLMP toxicity; this has previously been observed in cells transiently expressing GLMP (Eskild, W., Unpublished). Several transfection experiments with different plasmid concentrations were conducted to optimise the assay, but further optimisation may be necessary. The effect of adding a fluorophore tag might alter protein function, or the labelled protein might have a different localisation than the endogenous protein, possibly disrupting cell function [115].

Since GLMP expression might be inhibited in *Mfsd1*$^{ko/ko}$ cells, we investigated if transient expression of MFSD1 and simultaneous transient GLMP and MFSD1 expression could rescue the impaired uptake of the *Glmp*$^{gt/gt}$ MEF1 cells, but neither could. However, as the impaired EGF uptake capacity was later ruled an artefact of transformation in the *Glmp*$^{gt/gt}$ MEF1 cell line, these assays cannot give an insight into as whether a cooperation between these proteins exist or not.

Assuming that transiently expressed EGFR follows the same trafficking and sorting pathway as natural EGFR, we introduced additional transiently expressed EGFR to see whether the impaired uptake was due to improper sorting, increased degradation, or impaired synthesis. The uptake was significantly improved in cells transiently expressing additional EGFR, indicating some sort of impairment in the EGFR synthesis or increased degradation. The preliminary western blot experiment also indicated impaired synthesis or increased

degradation of EGFR, as the $Glmp^{gt/gt}$ MEF1 cells contained approximately 30% of the EGFR protein found in the $Glmp^{wt/wt}$ MEF1 cells.

As mentioned, control experiments in independent cell lines derived from the same transgenic mouse lineage and primary cells are important when investigating whether an observed trait is due to altered gene expression in studies of protein function [5]. The EGF-uptake capacity in both MEF2-T cells and in the MEF2-P cells did not differ between the genotypes, and therefore it was concluded that the impaired uptake capacity observed in the $Glmp^{gt/gt}$ MEF1 cells most likely is an artefact of the transformation event, and not a consequence of GLMP ablation. The EGF uptake capacity between SV40 TAg transformed MEF cells derived from $Mfsd1^{ko/ko}$ and $Mfsd1^{wt/wt}$ mice (MEF-M) did not differ either, further confirming some sort of deficiency in the $Glmp^{gt/gt}$ MEF1 cells, assuming $Mfsd1^{ko/ko}$ cells are GLMP ablated.

The new TAg transformed cell lines (MEF2-T and MEF3-T) were initially made to complement the MEF1 cell lines, and confirm GLMP ablations role in the impaired EGF uptake capacity observed in the $Glmp^{gt/gt}$ MEF1 cells. There was no difference in EGF uptake capacity between the genotypes of the MEF2-T cells, which was also confirmed in primary cells (MEF2-P). Based on this, the results obtained in the EGF uptake analysis of GLMP ablated MEF1 cells were rejected, and the low EGFR content in the $Glmp^{gt/gt}$ MEF1 cells deemed an artefact of transformation. If the reduced amount of EGFR, either by retention inside a cellular compartment, increased degradation or impaired synthesis, was directly linked to GLMP ablation, one would expect a different EGFR content in all GLMP ablated cell lines.

The uptake assays indicate that GLMP ablation does not alter the cellular uptake capacity through receptor-mediated endocytosis of Tf or EGF. Studying additional ligands and pathways (e.g. Autophagic pathways and clathrin-independent endocytosis) might provide further insight in GLMP function and role in the endosomal-lysosomal system.

5.3 EGFR and TfR content in GLMP ablated cells

The preliminary western blot experiment revealed that the *Glmp*$^{gt/gt}$ MEF1 cells contained approximately 30% of the EGFR protein found in *Glmp*$^{wt/wt}$ MEF1 cells. No difference was found when comparing the EGFR content between the genotypes of the primary MEF cells (MEF2-P) or the TAg transformed MEF cells (MEF2-T). The TfR did not appear to differ between the genotypes of any of the cell lines investigated, but additional replicates are needed to confirm these findings. As mentioned in section 5.1 the MEF1 *Glmp*$^{gt/gt}$ cells were found to be aneuploid, containing four alleles of the *Egfr* gene, with a chromosome cross over site on one of the chromosomes containing an *Egfr* allele (Eskeland, R., unpublished). Whether this impacts the synthesis rate or not is difficult to determine. However, it offers a possible explanation for the lower EGFR content observed in the *Glmp*$^{gt/gt}$ MEF1 cell line.

6   Conclusions and future studies

The aim of this study was to develop and characterise an *in vitro* model for studying the effect of GLMP ablation at the cellular level.

MEF cells from *Glmp^gt/gt* and *Glmp^wt/wt* mice were successfully harvested and cultivated (MEF2-P). Two cell lines from each genotype were stably transfected with SV40 TAg (MEF2-T and MEF3-T). Transformation was confirmed in both genotypes of the MEF2-T cells by a FBS depletion growth assay, confirming the establishment of a new *in vitro* model for studying GLMP ablation at the cellular level.

GLMP ablation has been shown to cause a slowly progressing liver fibrosis in the *Glmp^gt/gt* mouse model. We hypothesise that the liver fibrosis is a symptom of a yet undescribed lysosomal disorder. Spontaneously transformed *Glmp^gt/gt* and *Glmp^wt/wt* MEF cells (MEF1) have previously been made (Kong X. Y., unpublished) and impaired cellular EGF uptake capacity in *Glmp^gt/gt* MEF1 cells has previously been shown (Heyward, C. A., unpublished). The growth rate of the MEF1 cells is equal between the *Glmp^gt/gt* and *Glmp^wt/wt* cells, but the *Glmp^gt/gt* MEF1 cells are more sensitive to low cell density. The cellular uptake capacity of Tf and dextran did not differ between the genotypes of the MEF1 cells. The impaired EGF uptake capacity of the *Glmp^gt/gt* MEF1 cells was initially thought to be caused by GLMP ablation leading to deficient synthesis of EGFR or impaired EGFR traffic.

The impaired cellular uptake in the *Glmp^gt/gt* MEF1 cells could not be rescued by transient expression of GLMP alone, or by simultaneous transient expression of GLMP and MFSD1. In accordance with previous observations, GLMP appeared toxic to the cells when introduced in large amounts, (Eskild, W., unpublished). Increasing the EGFR content by transient expression did, however, improve the cellular uptake capacity. This initially led us to believe that GLMP ablation affected the synthesis or degradation rate of EGFR. The cellular uptake capacity of EGF and Tf was compared between TAg transformed *Glmp^gt/gt* and *Glmp^wt/wt* MEF cells (MEF2-T) cells, and between primary *Glmp^gt/gt* and *Glmp^wt/wt* MEF cells (MEF2-P). Neither MEF2-P nor MEF2-T displayed differences in the cellular uptake capacity of either EGF or Tf. The EGF uptake capacity did not differ between SV40 TAg transformed *Mfsd1^ko/ko* and *Mfsd1^wt/wt* MEF cells (MEF-M) either. Preliminary karyotyping experiments revealed that the *Glmp^gt/gt* MEF1 cells were aneuploid, containing four different *Egfr* alleles, with a chromosome crossover site on one of the *Egfr* containing chromosomes (Eskeland, R.,

unpublished). This might be the cause of the lower EGFR levels, and the reduced uptake capacity in the *Glmp*$^{gt/gt}$ MEF1 cells is most likely an artefact of the spontaneous transformation. Preliminary western blots showed that the *Glmp*$^{gt/gt}$ MEF1 cells contained approximately 30% of the EGFR protein found in the *Glmp*$^{wt/wt}$ MEF cells, whereas the EGFR content did not differ between the genotypes of the MEF2-P and MEF2-T cells. Tf content appeared equal when compared between the genotypes in the MEF1, MEF2-P, and MEF2-T cells.

Based on these findings, the MEF1 cell lines have been rejected as suitable models for studying the effect of GLMP ablation on the endocytic pathway.

Further characterisation might be necessary to determine whether the MEF2-T and MEF3-T cell lines are suitable as *in vitro* models for GLMP ablation at the cellular level. Transformation should be confirmed in the MEF3-T cells, and the growth rate should be compared between the genotypes of both MEF2-T and MEF3-T cells. The cellular uptake assays did not include ligand competition with unmarked ligand, and ligands adherent to the cell surface were not removed. New uptake assays that take these factors into account should be considered.

The apparent toxicity of GLMP when transiently expressed resulted in the use of concentrations too low to be detected properly at the applied microscope. Further optimisation for the reintroduction of transiently expressed fluorophore labelled GLMP should be performed. Subcellular localisation of GLMP in live cells, and co-localisation assays with the various compartments of the endocytic pathway should be investigated after transient transfection with fluorophore tagged GLMP.

Autophagic events have not been addressed and should be considered as areas of interest in future studies. Determining the degradation rate of the various ligands could possibly yield valuable information about GLMP function. The dextran uptake capacity should be investigated in the new cell lines as well.

To verify the EGFR and TfR content in the MEF2-T and MEF2-P is equal between the genotypes, additional western blot experiments should be performed. Investigating the content of additional endocytic receptors should also be considered.

References

1.   Nesset, C.K., X.Y. Kong, M. Damme, C. Schjalm, N. Roos, E.M. Loberg, and W. Eskild, *Age-dependent development of liver fibrosis in Glmp (gt/gt) mice.* Fibrogenesis Tissue Repair, 2016. **9**: p. 5.

2.   Kong, X.Y., C.K. Nesset, M. Damme, E.M. Loberg, T. Lubke, J. Maehlen, K.B. Andersson, P.I. Lorenzo, N. Roos, G.H. Thoresen, A.C. Rustan, E.T. Kase, and W. Eskild, *Loss of lysosomal membrane protein NCU-G1 in mice results in spontaneous liver fibrosis with accumulation of lipofuscin and iron in Kupffer cells.* Dis Model Mech, 2014. **7**: p. 351-362.

3.   Schieweck, O., M. Damme, B. Schroder, A. Hasilik, B. Schmidt, and T. Lubke, *NCU-G1 is a highly glycosylated integral membrane protein of the lysosome.* Biochem J, 2009. **422**: p. 83-90.

4.   Ballabio, A. and V. Gieselmann, *Lysosomal disorders: From storage to cellular damage.* Biochimica et Biophysica Acta (BBA) - Molecular Cell Research, 2009. **1793**: p. 684-696.

5.   Staycey, G., *Primary Cell Cultures and Immortal Cell Lines*, in *Encyclopedia Of Life Sciences*. 2001, John Wiley & Sons, Ltd.

6.   Ishibashi, H., M. Nakamura, A. Komori, K. Migita, and S. Shimoda, *Liver architecture, cell function, and disease.* Semin Immunopathol, 2009. **31**: p. 399-409.

7.   McCuskey, R.S., *Chapter 1 - Anatomy of the Liver A2 - by, Edited*, in *Zakim and Boyer's Hepatology (Fifth Edition)*, T.D. Boyer, T.L. Wright, M.P. Manns, C. Editor, and D. Zakim, Editors. 2006, W.B. Saunders: Edinburgh. p. 3-21.

8.   Trautwein, C., *Chapter 2 - Liver Regeneration A2 - by, Edited*, in *Zakim and Boyer's Hepatology (Fifth Edition)*, T.D. Boyer, T.L. Wright, M.P. Manns, C. Editor, and D. Zakim, Editors. 2006, W.B. Saunders: Edinburgh. p. 23-36.

9.   Fujiyoshi, M. and M. Ozaki, *Molecular mechanisms of liver regeneration and protection for treatment of liver dysfunction and diseases.* Journal of Hepato-Biliary-Pancreatic Sciences, 2011. **18**: p. 13-22.

10.   Bataller, R. and D.A. Brenner, *Liver fibrosis.* J Clin Invest, 2005. **115**: p. 209-218.

11.   Rockey, D.C. and S.L. Friedman, *Chapter 6 - Hepatic Fibrosis and Cirrhosis A2 - by, Edited*, in *Zakim and Boyer's Hepatology (Fifth Edition)*, T.D. Boyer, T.L. Wright, M.P. Manns, C. Editor, and D. Zakim, Editors. 2006, W.B. Saunders: Edinburgh. p. 87-109.

12.   Hernandez-Gea, V. and S.L. Friedman, *Pathogenesis of liver fibrosis.* Annu Rev Pathol, 2011. **6**: p. 425-456.

13.   Friedman, S.L., *Liver fibrosis—from bench to bedside.* J Hepatol, 2003. **38 Suppl 1**: p. 38-53.

14.   Moreira, R.K., *Hepatic stellate cells and liver fibrosis.* Arch Pathol Lab Med, 2007. **131**: p. 1728-1734.

15.   Friedman, S.L., *Mechanisms of hepatic fibrogenesis.* Gastroenterology, 2008. **134**: p. 1655-1669.

16.   Pellicoro, A., P. Ramachandran, J.P. Iredale, and J.A. Fallowfield, *Liver fibrosis and repair: immune regulation of wound healing in a solid organ.* Nat Rev Immunol, 2014. **14**: p. 181-194.

17.   Steffensen, K.R., M. Bouzga, F. Skjeldal, C. Kasi, A. Karahasan, V. Matre, O. Bakke, S. Guerin, and W. Eskild, *Human NCU-G1 can function as a transcription factor and as a nuclear receptor co-activator.* BMC Mol Biol, 2007. **8**: p. 106.

18. Sardiello, M., M. Palmieri, A. di Ronza, D.L. Medina, M. Valenza, V.A. Gennarino, C. Di Malta, F. Donaudy, V. Embrione, R.S. Polishchuk, S. Banfi, G. Parenti, E. Cattaneo, and A. Ballabio, *A gene network regulating lysosomal biogenesis and function.* Science, 2009. **325**: p. 473-477.

19. Barnett CP, N.N., Chedera B, Byrne A, Schwartz Q, Carney T, Hahn CN, Schreiber AW, Feng JH and Scott HS, *Mutations in C1orf85 associated with a novel craniofacial fibrous dysplasia syndrome with unusual palate and hand abnormalities (abstract).*

20. Pierce, A.M., W.J. Sampson, D.F. Wilson, and A.N. Goss, *Fifteen-year follow-up of a family with inherited craniofacial fibrous dysplasia.* J Oral Maxillofac Surg, 1996. **54**: p. 780-788.

21. Carpino, G., S. Morini, S. Ginanni Corradini, A. Franchitto, M. Merli, M. Siciliano, F. Gentili, A. Onetti Muda, P. Berloco, M. Rossi, A.F. Attili, and E. Gaudio, *Alpha-SMA expression in hepatic stellate cells and quantitative analysis of hepatic fibrosis in cirrhosis and in recurrent chronic hepatitis after liver transplantation.* Dig Liver Dis, 2005. **37**: p. 349-356.

22. Gressner, A.M. and M.G. Bachem, *Molecular mechanisms of liver fibrogenesis—a homage to the role of activated fat-storing cells.* Digestion, 1995. **56**: p. 335-346.

23. Sell, S. and H.A. Dunsford, *Evidence for the stem cell origin of hepatocellular carcinoma and cholangiocarcinoma.* Am J Pathol, 1989. **134**: p. 1347-1363.

24. Xu, J., *Preparation, culture, and immortalization of mouse embryonic fibroblasts.* Curr Protoc Mol Biol, 2005. **28**: p. 1.

25. Puigserver, P., G. Adelmant, Z. Wu, M. Fan, J. Xu, B. O'Malley, and B.M. Spiegelman, *Activation of PPARgamma coactivator-1 through transcription factor docking.* Science, 1999. **286**: p. 1368-1371.

26. Moore, C.B. and I.C. Allen, *Primary ear fibroblast derivation from mice.* Methods Mol Biol, 2013. **1031**: p. 65-70.

27. Rattan, S.I.S., *Cell Senescence In Vitro*, in *eLS*. 2001, John Wiley & Sons, Ltd.

28. Kaur, G. and J.M. Dufour, *Cell lines.* Spermatogenesis, 2012. **2**: p. 1-5.

29. Hughes, P., D. Marshall, Y. Reid, H. Parkes, and C. Gelber, *The costs of using unauthenticated, over-passaged cell lines: how much more data do we need?* Biotechniques, 2007. **43**: p. 575.

30. Geraghty, R.J., A. Capes-Davis, J.M. Davis, J. Downward, R.I. Freshney, I. Knezevic, R. Lovell-Badge, J.R. Masters, J. Meredith, G.N. Stacey, P. Thraves, M. Vias, and U.K. Cancer Research, *Guidelines for the use of cell lines in biomedical research.* Br J Cancer, 2014. **111**: p. 1021-1046.

31. Mericko, P., A. Helmirch, L. Chen, K. Kusamoto, A. Toumadje, C. Chapline, D. Sato, and D.W. Barnes, *Cell Culture: Basic Procedures*, in *eLS*. 2001, John Wiley & Sons, Ltd.

32. Gollin, S.M. and D.W. Lewis, *Cell Culture Contamination*, in *eLS*. 2001, John Wiley & Sons, Ltd.

33. Singhal, P.K., S. Sassi, L. Lan, P. Au, S.C. Halvorsen, D. Fukumura, R.K. Jain, and B. Seed, *Mouse embryonic fibroblasts exhibit extensive developmental and phenotypic diversity.* Proceedings of the National Academy of Sciences, 2016. **113**: p. 122-127.

34. Huotari, J. and A. Helenius, *Endosome maturation.* The EMBO Journal, 2011. **30**: p. 3481-3500.

35. Hu, Y.B., E.B. Dammer, R.J. Ren, and G. Wang, *The endosomal-lysosomal system: from acidification and cargo sorting to neurodegeneration.* Transl Neurodegener, 2015. **4**: p. 18.

36. Doherty, G.J. and H.T. McMahon, *Mechanisms of endocytosis.* Annu Rev Biochem, 2009. **78**: p. 857-902.

37. Hyttinen, J.M.T., M. Niittykoski, A. Salminen, and K. Kaarniranta, *Maturation of autophagosomes and endosomes: A key role for Rab7.* Biochimica et Biophysica Acta (BBA) - Molecular Cell Research, 2013. **1833**: p. 503-510.

38. Seaman, M.N.J., *The retromer complex – endosomal protein recycling and beyond.* Journal of Cell Science, 2012. **125**: p. 4693-4702.

39. Luzio, J.P., P.R. Pryor, and N.A. Bright, *Lysosomes: fusion and function.* Nat Rev Mol Cell Biol, 2007. **8**: p. 622-632.

40. Lopez, S.A., C., *How Viruses Hijack Endocytic Machinery.* Nature Education, 2010. **3**: p. 1.

41. McMahon, H.T. and E. Boucrot, *Molecular mechanism and physiological functions of clathrin-mediated endocytosis.* Nat Rev Mol Cell Biol, 2011. **12**: p. 517-533.

42. Madshus, I.H. and E. Stang, *Internalization and intracellular sorting of the EGF receptor: a model for understanding the mechanisms of receptor trafficking.* Journal of Cell Science, 2009. **122**: p. 3433-3439.

43. Sorkin, A. and M. von Zastrow, *Signal transduction and endocytosis: close encounters of many kinds.* Nat Rev Mol Cell Biol, 2002. **3**: p. 600-614.

44. Sigismund, S., E. Argenzio, D. Tosoni, E. Cavallaro, S. Polo, and P.P. Di Fiore, *Clathrin-Mediated Internalization Is Essential for Sustained EGFR Signaling but Dispensable for Degradation.* Developmental Cell, 2008. **15**: p. 209-219.

45. Tortorella, S. and T.C. Karagiannis, *Transferrin receptor-mediated endocytosis: a useful target for cancer therapy.* J Membr Biol, 2014. **247**: p. 291-307.

46. Kiss, A.L. and E. Botos, *Endocytosis via caveolae: alternative pathway with distinct cellular compartments to avoid lysosomal degradation?* Journal of Cellular and Molecular Medicine, 2009. **13**: p. 1228-1237.

47. Nabi, I.R. and P.U. Le, *Caveolae/raft-dependent endocytosis.* The Journal of Cell Biology, 2003. **161**: p. 673-677.

48. Parton, R.G. and K. Simons, *The multiple faces of caveolae.* Nat Rev Mol Cell Biol, 2007. **8**: p. 185-194.

49. Lim, J.P. and P.A. Gleeson, *Macropinocytosis: an endocytic pathway for internalising large gulps.* Immunol Cell Biol, 2011. **89**: p. 836-843.

50. Richards, David M. and Robert G. Endres, *The Mechanism of Phagocytosis: Two Stages of Engulfment.* Biophysical Journal, 2014. **107**: p. 1542-1553.

51. Glick, D., S. Barth, and K.F. Macleod, *Autophagy: cellular and molecular mechanisms.* The Journal of pathology, 2010. **221**: p. 3-12.

52. *Microautophagy in mammalian cells: Revisiting a 40-year-old conundrum.* Autophagy, 2011. **7**: p. 673-682.

53. Li, W.W., J. Li, and J.K. Bao, *Microautophagy: lesser-known self-eating.* Cell Mol Life Sci, 2012. **69**: p. 1125-1136.

54. Mizushima, N., *Autophagy: process and function.* Genes Dev, 2007. **21**: p. 2861-73.

55. Bejarano, E. and A.M. Cuervo, *Chaperone-Mediated Autophagy.* Proceedings of the American Thoracic Society, 2010. **7**: p. 29-39.

56. Bandyopadhyay, U., S. Kaushik, L. Varticovski, and A.M. Cuervo, *The chaperone-mediated autophagy receptor organizes in dynamic protein complexes at the lysosomal membrane.* Mol Cell Biol, 2008. **28**: p. 5747-5763.

57.   Saftig, P. and J. Klumperman, *Lysosome biogenesis and lysosomal membrane proteins: trafficking meets function.* Nat Rev Mol Cell Biol, 2009. **10**: p. 623-635.

58.   Braulke, T. and J.S. Bonifacino, *Sorting of lysosomal proteins.* Biochimica et Biophysica Acta (BBA) - Molecular Cell Research, 2009. **1793**: p. 605-614.

59.   De Duve, C. and R. Wattiaux, *Functions of lysosomes.* Annu Rev Physiol, 1966. **28**: p. 435-492.

60.   Turk, V., V. Stoka, O. Vasiljeva, M. Renko, T. Sun, B. Turk, and D. Turk, *Cysteine cathepsins: From structure, function and regulation to new frontiers.* Biochimica et Biophysica Acta (BBA) - Proteins and Proteomics, 2012. **1824**: p. 68-88.

61.   Reczek, D., M. Schwake, J. Schröder, H. Hughes, J. Blanz, X. Jin, W. Brondyk, S. Van Patten, T. Edmunds, and P. Saftig, *LIMP-2 Is a Receptor for Lysosomal Mannose-6-Phosphate-Independent Targeting of β-Glucocerebrosidase.* Cell, 2007. **131**: p. 770-783.

62.   Beyenbach, K.W. and H. Wieczorek, *The V-type H+ ATPase: molecular structure and function, physiological roles and regulation.* Journal of Experimental Biology, 2006. **209**: p. 577-589.

63.   Schwake, M., B. Schröder, and P. Saftig, *Lysosomal Membrane Proteins and Their Central Role in Physiology.* Traffic, 2013. **14**: p. 739-748.

64.   Fukuda, M., *Lysosomal membrane glycoproteins. Structure, biosynthesis, and intracellular trafficking.* Journal of Biological Chemistry, 1991. **266**: p. 21327-21330.

65.   Hunziker, W. and H.J. Geuze, *Intracellular trafficking of lysosomal membrane proteins.* Bioessays, 1996. **18**: p. 379-389.

66.   Eskelinen, E.-L., Y. Tanaka, and P. Saftig, *At the acidic edge: emerging functions for lysosomal membrane proteins.* Trends in Cell Biology, 2003. **13**: p. 137-145.

67.   Eskelinen, E.-L., *Roles of LAMP-1 and LAMP-2 in lysosome biogenesis and autophagy.* Molecular Aspects of Medicine, 2006. **27**: p. 495-502.

68.   Carlsson, S.R., J. Roth, F. Piller, and M. Fukuda, *Isolation and characterization of human lysosomal membrane glycoproteins, h-lamp-1 and h-lamp-2. Major sialoglycoproteins carrying polylactosaminoglycan.* Journal of Biological Chemistry, 1988. **263**: p. 18911-18919.

69.   Eskelinen, E.-L., A.M. Cuervo, M.R.G. Taylor, I. Nishino, J.S. Blum, J.F. Dice, I.V. Sandoval, J. Lippincott-Schwartz, J.T. August, and P. Saftig, *Unifying Nomenclature for the Isoforms of the Lysosomal Membrane Protein LAMP-2.* Traffic, 2005. **6**: p. 1058-1061.

70.   Huynh, K.K., E.L. Eskelinen, C.C. Scott, A. Malevanets, P. Saftig, and S. Grinstein, *LAMP proteins are required for fusion of lysosomes with phagosomes.* The EMBO Journal, 2007. **26**: p. 313-324.

71.   Kuronita, T., E.-L. Eskelinen, H. Fujita, P. Saftig, M. Himeno, and Y. Tanaka, *A role for the lysosomal membrane protein LGP85 in the biogenesis and maintenance of endosomal and lysosomal morphology.* Journal of Cell Science, 2002. **115**: p. 4117-4131.

72.   Sagné, C. and B. Gasnier, *Molecular physiology and pathophysiology of lysosomal membrane transporters.* Journal of Inherited Metabolic Disease, 2008. **31**: p. 258-266.

73.   Platt, F.M., B. Boland, and A.C. van der Spoel, *Lysosomal storage disorders: The cellular impact of lysosomal dysfunction.* The Journal of Cell Biology, 2012. **199**: p. 723-734.

74.   Parkinson-Lawrence, E.J., T. Shandala, M. Prodoehl, R. Plew, G.N. Borlace, and D.A. Brooks, *Lysosomal Storage Disease: Revealing Lysosomal Function and Physiology.* Physiology, 2010. **25**: p. 102-115.

75.   Kiselyov, K., J.J. Jennigs, Y. Rbaibi, and C.T. Chu, *Autophagy, mitochondria and cell death in lysosomal storage diseases.* Autophagy, 2007. **3**: p. 259-262.

76.   Walkley, S.U. and M.T. Vanier, *Pathomechanisms in Lysosomal Storage Disorders.* Biochimica et biophysica acta, 2009. **1793**: p. 726-736.

77.   Wilcox, W.R., *Lysosomal storage disorders: the need for better pediatric recognition and comprehensive care.* The Journal of Pediatrics, 2004. **144**: p. S3-S14.

78.   Nagral, A., *Gaucher Disease.* Journal of Clinical and Experimental Hepatology, 2014. **4**: p. 37-50.

79.   Dandana, A., S. Ben Khelifa, H. Chahed, A. Miled, and S. Ferchichi, *Gaucher Disease: Clinical, Biological and Therapeutic Aspects.* Pathobiology, 2016. **83**: p. 13-23.

80.   Aflaki, E., B.K. Stubblefield, E. Maniwang, G. Lopez, N. Moaven, E. Goldin, J. Marugan, S. Patnaik, A. Dutra, N. Southall, W. Zheng, N. Tayebi, and E. Sidransky, *Macrophage Models of Gaucher Disease for Evaluating Disease Pathogenesis and Candidate Drugs.* Science Translational Medicine, 2014. **6**: p. 240ra73-240ra73.

81.   Lachmann, R.H., D.G. Wight, D.J. Lomas, N.C. Fisher, J.P. Schofield, E. Elias, and T.M. Cox, *Massive hepatic fibrosis in Gaucher's disease: clinico-pathological and radiological features.* QJM, 2000. **93**: p. 237-244.

82.   Hers, H.G., *alpha-Glucosidase deficiency in generalized glycogenstorage disease (Pompe's disease).* Biochem J, 1963. **86**: p. 11-16.

83.   van der Ploeg, A.T. and A.J.J. Reuser, *Pompe's disease.* The Lancet. **372**: p. 1342-1353.

84.   Lim, J.-A., L. Li, and N. Raben, *Pompe disease: from pathophysiology to therapy and back again.* Frontiers in Aging Neuroscience, 2014. **6**: p. 177.

85.   Palmieri, M., S. Impey, H. Kang, A. di Ronza, C. Pelz, M. Sardiello, and A. Ballabio, *Characterization of the CLEAR network reveals an integrated control of cellular clearance pathways.* Human Molecular Genetics, 2011. **20**: p. 3852-3866.

86.   Chapel, A., S. Kieffer-Jaquinod, C. Sagné, Q. Verdon, C. Ivaldi, M. Mellal, J. Thirion, M. Jadot, C. Bruley, J. Garin, B. Gasnier, and A. Journet, *An Extended Proteome Map of the Lysosomal Membrane Reveals Novel Potential Transporters.* Molecular & Cellular Proteomics, 2013. **12**: p. 1572-1588.

87.   David Massa Lopez, M.D.P.S., *Characterising the role of the lysosomal membrane proteins MFSD1 and TMEM106b in osteoclasts (abstract).* 2016.

88.   Perland, E., S.V. Hellsten, E. Lekholm, M.M. Eriksson, V. Arapi, and R. Fredriksson, *The Novel Membrane-Bound Proteins MFSD1 and MFSD3 are Putative SLC Transporters Affected by Altered Nutrient Intake.* Journal of Molecular Neuroscience, 2017. **61**: p. 199-214.

89.   *The Countess™ Automated Cell Counter FAQs.* 2009 [cited 2017; Retrieved from: http://uic.umn.edu/sites/uic.umn.edu/files/Countess-Cell-Counter-FAQ.pdf.

90.   Brand.de. *Counting chambers.* 2017; Retrieved from: http://www.brand.de/fileadmin/user/pdf/GK900/Zaehlkammern/GK900_05_Clinical_Lab_Zaehlkammern_e.pdf.

91.   *What is Transfection?* 2017; Retrieved from: http://www.polyplus-transfection.com/technologies/what-is-transfection/.

92.   Ahuja, D., M.T. Saenz-Robles, and J.M. Pipas, *SV40 large T antigen targets multiple cellular pathways to elicit cellular transformation.* Oncogene, 2005. **24**: p. 7729-7745.

93.   Sciences, G.H.L., *Amersham ECL Prime Western Blotting detection reagent.* 2017.

94.   Spence, M.T.Z., *The molecular probes handbook.* 2010: Live Technologies Corporation

95.   Miller, L. *Analyzing gels and western blots with ImageJ* 2017; Retrieved from: http://lukemiller.org/index.php/2010/11/analyzing-gels-and-western-blots-with-image-j/.

96.   Emptage, N.J., *Fluorescent imaging in living systems.* Current Opinion in Pharmacology, 2001. **1**: p. 521-525.

97.   Davidson, S.W.P.T.J.F.a.M.W. *Introductory Confocal Concepts*. [cited 2017; Retrieved from: https://www.microscopyu.com/techniques/confocal/introductory-confocal-concepts.

98.   Olympus. *Principles of Laser Scanning Microscopes*. Basic Principles of Laser Scanning Microscopes [cited 2017; Retrieved from: http://www.olympus-ims.com/en/knowledge/metrology/lext_principles/basic/.

99.   Irfan Maqsood, M., M.M. Matin, A.R. Bahrami, and M.M. Ghasroldasht, *Immortality of cell lines: challenges and advantages of establishment.* Cell Biology International, 2013. **37**: p. 1038-1045.

100.   Di Micco, R., A. Cicalese, M. Fumagalli, M. Dobreva, A. Verrecchia, P.G. Pelicci, and F. di Fagagna, *DNA damage response activation in mouse embryonic fibroblasts undergoing replicative senescence and following spontaneous immortalization.* Cell Cycle, 2008. **7**: p. 3601-3606.

101.   Amand, M.M., J.A. Hanover, and J. Shiloach, *A comparison of strategies for immortalizing mouse embryonic fibroblasts.* 2016, 2016.

102.   Stubdal, H., J. Zalvide, K.S. Campbell, C. Schweitzer, T.M. Roberts, and J.A. DeCaprio, *Inactivation of pRB-related proteins p130 and p107 mediated by the J domain of simian virus 40 large T antigen.* Molecular and Cellular Biology, 1997. **17**: p. 4979-4990.

103.   Zalvide, J., H. Stubdal, and J.A. DeCaprio, *The J Domain of Simian Virus 40 Large T Antigen Is Required To Functionally Inactivate RB Family Proteins.* Molecular and Cellular Biology, 1998. **18**: p. 1408-1415.

104.   Gaubatz, S., G.J. Lindeman, S. Ishida, L. Jakoi, J.R. Nevins, D.M. Livingston, and R.E. Rempel, *E2F4 and E2F5 Play an Essential Role in Pocket Protein–Mediated G1 Control.* Molecular Cell, 2000. **6**: p. 729-735.

105.   Zalvide, J. and J.A. DeCaprio, *Role of pRb-related proteins in simian virus 40 large-T-antigen-mediated transformation.* Molecular and Cellular Biology, 1995. **15**: p. 5800-5810.

106.   Sullivan, C.S., S.P. Gilbert, and J.M. Pipas, *ATP-Dependent Simian Virus 40 T-Antigen–Hsc70 Complex Formation.* Journal of Virology, 2001. **75**: p. 1601-1610.

107.   Srinivasan, A., A.J. McClellan, J. Vartikar, I. Marks, P. Cantalupo, Y. Li, P. Whyte, K. Rundell, J.L. Brodsky, and J.M. Pipas, *The amino-terminal transforming region of simian virus 40 large T and small t antigens functions as a J domain.* Molecular and Cellular Biology, 1997. **17**: p. 4761-4773.

108.   Ali, S.H. and J.A. DeCaprio, *Cellular transformation by SV40 large T antigen: interaction with host proteins.* Seminars in Cancer Biology, 2001. **11**: p. 15-22.

109.   White, E., *Autophagy and p53.* Cold Spring Harbor Perspectives in Medicine, 2016. **6**.

110.   Carter, R.E. and A. Sorkin, *Endocytosis of Functional Epidermal Growth Factor Receptor-Green Fluorescent Protein Chimera.* Journal of Biological Chemistry, 1998. **273**: p. 35000-35007.

111.   Walker-Daniels, J. *Live Cell Imaging Review*. 2012 2015-10-06 [cited 2017 060617]; Retrieved from: https://www.labome.com/method/Live-Cell-Imaging-Methods-Review.html.

112. Copeland, R.A., *Protein-ligand binding equilibria*, in *Enzymes. A Practical Introduction to Structure, Mechanism, and Data Analysis*, 2000, 76-108.

113. Ghosh, R.N., W.G. Mallet, T.T. Soe, T.E. McGraw, and F.R. Maxfield, *An Endocytosed TGN38 Chimeric Protein Is Delivered to the TGN after Trafficking through the Endocytic Recycling Compartment in CHO Cells.* The Journal of Cell Biology, 1998. **142**: p. 923-936.

114. Nordberg, E., M. Friedman, L. Göstring, G.P. Adams, H. Brismar, F.Y. Nilsson, S. Ståhl, B. Glimelius, and J. Carlsson, *Cellular studies of binding, internalization and retention of a radiolabeled EGFR-binding affibody molecule.* Nuclear Medicine and Biology, 2007. **34**: p. 609-618.

115. Rappoport, J.Z. and S.M. Simon, *A functional GFP-fusion for imaging clathrin-mediated endocytosis.* Traffic 2008. **9**: p. 1250-1255.

116. Campbell, R.E., O. Tour, A.E. Palmer, P.A. Steinbach, G.S. Baird, D.A. Zacharias, and R.Y. Tsien, *A monomeric red fluorescent protein.* Proceedings of the National Academy of Sciences of the United States of America, 2002. **99**: p. 7877-7882.

Appendix A – Abbreviations

ATP	Adenosine Triphosphate
cDNA	complementary Deoxyribonucleic acid
CIE	Clathrin-Independent Endocytose
CME	Clathrin-Mediated Endocytosis
DMEM	Dulbecco's Modified Eagle's Medium
DMSO	Dimethyl Sulfoxide
DNA	Deoxyribonucleic acid
ECL	Enhanced Chemiluminescence
ECM	Extracellular Matrix
EDTA	Ethylenediaminetetraacetic acid
EE	Early Endosome
EGF	Epidermal Growth Factor
EGFP	Enhanced Green Fluorescence Protein
ER	Endoplasmic Reticulum
ESCRT	Endosomal Sorting Complexes Required for Transport
FBS	Fetal Bovine Serum
GD	Gaucher Disease
GDP	Guanosine Diphosphate
GDS	Glycogen Storage Disorder
GFP	Green Fluorescence Protein

GLMP	Glycosylated Lysosomal Membrane Protein
gt	gene-trap
GTP	Guanosine Triphosphate
HCSs	Hepatic Stellate Cells
HRP	Horseradish Peroxidase
ILVs	Intraluminal Vesicles
KCs	Kupffer Cells
LAMP	Lysosome-Associated Membrane Protein
LB	Lysogeny broth
LD	Lysosomal Disorders
LE	Late Endosome
LIMP	Lysosome-Integral Membrane Protein
LMPs	Lysosomal Membrane Proteins
LSECs	Liver Sinusoidal Endothelial Cells
M6P	Mannose-6-Phosphate
M6PR	Mannose-6-Phosphate Receptor
MEF	Mouse Embryonic Fibroblasts
MFSD1	Major Facilitator Superfamily Domain containing protein 1
MT	Microtubules
OD	Optical Density
PBS	Phosphate Buffered Saline

PCR	Polymerase Chain Reaction
pRB	Retinoblastoma
PVDF	Polyvinyldene difluoride
RE	Recycling Endosome
RFP	Red Fluorescence Protein
ROI	Region Of Interest
S.O.B	Super Optimal Broth
S.O.C	Super Optimal broth with Catabolite repression
SDS-PAGE	Sodium Dodecyl Sulfate Polyacrylamide Gel Electrophoresis
SV40	Simian vacuolating virus 40
TAg	Large T antigen
TB	Terrific Broth
TBS	Tris Buffered Saline
Tf	Transferrin
TFEB	Transcription Factor EB
TfR	Transferrin receptor
TGF-α	Transforming Growth Factor-Alpha
TGN	Trans Golgi Network
α-SMA	Alpha-Smooth Muscle Actin

Appendix B – Materials

B1   Chemicals

	Manufacturer
Bacroagar	Merck, 1078890500
Bactotrypton	BD Biosciences, Cat No. 211705
CaCl2 x 2H2O	Sigma-Aldrich
Coomassie Brilliant Blue R-250	Bio-Rad, Cat No. 1610436
Dextran, Alexa Fluor™ 546	Thermo Fischer, Cat No. D22911
DMEM w/o L-glutamine w/ phenol red	Lonza, BE12-614F
DMEM w/o L-glutamine w/o phenol red	Lonza, BE12-917F
Dimethyl sulfoxide (DMSO)	Sigma-Aldrich, Prod. No. D8418
EGF complexed to Alexa Fluor™ 647	Thermo Fischer, Cat No. E35351
FBS	Loza
Glucose	Sigma-Aldrich
KCl	Merck
KH2PO4	Meck
KOH	Prolab Technologies
L-glutamine	Lonza, BE17-605F
MgCl2	Sigma-Aldrich
MGgSO4	Sigma-Aldrich
MnCl2	Sigma-Aldrich
Na2HPO4 x 2H2O	Merck
NaCl	vwr Chemicals

NaOH	Sigma-Aldrich
NuPAGE Bis-Tris SDS-PAGE gel 4-12%	Invitrogen, Cat No. NP0322
NuPage LDL sample buffer 4x	Invitrogen, Cat No. NP007
PageRuler™ Prestained Protein Ladder	Fermentas, Cat No. SM0671
Penicillin/streptomycin	Lonza, Cat No. 17-602^E
Pipes	Sigma-Aldrich
Transferrin Alexa Fluor™ 488	Thermo Fischer, Cat No. T13342
Trypsin EDTA	Lonza, Cat No. CC-5012
Trypan Blue 0.4%	Thermo Fischer, Cat No. T10282
Yeast extract	BD Biosciences, Cat No. 211750
XT MOPS	Bio-Rad, Cat No. 161-0788
XT Sample Buffer	Bio-Rad, Cat No. 161-0791

B2   Kits

Product name	Manufacturer
NucleoSpin® RNA	Macherey-Nagel, Cat No. 740588.50
jetPRIME® DNA/siRNA transfection	PolyPlus, Cat No. 114-01
ECL Select™ Wester Blotting Detection Reagent	GE Lifesciences, Cat No. RPN2235

Appendix C- solutions and mediums

C1   Cell culture mediums

Table C1.1: **Cell growth medium**

Growth medium
500 mL DMEM with phenol red
Add sterile filtered:
50 mL FBS
5 mL L-Glutamine (2nM)
5 mL Pen/strep
Store in dark at 4 °C

Table C1.2: **Freeze stable medium**

Freeze medium
Prepare fresh
Sterile filtered:
8 mL growth medium
1 mL DMSO
1 mL FBS
Do not store, use at once.

Table C1.3: **Microscope medium**

Microscope medium
500 mL DMEM without phenol red
Add sterile filtered:
50 mL FBS
5 mL L-Glutamine (2nM)
5 mL Pen/strep
Store in dark at 4 °C

C2   Bacterial growth mediums

Table C2.1: **LB medium and LB-agar plates**

LB (500 mL)
5 g bactotrypton 2.5 g yeast extract 2.5 g NaCl 0.5 mL NaOH milliQ to 500 mL autoclave at 121 ℃ for 20 min Store in RT
LB-plates
Mix 1,5 g bactoagar / 100 mL LB Autoclave at 121 ℃ for 20 min When solution cools to under 50 ℃ antibiotics might be added Pour into petri dishes Let set store in concealed plastic bag at 4 ℃

Table C2.2: **S.O.C. medium**

S.O.C. (50 mL)
1 g bactotrypton 0.25 g yeast extract 0.03 g NaCl 62,5 µl 2M KCl milliQ to 49 mL Autoclave at 121 ℃ for 20 min Add: 0,5 mL 1M $MgCl_2$ 0,5 mL 1M MgSO4 1 mL 20 mM glucose Adjust pH to 7 with 1M NaOH Sterile filter solution Store in aliquots of 2 mL in – 4 ℃

Table C2.3: **S.O.B medium**

S.O.B.
10 g bactotrypton
2,5 g yeast extract
0.29 g NaCl
625 µl 2M KCl
Add milliQ H_2O to 490 mL
autoclave at 121 ºC for 20 min
store at 4 ºC
Right before use add:
5 mL 1M MgCl2 5 mL 1M MgSO4
Sterile filter

C3   Solutions

Table C3.1: **PBS buffer**

10 x PBS
80 g NaCl
2 g KCl
7.64 g Na2HPO4 x 2 H2O
2 g KH2PO4
milliQ to 1 litre
1 x PBS:
Dilute 10 x PBS stock 1:10 with milliQ H_2O
Autoclave 20 min at 121ºC

Table C3.2: **TB buffer**

TB
1.5 g Pipes
1.1 g $CaCl_2$ x $2H_2O$
9.3 g KCl
5.3 g $MnCl_2$
465 mL milliQ
Mix all except $MnCl_2$
adjust pH to 6.7 with KOH
Add $MnCl_2$

Table C3.3: **RIPA lysing buffer**

RIPA
20 mM Tris pH 7.5
150 mM NaCl
1mM Na_2EDTA

| 1 % Triton |
| 2.5 mM Na-pyrophosphate |
| 1 mM β-glycerol phosphate |
| 1 mM Na_3VO_4 |

Table C3.4: **Blotting buffer**

Blotting buffer
15 g Tris base
72.5 g Glycine
1 L methanol
milliQ to 5 L

Table C3.4: **Blocking buffer**

Blocking buffer
1 x PBS (Table C3.1)
0.1% tween
5 % dry milk powder

Appendix D – Plasmids

The pSG5 Vector
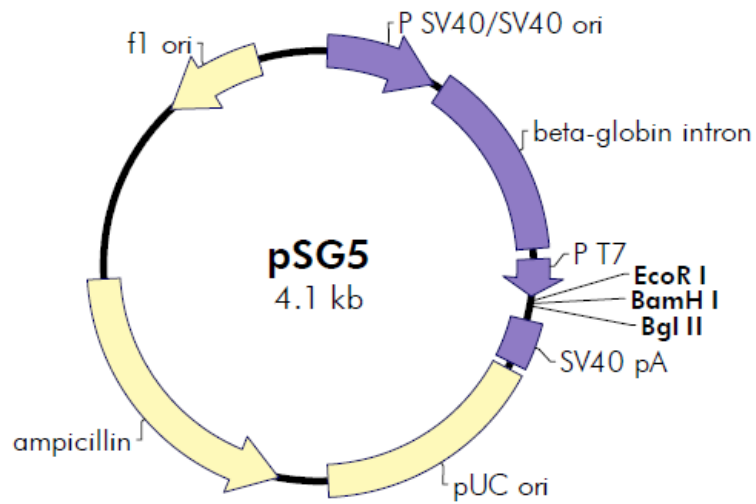
Feature	Nucleotide Position
SV40 promoter and SV40 origin of replication	28–366
β-globin intron	395–967
T7 promoter	1022–1040
EcoR I	1043
BamH I	1049
Bgl II	1055
SV40 polyA signal	1069–1202
pUC origin of replication	1342–2009
ampicillin resistance (bla) ORF	2160–3017
f1 origin of ss-DNA replication	3587–3893

Plasmid D1: **pSG5.** Circular map with features of pSG5, complete sequence and list available from www.genomics.agilent.com

pEGFP-N1 Vector Information

GenBank Accession #U55762

PT3027-5

Catalog #6085-1
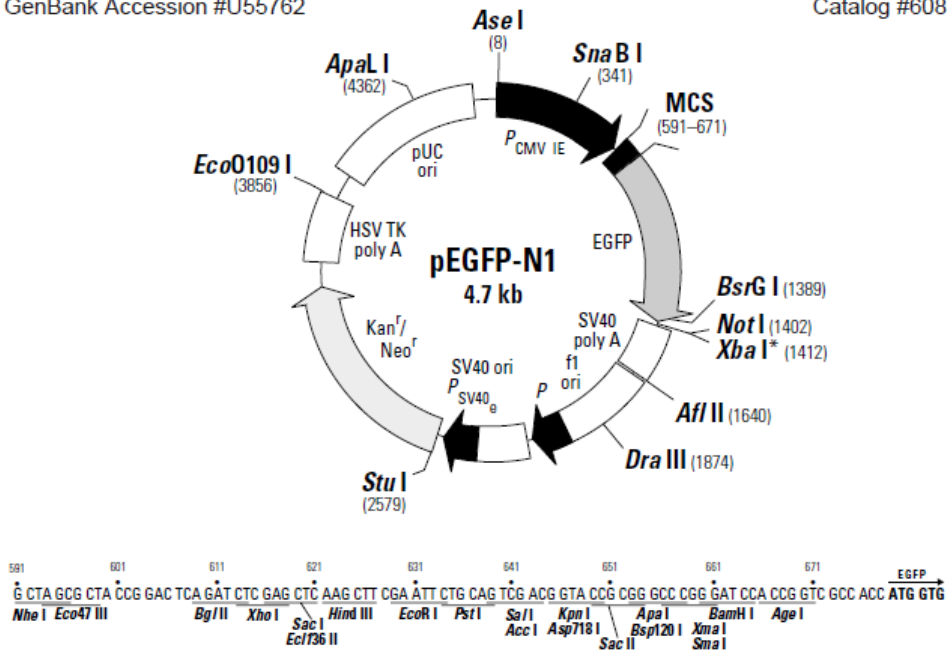
Plasmid D 2 **pEGFP-C2 Vector**. The pEGFP-GLMP constructed applied in this thesis was constructed by previous student Orby, R. *Glmp* ORF is inserted at Age1/EcoR1 as described in [17].
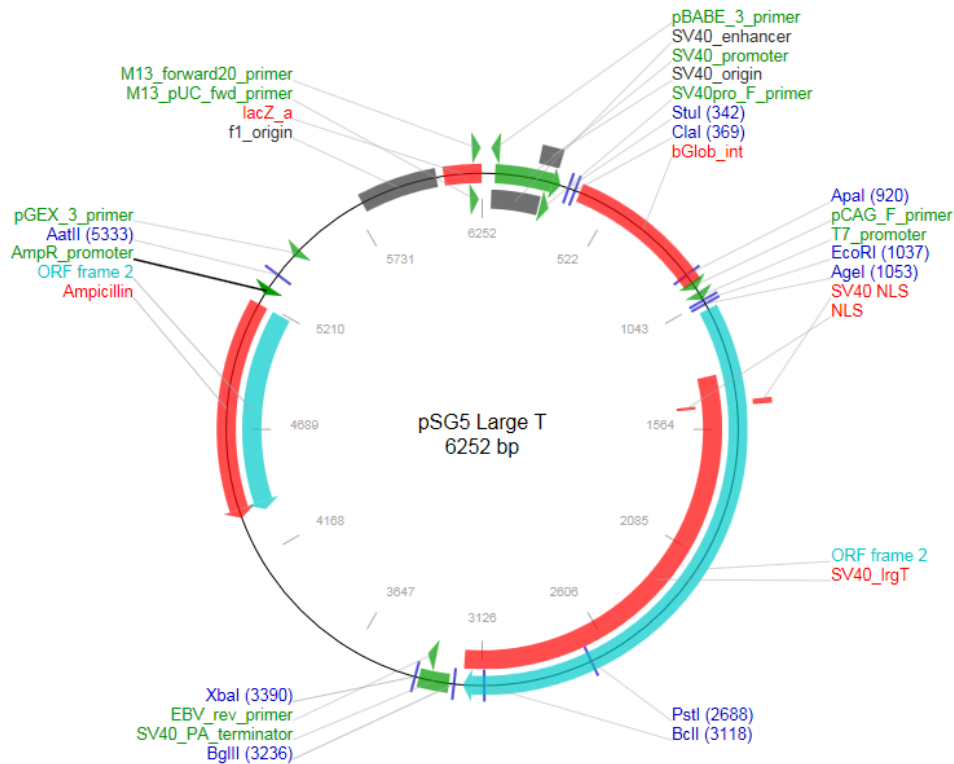
Plasmid D3. **pSG5 Large T.** SV40 Large T antigen available from Addgene, Catalog #9053
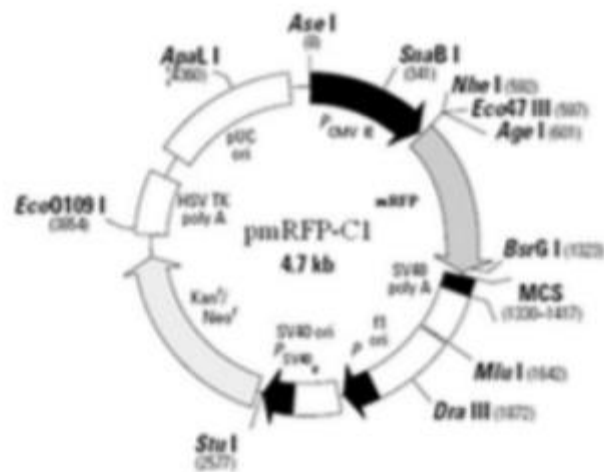
Plasmid D4. **pmRFP-C1.** RFP expression plasmid, constructed by Robert E. Campbell [116].
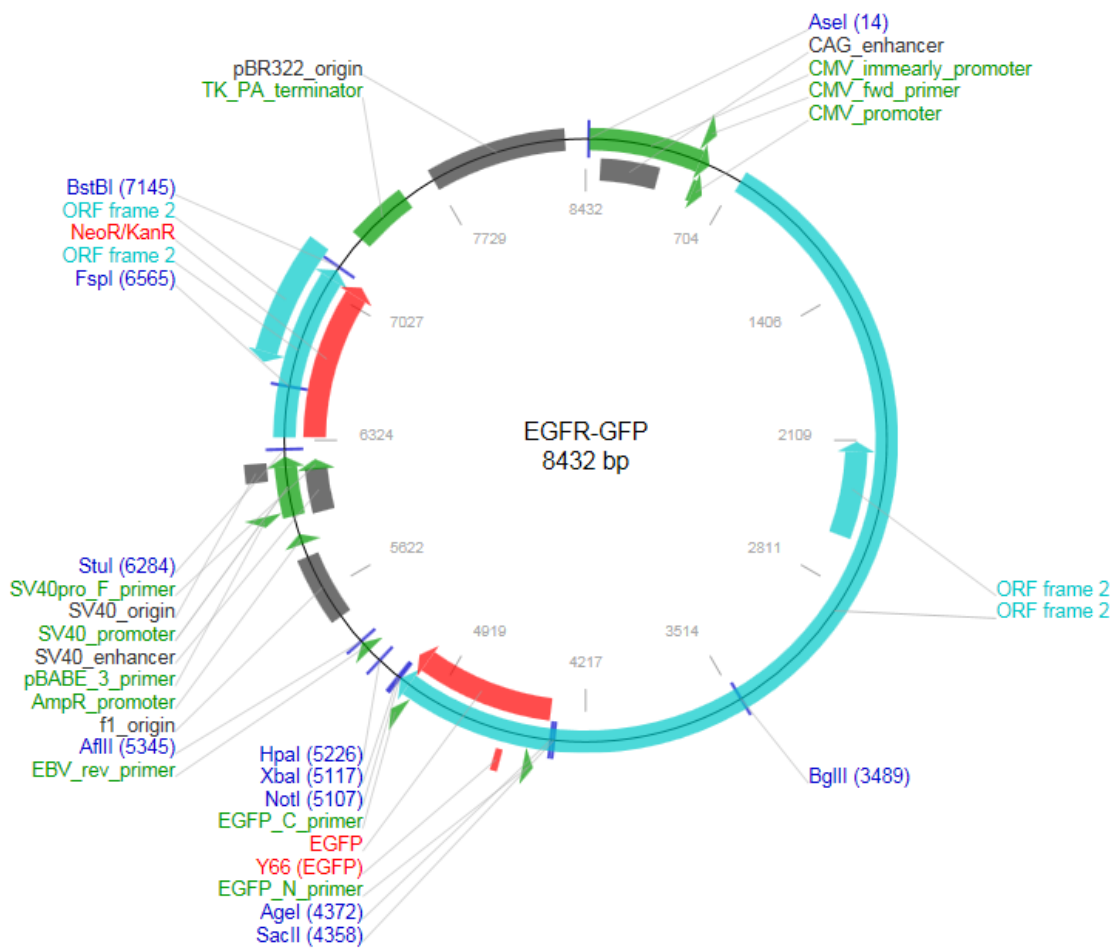
Plasmid D5. **pEGFR-EGFP.** Available from Addgene, Catalog #32751